UNIVERSITA' DEGLI STUDI "ROMA TRE"
SCUOLA DOTTORALE IN GEOLOGIA DELL'AMBIENTE E DELLE RISORSE (SDIGAR)
SEZIONE: GEOLOGIA DELL'AMBIENTE E GEODINAMICA
- XXVII CICLO-

"Cenozoic tectonic evolution and paleomagnetic rotation in Iran"

PhD Candidate

Hamideh Rashid

Advisors: ***Prof. Massimo Mattei***
Prof. Mohammad Mohajjel Kafshduz

Co-advisor: ***Dr. Francesca Cifelli***

Head of the Doctoral School:
Prof. Claudio Faccenna

11/2/2016

Abstract

To provide insights on the late Mesozoic-Cenozoic paleogeographic and tectonic evolution of Iran, I present new paleomagnetic, anisotropy of magnetic susceptibility (AMS) and structural data from the Upper Jurassic Bidou and Garedu Formation of Central Iran and the Miocene Upper Red Formation (URF) of Central Iran and Alborz Mountain, which we used in conjunction with published paleomagnetic data.

Palemagnetic results demonstrate two main episodes of counter-clockwise (CCW) vertical axis rotations that occurred in Central Iran in the Late Jurassic–Early Cretaceous and after the Middle–Late Miocene. Paleomagnetic inclination values indicate that, during the Late Jurassic, the Central-East-Iranian Microcontinent (CEIM), consisting of the Yazd, Tabas, and Lut continental blocks, was located at low latitudes close to the Eurasian margin and the CEIM was oriented WSW–ENE, with the Lut Block bordered to the south by the Neo-Tethys Ocean and to the southeast by the Neo-Sistan oceanic seaway. Subsequently, the CEIM underwent the first significant counter-clockwise (CCW) rotation during the Early Cretaceous with an average amount of ~30°. This rotation may have resulted from the northward propagation of the Sistan rifting-spreading axis during Late Jurassic–Early Cretaceous, or to the subsequent (late Early Cretaceous?) eastward subduction and closure of the Sistan oceanic seaway underneath the continental margin of the Afghan Block. The second episode of counter-clockwise (CCW) vertical axis rotations in Central Iran, occurred after the Middle–Late Miocene with an average amount of ~20°. Paleomagnetic results show that crustal blocks bounded by sets of N-S right lateral strike slip faults are rotated CCW to accommodate NNE-SSW shortening related the convergence between Arabia-Eurasia during the Cenozoic.

The paleomagnetic results of URF sediments in the Northern sector of Arabia-Eurasia collision zone (Alborz Mountain) document clockwise, counter-clockwise and clockwise rotations along vertical axis for the western, central and eastern arms of the Alborz thrust-fault system, respectively. My results suggest orocline bending mechanism for the origin of the curved Alborz Mountains, which acquired most of its curvature in the last 8 Myr. Most likely, the bending processes caused by relative motion between the stable and rigid blocks (Caspian Sea and Central

Iran) within Arabia-Eurasia collision zone. In the Southern part of Lut Block (Central Iran), opposite vertical axis rotations have been recorded in the Middle-Upper Miocene units cropping out along the Northern and Southern parts of Shahdad thrust-fold system which may due to an orocline bending mechanism acquired most of its curvature after deposition of Upper Red Formation in the Late Miocene.

I used the integration of AMS and structural data for understanding the continental deformation in collision zone of Arabia-Eurasia. At the tectonic boundary between the Lut and the Tabas blocks of Central Iran, the results of Garedu Red Beds, outcropping in the core of a NNE–SSW oriented syncline in the northern Shotori Range, confirm that the Garedu Red Beds syncline is a transected fold which formed as a consequence of right-lateral transpressional tectonics. It may have related to the shortening phase which caused the closure of the small oceanic basins around Central Iran, as a result of the motion of the Arabian Plate and the closure of the Neotethys oceanic basin.

My results in the Ferdows Thrust-fold system (Lut block), show two sets of the magnetic fabrics. In most cases magnetic fabric, acquired when the bedding were still horizontal, is related to different degrees of LPS shortening and in some cases magnetic fabric has been developed as a consequence of later shortening related to the activity of the thrust system responsible of the recent earthquakes in the area. These results appears in agreement with the overall tectonic history of the Ferdows thrust–fold system which is characterized by two distinct phases of fold growing, marked by a sharp angular unconformity between the middle-upper Miocene URF and the overlying alluvial and fluvial Quaternary deposits.

Acknowledgments

I would like to thank many people who contributed to make this work possible. First of all, I am very grateful to my supervisor Prof. Mssimo Mattei for giving me the chance to do this PhD and for sharing his knowledge and experience with me. Thank you for teaching me self-confidence. I wish to thank my Iranian supervisor Prof. Mohammad Mohajjel for his guidance and supervision throughout my PhD. Many thanks to my co-supervisor Dr. Francesca Cifelli for her guidance in the field work and paleomagnetic laboratory. I learned many things through her comments and corrections of my manuscript. I am very grateful to Prof. Leonardo Sagnotti and the other members of the paleomagnetic laboratory at the National Institute of Geophysics and Volcanology of Italy (INGV).

During my PhD, I have had the opportunity to be a part of the Geodynamic Group which I have benefited from the interesting discussion and seminars. Thanks to all of them.

For this dissertation I would like to thank my reading committee members: Prof. Leonardo Sagnotti and Eugenio Carminati for their time, interest, and helpful comments.

My special thanks to Dr. Mohammad Reza Ghassemi and Manuchehr Ghorashi who encouraged me to make research in the paleomagnetic field in Italy. I would like to appreciate to deputy of geology of the Geological Survey of Iran (GSI), Dr. Jalil Ghalamghash who helped and supported me very much and also Dr. Habib Alimohamadian who helped me in field.

Many thanks to my Iranian friends Benyamin and Meysam for their nice friendship and continuous presence.

I thank Mrs. Ghanipour and her Colleagues for all their help in this period. I also thank my friends in Iran and Italy (too many to list here but you know who you are!) for providing support and friendship that I needed Lastly, I would like to thank my family for all their love and encouragement. For my parents who are the most important people in my world and I dedicate this thesis to them.

Table of Contents

Chapter I- Introduction

Chapter II- Post-Cimerian paleogeography

Chapter III- Oroclines in the Alborz and Central Iran

Chapter IV- Right-lateral transpressional tectonics

Chapter V- Late folding-related magnetic foliation

Chapter VI- Discussion and conclusion

Bibliography

Chapter I

Introduction

1. General overview

This thesis deals with the determination of the late Mesozoic and Cenozoic tectonic evolution of Central Iran and Alborz Mts. through paleomagnetic and AMS studies. Structural data, magnetic fabrics and paleomagnetic results from Oligocene-Miocene sedimentary units in Alborz range and central Iran are used to reconstruct the history of Neogene tectonic deformation of this region.

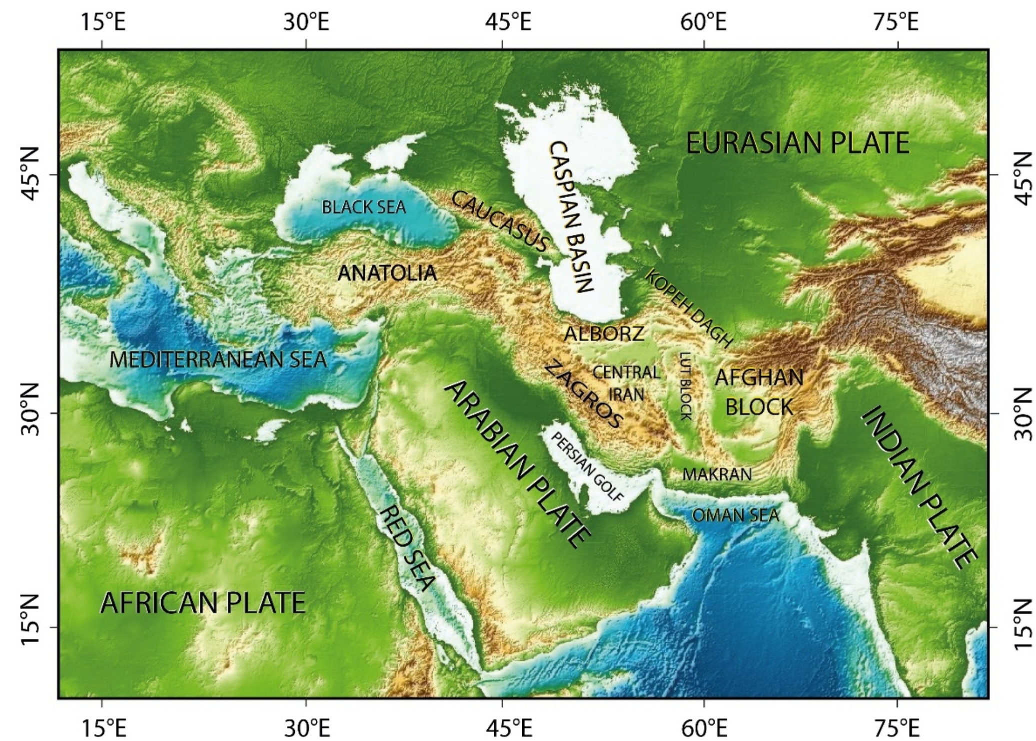

Fig. 1. Topographic map (SRTM data) of Iran in Alpine-Himalayan orogenic bet.

Iran is situated in the Alpine–Himalayan orogenic belt and has a complex tectonic history in late Mesozoic and Cenozoic which results from the convergence and collision of the Arabian Plate towards Eurasia (Fig. 1). The onset age of Arabia-Eurasia continent-continent collision matter of discussion (e.g., McQuarrie et al., 2003; Guest et al., 2006b). Timing estimates for the inception of the collision include Late Cretaceous (Stocklin, 1974; Berberian and Berberian, 1981; Alavi, 1994), Eocene (Hempton, 1987), latest Eocene–Early Oligocene (Jolivet and Faccenna, 2000; Hessami et al., 2001; Robertson et al., 2006; Allen and Armstrong, 2008; McQuarrie and van Hinsbergen, 2013, Neill et all., 2015), Oligocene (Yilmaz, 1993), Oligocene–Miocene (Berberian et al., 1982), Early to Middle Miocene (Robertson, 2000), Middle Miocene (Dewey and Sengör, 1979; Sengör and Kidd, 1979, Guest et al., 2006b), Middle to Late Miocene (Homke et al., 2004), Late Miocene (Stoneley, 1981).

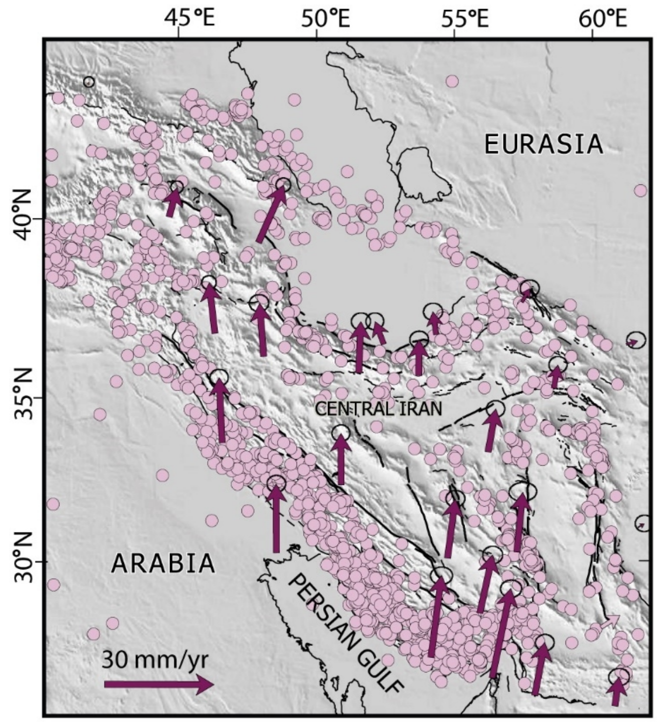

Fig. 2. Teleseismically recorded earthquakes of Iran in a period 1964–2004 (pink dots), from Tartar et al, (2007), with GPS velocities of points in Iran relative to stable Eurasia from Vernant et al., (2004) shown by red arrows.

Maximum deformation related to Arabia-Eurasia convergence in the Cenozoic has been-and is at present day- accommodated mainly by displacement in the active fold-and-thrust belts of the Zagros, Alborz and Kopeh Dagh (e.g., Berberian and King, 1981; Allen et al., 2004, Mattei et al., 2012), whereas, the fault-bounded crustal blocks of central Iran (Yazd, Tabas, and Lut blocks), show little internal deformation (Vernant et al., 2004, Mattei et al., 2012, 2015). This deformation model is in agreement with the distribution of seismic and geodetic data (Fig. 2) and shows that at longitude 55°E, the ~22 ± 2 mm/yr of Arabia-Eurasia convergence rate is mostly accommodated in the Zagros fold-and-thrust belt (~9 ± 2 mm/yr) and in the Alborz and KopehDagh Mountains (~8 ± 2 mm/yr), whereas only ~4 ± 2 mm/yr is taken up in central Iran (Vernant et al., 2004). Since initial collision along the Bitlis-Zagros suture, the Arabian plate has shifted ~300–500 km toward the north with respect to stable Eurasia (Allen et al., 2004).

2. Study Area

2.1. Alborz Range

The Alborz (also written as Alburz, Elburz or Elborz) Mountains system is located along the northern margin of Arabia-Eurasia collision zone (Fig. 1) and forms a gently curved east-west range (Fig.3) in northern Iran (Stöcklin, 1974). It extends in a sinuous shape for ca. 1200 km from the Talesh in north-west to the Parapamisus Mountains of northern Afghanistan, to the east, and could be divided into three main parts including: Western Alborz, Central Alborz and Eastern Alborz respectively. Mount Damavand (Fig. 3), a dormant volcano and the highest peak in Iran and the Middle East with ~5671 m elevation, is situated in the Central Alborz range.

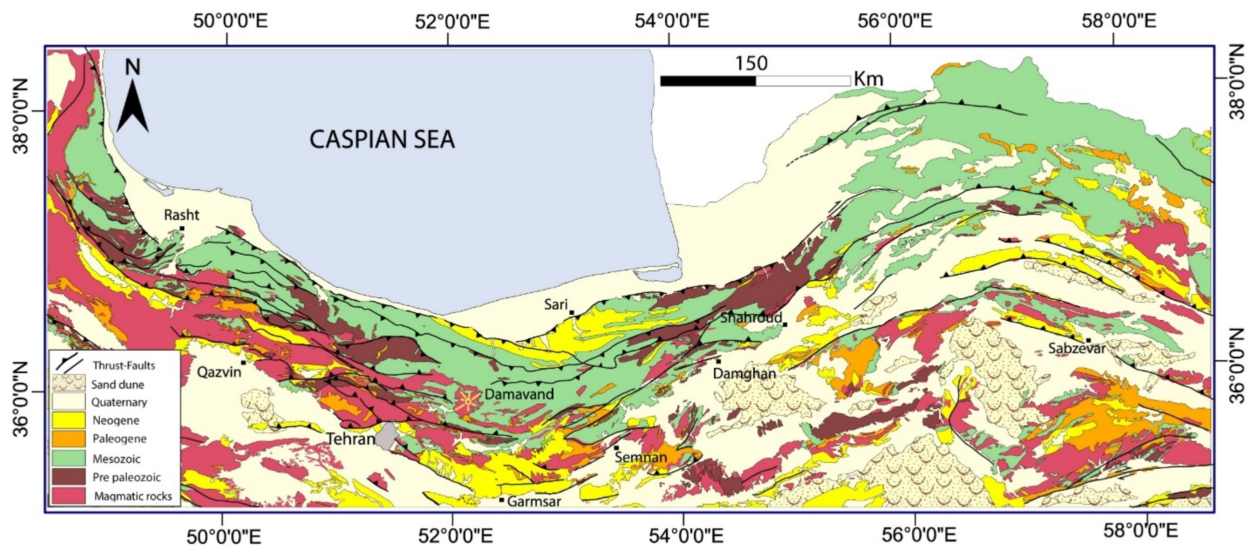

Fig. 3. Generalized geological-structural map of the Alborz. Geological unites modified from geological maps of Iran published by Geological Survey of Iran, and the faults modified from Tectonic Map of Iran. Nogole Sadat et al, (1993).

The Alborz range is the result of several tectonic events (e.g., Alavi, 1996) from the early Mesozoic, Cimmerian orogeny, to the present-day stage of intracontinental deformation related to the convergence between Arabian and Eurasian plates (Allen et al., 2003; Zanchi et al., 2006; Guest et al., 2007; Ballato et al., 2008; Zanchi et al., 2009).

During Permian to earliest Triassic times, the Neotethys ocean opened (Fig. 4) between the Arabian and Central Iranian blocks (Wilmsen et al., 2009) and in the Late Permian–Middle Triassic Neotethys spreading rates~20 cm/a) rapidly decreased to about 6cm/ a (Stampfli and Borel, 2002; Muttoni et al., 2009). Primary collision between Iranian microplate and southern margin of Eurasia occurred in Late Permian – Early Triassic (260 – 249 Ma) (Sengör, 1984; Zanchi et al., 2006; Zanchi et al., 2009; Muttoni et al., 2009; Wilmsen et al., 2009).

Fig. 4. Paleogeographic reconstruction of Pangea A for the Late Permian – Early Triassic based on paleomagnetic poles modified from Muttoni et al, (2009a). The star to the northeast of Adria indicates the hypothetical location of a ridge-trench-fault (RTF) triple junction adjoining the Gondwana, Laurasia, and Paleo-Tethys plates.

The Cimmerian orogeny is related to the Middle-Late Triassic collision of Iran (Fig. 4), a microplate of Gondwanan affinity, with Eurasia and to the closure of the Palaeotethys (Stöcklin, 1974; Davoudzadeh and Schmidt, 1984; Sengör, 1984; Stampfli et al., 1991; Stampfli and Borel, 2002). Most researchers suppose that the collision occurred in the Late Triassic (Fig. 5a) along a north dipping subduction zone (Stöclin, 1974; Alavi, 1991; Ruttner, 1993; Ricou, 1996; Alavi et al., 1997; Stampfli et al., 2001; Allen et al., 2003) which is now located at the latitude of the southern Caspian coast (Berberian & King, 1981; Alavi, 1991; Ruttner, 1993). Remnants of Paleo-Tethys suture are recognized as the Aghdarband suture in the Binnalud Mauntain NE Iran and eastward (Stöcklin, 1968; Baud and Stampfli, 1991; Alavi, 1991; Ruttner, 1993; Sheikholeslami & Kouhpeyma, 2012). The continuation of the suture zone to the west, was introduced by Alavi (1996) along the Central and Western Alborz (Talesh Mountain) is debatable (Zanchi et al., 2009b).The collision is distinguished by an angular unconformity between the Upper Precambrian to Middle Triassic sequences of North Iran and the Upper Triassic to Lower Jurassic

Shemshak Formation (Seyed-Emami, 2003; Fursich et al., 2005; Zanchi et al., 2009a, Wilmsen et al., 2009).

Long lived subduction of the Neo-Tethys Ocean beneath the south Eurasian margin led to opening of the Great Caucasus-Caspian back arc rifting (Fig. 5b)(Brunet et al., 2003; Kaz'min and Verzhbitskii., 2011) which reached its maximum extent during the late Cretaceous–early Paleogene. (Golonka, 2000; Golonka et al., 2006, 2007; Kaz'min and Tikhonova, 2006). Some researchers proposed that this Ocean was connected to the Sistan Ocean, which separated Lut

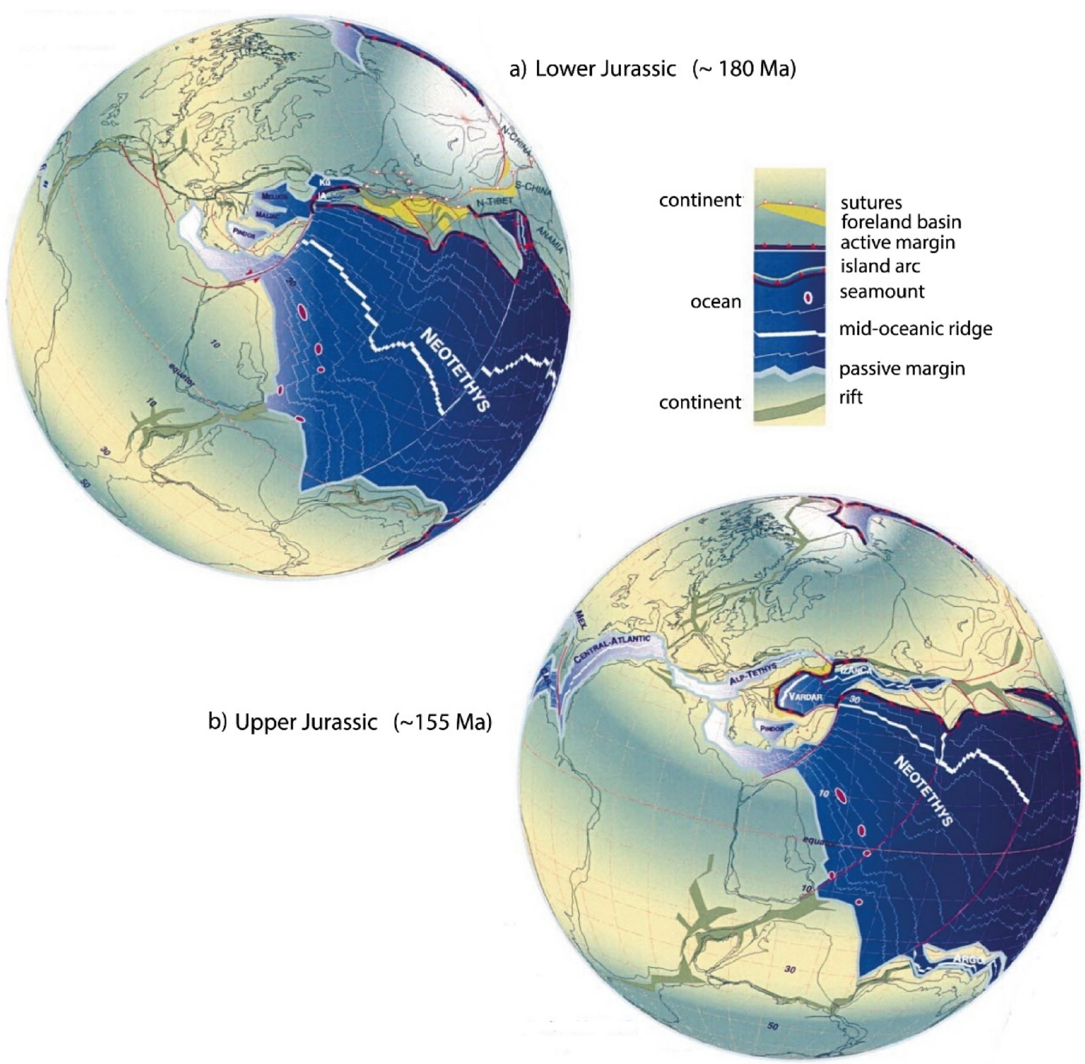

Fig. 5. Orthographic projection with Europe fixed in its present-day position from Stampfly and Borel, (2002). a) ~180, b) ~155 Ma. Paleopoles of Baltica are used as reference for the paleolatitudes.

from Afghanistan and Kopet-Dagh area (Golonka et al., 2006, 2007; Kaz'min and Tikhonova, 2006). The closure of this ocean is marked by ophiolites in northern Iran (Ricou, 1996; Sengör and Natalin, 1996). From the Early Cretaceous to Paleogene (Fig. 6a, b, c), the Turan platform was characterized by a tectonic quiescence (Golonka et al., 2007). In contrast, various pre-existing rock units (from Cambrian to Upper Cretaceous in age) in the southern Alborz and over the greater part of central Iran underwent a regional phase of shortening, uplift, and erosion (Stöcklin, 1968; Berberian and King, 1981, Guest et al., 2006) during the closure of some small oceanic basins further south in Iran, now preserved as Late Cretaceous ophiolite complexes. In the Alborz Mountains, this uplift and folding was associated with the deposition of Paleocene Fajan conglomerate (Allen et al., 2003; Zanchi et al., 2006, 2009, Ballato et al., 2013).

Before the Arabia–Eurasia collision, the Eurasian continental margin experienced arc magmatism as the result of the northwards subduction of Neo-Tethyan oceanic crust (Allen and Armestrong, 2008). A highly generative magmatic arc/back arc system (e.g., Kazmin et al., 1986; Verdel et al., 2011; Allen and Armestrong, 2008) was dominated across most part of Iran and Turkey between ~50 and ~35 Ma (Allen and Armestrong, 2008). Volcanism happened in an extensional setting during the Eocene along the southern margin of the Eurasian plate which was coincident with the renewal of northern motion of Africa–Arabia with respect to Eurasia and subduction of Neotethyan oceanic crust (e.g., Dewey et al., 1973, 1989). The pick of these volcanic activities was during the middle Eocene (Allen and Armestrong, 2008). In the southern margin of the Alborz, this volcanic arc was specified by the accumulation of a thick (up to 5 km) andesitic volcanics and volcanoclastics of the Karaj Formation (Stöcklin, 1974; Alavi, 1996). The volcanic activities decreased in the late Eocene and was little in the Oligocene time, although minor and scattered volcanism is maintained to the present day at the most part of collision zone (Pearce et al., 1990; Allen and Armestrong, 2008). Eocene normal faults in the Alborz Mountains (Guest et al., 2006a), stratigraphic evidence of Eocene subsidence in the Alborz Mountains and central Iran (Brunet et al., 2003; Hassanzadeh et al., 2004; Vincent et al., 2005; Guest et al., 2007b; Morley et al., 2009), geochemical and geochronological data (Verdel et al., 2011) and an Eocene metamorphic core complex in central and eastern Iran (Moritz et al., 2006; Verdel et al., 2007) indicate that this magmatic episode occurred during regional extension.

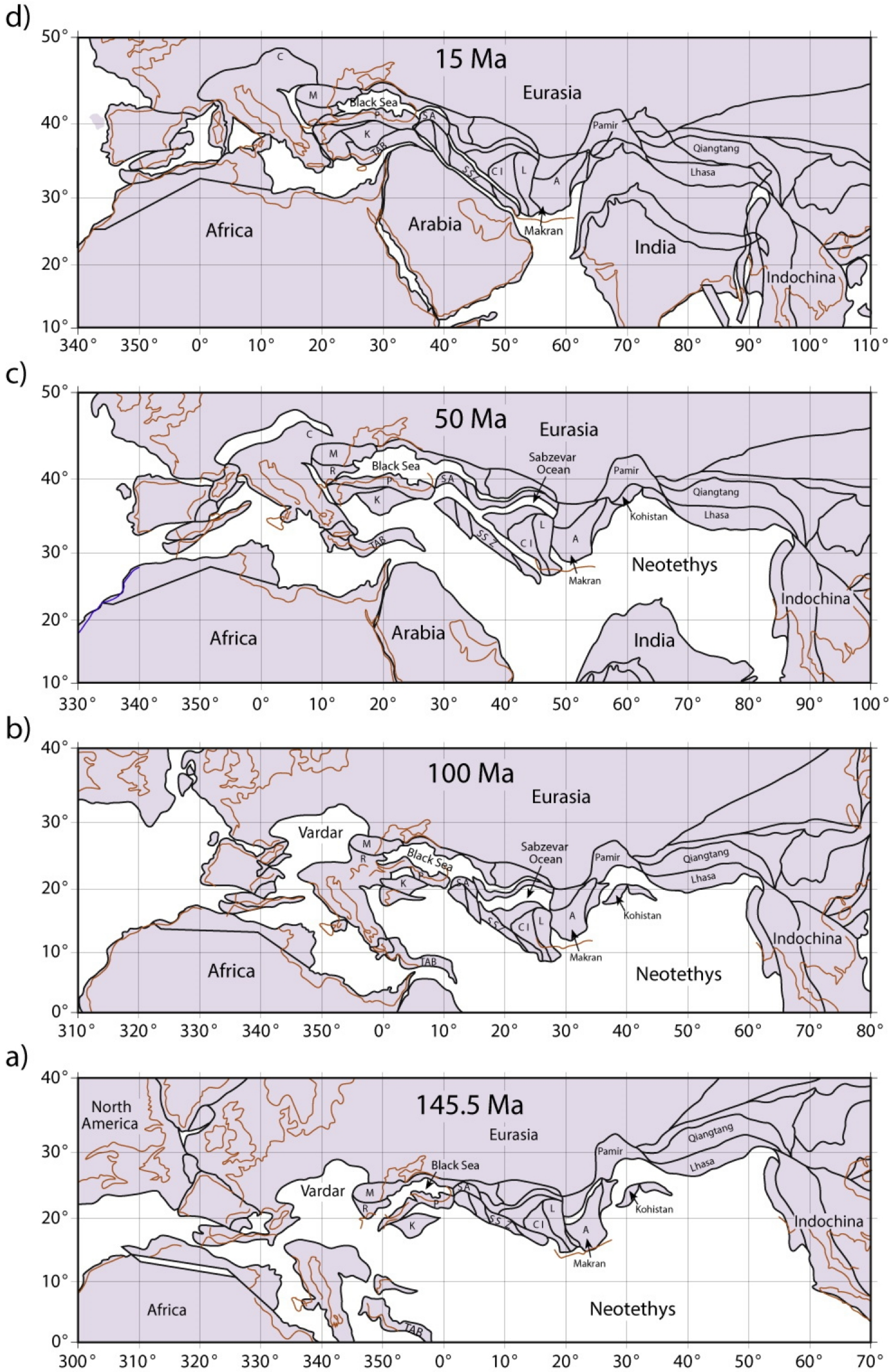

Fig. 6. Paleogeographic reconstructions of the Neotethyan region at (a) 145.5, (b) 100 Ma, (c) 50 Ma, (d) 15 Ma, modified from Richards, (2015). Abbreviations: A: Afghan block; C: Carpathians; CI: Central Iranian block; K =Kirsehir block; L: Lut block; M: Moesian Platform; P: Pontides; R: Rhodopes; SA: South Armenian block; SSZ: Sanandaj–Sirjan Zone; TAB: Tauride–Anatolide block.

During the late Eocene–early Oligocene, a regional phase of shortening developed in Alborz Mountains (Stöcklin, 1968; Berberian and King, 1981). The volcanic and volcanoclastic rocks of the Karaj Formation and marine evaporates of Kond Formation are unconformably overlain by terrestrial clastic and evaporite deposits (Fig. 7) of the Oligocene Lower Red Formation (e.g., Jackson et al., 1990; Amini, 1997; Davoudzadeh et al., 1997). Change in kinematics from an extensional to a compressional tectonic regime and ending of arc magmatism is concordant with the initiation of continental collision with the subduction of stretched continental Arabian lithosphere ("soft" collision) beneath Eurasia (Ballato et al., 2011). Reduction of convergence rate by 20 Ma was associated with the "hard"collision of unstretched and buoyant Arabian lithosphere, which ultimately caused widespread upper-plate deformation (Ballato et al., 2011; McQuarrie et al., 2013).

During the late Oligocene–early Miocene a shallow-water carbonate shelf (Qom Formation) developed over the central and northern Iran more than 1 km in thickness (Stöcklin and Setudehnia, 1977; Reuter et al., 2009). Acceleration of shortening rates, the development of higher topography and rapid exhumation in Southern Alborz must have been started from ~20 Ma (Fig. 7) (Allen et al., 2003; Ballato et al., 2008, 2010, 2011; Rezaeian et al., 2012, Ballato et al., 2013) which has been interpreted as a hard stage of collision by Ballato et al., (2011). Stratigraphic data confirm extension and subsidence during deposition of the Qom Formation (e.g., Hassanzadeh and Fakhari, 1997). In the Middle Miocene shallow marine deposits of the Qom Formation have been covered by basal conglomerates of the Middle-Late Miocene Upper Red Formation extended in the southern Alborz (Reuter et al., 2009; Ballato et al., 2011). The deposition of the Upper Red Formation occurred between 17.5-7.5 Ma. (Ballato et al., 2008). Thermo chronological data illustrate a significant tectonic event which is characterized by acceleration of exhumation and sedimentation rates in the Alborz Mountains (Ballato et al., 2011; Rezaeian et al., 2012).

Finally, in the latest Miocene (Fig. 7) the regional stratigraphy shows an erosional unconformity (or facies change from fine to coarse clastics) (Rezaeian et al., 2012) and tectonic tilting (Ballato et al., 2008) above the Upper Red Formation along the Southern flank of Alborz Mountains. The Upper Rea Formation has been overlain by thick conglomerates and sandstones of the

Hezardarreh and Kahrizak formations which were formed into an alluvial fan system in Southern Alborz. (Rieben, 1955). Rezaeian et al., (2012) suggest an exhumation from 6 to 4 Ma, which could be as a result of a regional re-organization of the Arabia-Eurasia collision (Allen et al., 2004) or to climate change, or both in conjunction.

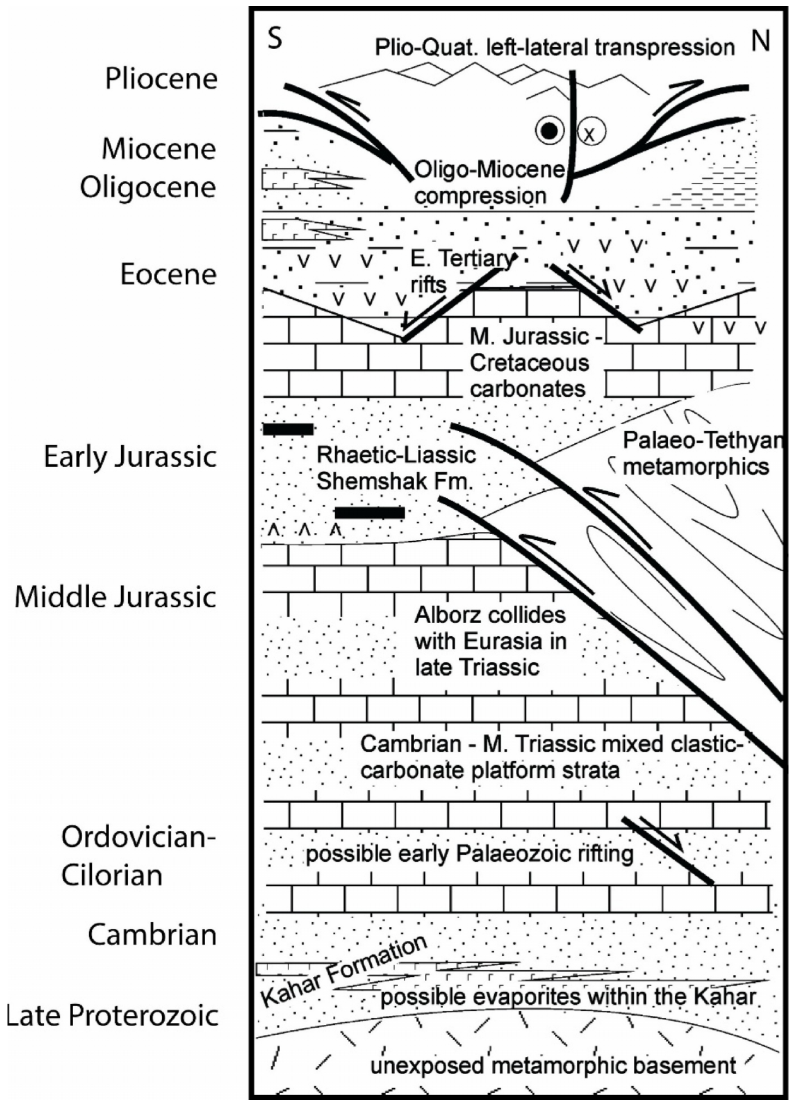

Fig. 7. Simplified tectonostratigraphy of the Alborz modified from Allen et al. (2003).

2.2. Central – East Iranian Microcontinent (CEIM)

Central Iran is a complex mosaic of several microcontinental blocks (Berberian 2014) with moderate relief surrounded by fold-and-thrust belts, within the Alpine-Himalayan orogenic system (Ramezani and Tucker, 2003) bounded by Alborz and Kopeh Dagh mountains to the North, the east Iranian ranges to the East and Zagros Chain and Makran to the West and South enclose the Central Iranian Plateau (Fig. 1). The microplate of Central Iran contains of three major tectonic blocks (Fig. 8) of the Lut Block, Tabas Block and the Yazd Block from East to West respectively (Davoudzadeh et al., 1981; Berberian and King 1981; Alavi, 1991) that are separated by mostly N-S right lateral strike slip major faults (e.g., the Nayband right lateral strike slip fault), and are separated from the Alborz belt by NE-SW left-lateral strike-slip and thrust faults (e.g., The Doruneh left lateral strike slip Fault),which have their individual stratigraphy, deformation style, and pattern of recent seismicity (Berberian and King, 1981; Berberian, 2014).

The Central and East Iranian Microcontinent (CEIM) (Takin, 1972), as an element of the Cimmerian microplate assemblage, has a complex history of geodynamic events. During the Cimmerian orogeny, the Iranian microplates detached from Northern Gondwana (Sengör, 1979; Berberian and King, 1981; Stampfli et al., 1991; Stampfli and Borel, 2002; Brunet et al., 2003; Angiolini et al., 2007; Zanchi et al., 2009a, 2015) in the Early Permian, during the opening of the Neotethys Ocean (Fig. 4), and collided with the Turan block (Eurasian) at the Early-Late Triassic or Early Jurassic (Fig.5. a) after the final consumption of the Palaeotethys ocean along a northward subduction zone (Stöcklin, 1974; Alavi, 1991; Ruttner, 1993; Alavi et al., 1997; besse et al., 1998; Allen et al., 2003; Muttoni et al., 2009; Mirnejad et al., 2013a). Paleomagnetic studies by Soffel et al., (1975); Wensink (1979, 1981, 1982); Wensink and Varekamp, (1980); Soffel and Förster, (1980); Soffel et al, (1995, 1996), Besse et al, (1998), Muttoni et al, (2009a), Mattei et al, (2014, 2015) is confirmed this scenario. The final collision happened during the late Triassic and is marked by deep erosion of the Eo-Cimmerian orogen and deposition of the Nayband and Shemshak molassic formations south of the orogenic belt (Bagheri and Stampfli, 2008; Fürsich et al., 2009; Zanchi et al., 2009). Since that time, the evolution of Central Iran was controlled by a sequence of back arc extentional and compressional events that were related to the north-dipping Neo-Tethyan subduction zone (Berberian and King, 1981; Dercourt et al., 1986; Bagheri and Stampfli, 2008; Rossetti et al., 2010).

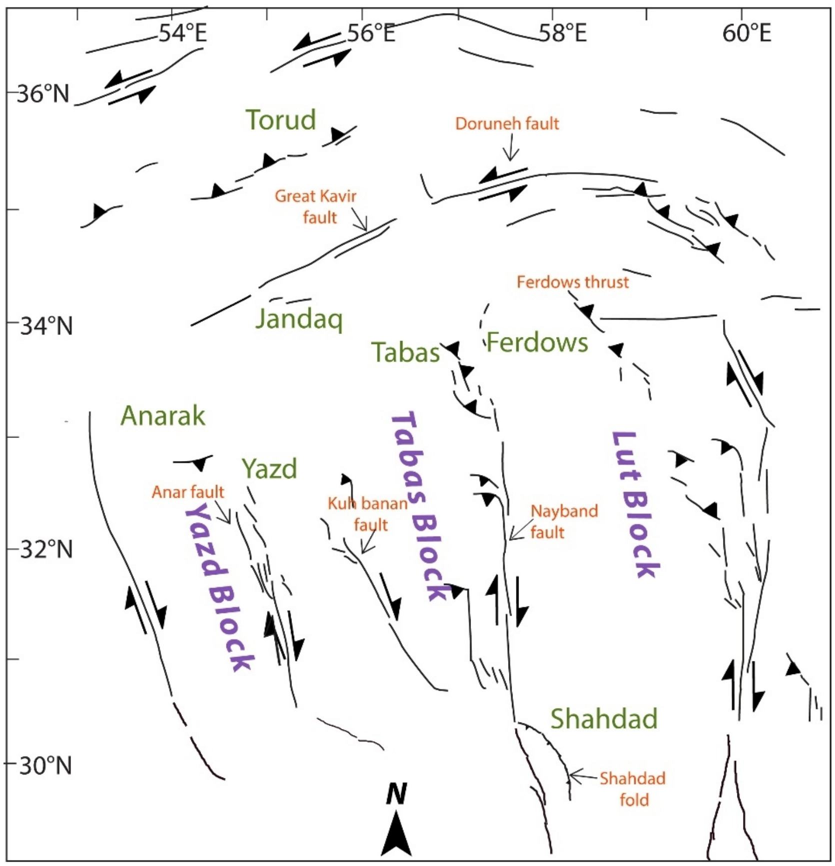

Fig. 8. Schematic fault map of central. The major tectonic domains and the study areas are shown.

These events caused the emplacement of the ophiolite melange belts around the Central East Iranian Microcontinent (Bagheri et al., 2008; Rossetti et al., 2010; shafaei moghaddam, 2014) (Fig.6.b). These ophiolites are the remnants of the branches of Neotethys oceanic basins (Sistan Ocean in the east, Sabzevar Ocean in the north, Nain–Baft Ocean in the west (Lindenberg et al., 1983; Tirrul et al., 1983; Dercourt et al., 1986; Stamfly and Borel, 2002; Philip and Floquet, 2000; Barrier and Vrielynck, 2008) that opened during the Early Cretaceous (Neocomian; e.g., Seyed-Emami et al.,1972) and closed during the late part of the Cretaceous (Dercourt et al., 1986; McCall, 1997, Bagheri and Stampfli, 2008, Shafaii Moghadam et al., 2009; 2014; 2015) and and document a polyphase tectonic evolution its Mesozoic–Cenozoic consumption along the Sanandaj–Sirjan Zone (Stöcklin, 1974; Sengör et al., 1988; Rossetti et al., 2010).

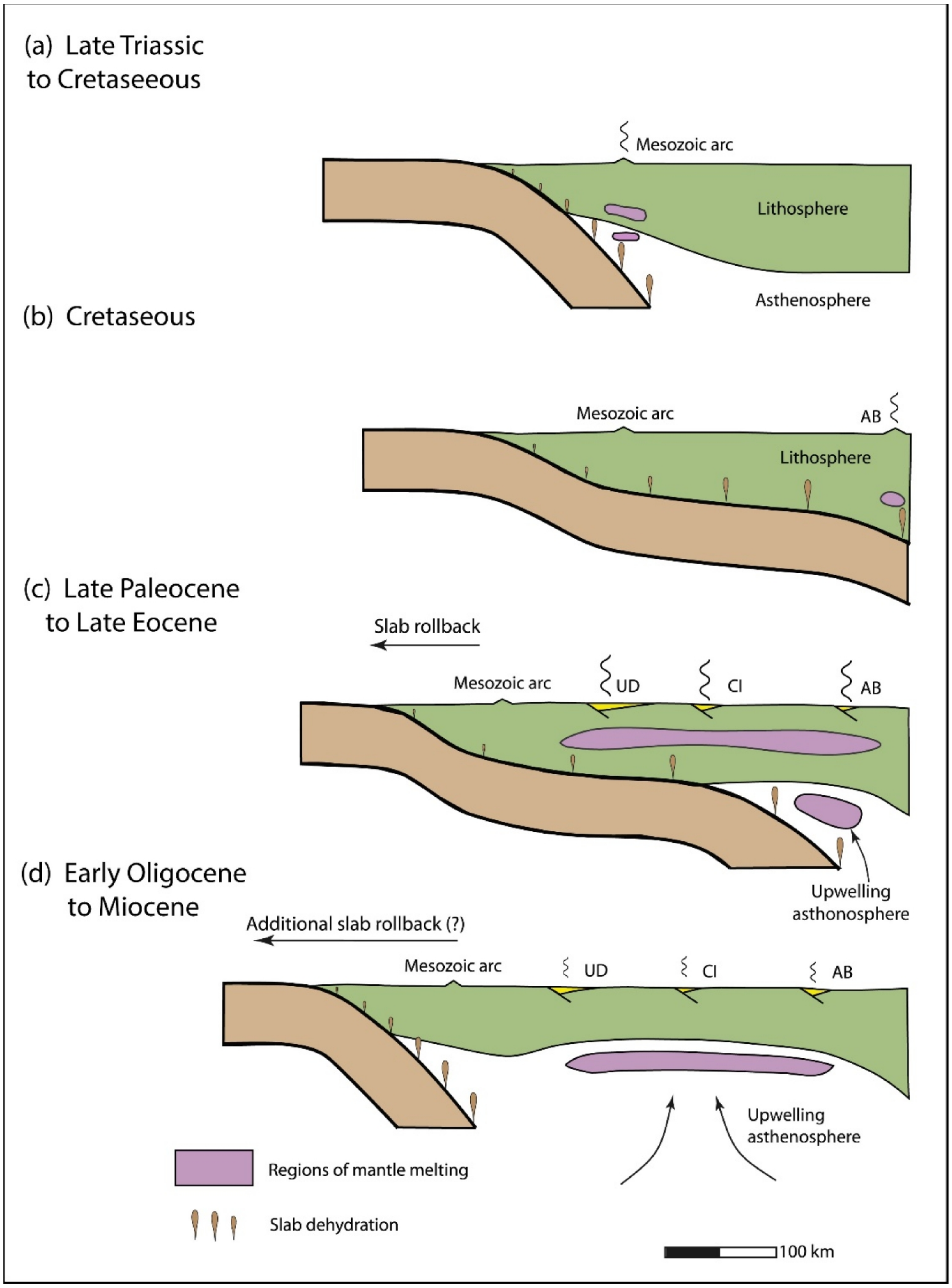

Figure 9. Summary of the development of the Iranian Eocene flare-up and subsequent asthenosphere-derived Oligocene magmatism in stages (a)-(d), modified from Verdel et al., (2011). Abbreviations: UD, Urumieh-Dokhtar magmatic belt; AB, Alborz Mountains; CI, central Iranian Eocene volcanics between Urumieh-Dokhtar and the Alborz Mountains.

Tertiary volcanic rocks are distributed over a large area in Iran, the Urumieh-Dokhtar belt (e.g., Omrani et al., 2008; Verdel et al., 2011), the Alborz Mountains (e.g., Brunet et al., 2003), northern parts of Lut Block (e.g., Jung et al., 1984) and many relatively small locations in central Iran (e.g., Amidi et al., 1984). The Paleogene in Central Iran has begun with a basal conglomerate and sandstone which rests unconformably on older rocks, followed by an extensive volcanogenic unit consisting mainly of submarine and continental lava flows (from rhyolite to basalt) and dacitic tuffs (Berberian and King, 1981). The extensive and severe Eocene volcanic activity of Central Iran was explained as a result of the subduction of Neotethyan oceanic crust beneath Iran along the Main Zagros reverse fault (e.g., Jung et al., 1976; Verdel et al., 2011).

Several Eocene age metamorphic core complexes in central and eastern Iran (Moritz et al., 2006a; Kargaran et al., 2006; Verdel et al., 2007), Syndepositional Eocene normal faults in the Alborz and Central Iran (Guest et al., 2006a; Kargaran et al., 2011) and stratigraphic evidences of Eocene subsidence in Alborz and Central Iran(Brunet et al., 2003; Hassanzadeh et al., 2004; Morley et al., 2009), indicate that this magmatic stage occurred in a back arc extensional basin related to the rollback of the Neotethys slab(Fig. 9c) (e.g., Brunet et al., 2003; Vincent et al.,2005;Verdel, 2008; Verdel et al., 2011). A regional phase of shortening happened during the late Eocene–early Oligocene (Stöcklin, 1968; Berberian and King, 1981) represented by a regional unconformity at the base of the terrestrial clastic and evaporitic deposits of the Oligocene Lower Red Formation (e.g., Jackson et al., 1990; Amini, 1997). During this phase, the Lut Block experienced uplift (major Lut uplift) and no Oligocene-Miocene sediments were obviously deposited (e.g., Berberian, 1974; Berberian and King, 1981). The Lower Red Formation is overlain conformably by marine limestones and marls of Rupelian–Burdigalian age of the Qom Formation (Daneshian and Ramezani Dana, 2007). Bottrill et al. (2012) proposed that the Late Oligocene-Early Miocene marine carbonates were deposited as a result of roll-back of the southern Neo-Tethys slab shortly before breakoff. Although it is not clear when extension-related subsidence terminated (e.g., Guest et al., 2007), but the transition from marine to terrestrial clastics of Upper Red Formation during the Burdigalian (Amini, 1991, 1997) recommends a major shift in subsidence scheme at this time (Guest et al.,2007). The Qom Formation is conformably replaced by gypsum-bearing red beds of the Miocene Upper Red Formation which has been dated between 17.5 and 7.5 Ma (Ballato et al., 2008). The Upper Red Formation is overlain by the Pliocene conglomerate, has been dated ~6.2 Ma by Ballato et al. (2008), which has been correlated with the Hezardarreh and

Bakhtiyari Formations of the Alborz basin and the Zagros mountains respectively (e.g., Rieben, 1955).

3. Overviews of previous Paleomagnetic studies in Iran

The paleomagnetic investigations of Iran have been done to clarify three main issues:

- Affinity of Iran to Gondwana during the Paleozoic.

- The reconstruction of the late Paleozoic–early Mesozoic northward drift of the Cimmerian blocks

- Large counterclockwise Rotation of Central East Iranian Microplate (CEIM) respect to the Eurasia from Triassic.

The first paleomagnetic studies in Iran, have been done to reconstruct the pre-Cimmerian tectonic evolution of Iran. Becker et al. (1973) reported paleomagnetic results of late Precambrian to Lower Cambrian rocks and iron ores of Bafq area and suggested that, like India, Central Iran was previously part of Gondwanaland. Soffel et al. (1975) published the paleomaganetic data of Infracambrian, Ordovician and Permian rocks of Central Iran which support the similarity of polar wander paths of India and Central Iran. Paleomagnetic results of Basaltic rocks of Late Devonian Early Carboniferous Geirud Formation of the Alborz Mountain confirm that during the Paleozoic, the Alborz range was part of former Gondwanaland (Wensink et al., 1978). Wensink, (1983) used the Paleomagnetic results of Lower Devonian Red beds of Central Iran to show a Gonadwana position for the Iranian- Afghan microcontinent in Paleozoic time. Besse et al. (1998) compiled a selection of paleopoles of the Carboniferous to present and revealed the Central Iran and Alborz were part of Gondwana during the Palaeozoic and rifted away by the end of the Permian. Investigation of the palaeomagnetic poles of Late Ordovician-earliest Carboniferous red bioclastic sediments of Shirgesht Formation in Anarak area by Muttoni et al., (2009), supported the affinity of Iran with Arabia (Gondwana) during this period of time.

Wensink (1979) studied the paleomagnetic properties of the upper Permian Ruteh Lavas in the Alborz Range and believed that in Paleozoic and Mesozoic times these areas were placed the coast of Arabia. This study was confirmed by Beese et al., (1998) in the same area and suggested a southern hemisphere of deposition during a reversed-polarity period.

The paleomagnetic results from Central Iran reported by Soffel and Forster, (1980) indicated that the reference point of Central Iran was in an intermediate latitude position between Eurasia and the Gondwanaland since the Late Paleozoic. After a slight tendency towards the south during the Permian, Central Iran moved again northward between the Permian and the Triassic. Besse et al. (1998) reported the paleomagnetic results of the Permo-Triassic boundary in the Upper Permian Hambast Formation close to city of Shahreza and from the Early Triassic Elika Formation close to city of Abadeh which sampled units were located at subequatorial paleolatitudes north of Arabian margin of West Gondwana as well reported by Gallet et al. (2000) in Hambast- Elika Formations of Abadeh section. Paleomagnetic data of Aruh laterite suggest equatorial paleolatitudes of c. 1°S to 1°N ± 5° for the Alborz area of northern Iran in the Late Permian (Muttoni et al., 2009). Wensink, (1982) discussed that the Early Jurassic Sorkh Shale Formation of Tabas region placed at 11°S, close to the coast of Arabia. Soffel et al. (1995, 1996) investigated the Triassic basalts in the Sirjan area and the Early Triassic Abyaneh Formation of Natanz area. They concluded that the Triassic pole is situated in the vicinity of other Late Palaeozoic-Early Mesozoic poles of the CEIM and is far away from the Triassic pole position for the Turan Plate. They argued that the Triassic pole position from the Natanz area (outside the CEIM) is in good agreement with the mean Triassic pole of the Turan plate indicating that the area to the west of the CEIM was close to the Turan Plate during the Triassic. Besse et al. (1998) suggested that the poles from the Early Triassic Sorkh Shales (Wensink, 1982) and Natanz (Soffel et al., 1995, 1996), both from central Iran, are situated at the same angular distance from their sampling sites as the Sirjan poles (Soffel et al., 1995, 1996), which are from the southernmost continental sliver of Iran. Muttoni et al. (2009) reported paleomagnetic results in the same area with Wensink, (1982) in the Early Triassic (Brönnimann et al., 1973) Sorkh Shale Formation in the Shotori Range near the town of Tabas. Interpretation of the inclination data from sampled sites indicate a palaeolatitude of approximately 9°±2.5°which is similar to Wensink, (1982) palaeolatitude (c.11°±8°) for Sorkh Shale sites from the same general area of this study. Despite of Wensink, (1982), Muttoni et al. (2009) chose a northern hemisphere palaeolatitude, as suggested by Besse et al., (1998). Soffel et al. (1996) sampled broadly in Nakhlak, Natanz, Saghand and Sirjan areas of the Early, Middle and Late Triassic ages and suggested that the Iranian Plate (without the CEIM, which is considered

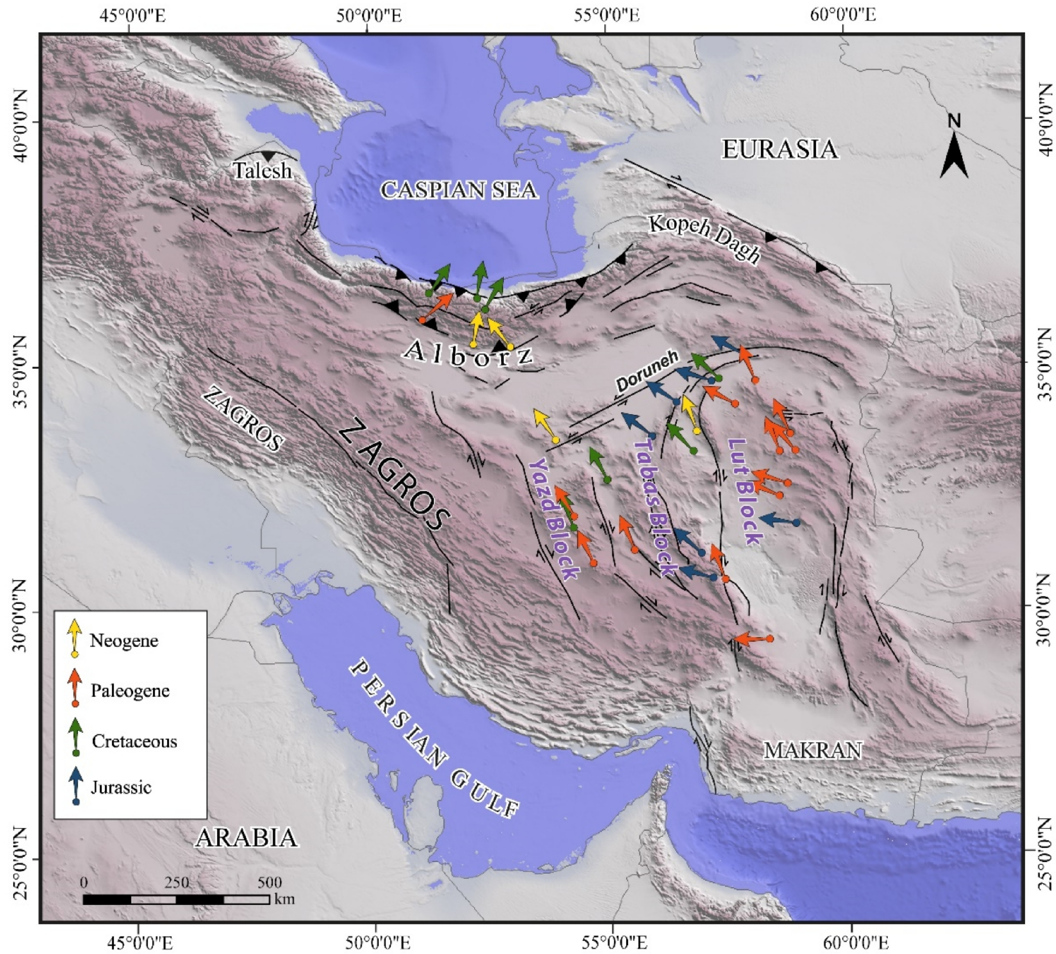

Fig. 11. Most reliable Paleomagnetic rotations from the Central Iran-East Iranian Microcontinent (CEIM) and the Alborz Mauntain. For more details see chapter 2.

as a separate unit) was located close to the southern margin of the Turan Plate, whereas the CEIM was in a more southeast position.

Late Triassic reddish limestones have been sampled by Besse et al., (1998) in the Abadeh area, close to the town of Waliabad which confirm a period of rapid northward motion of Iran. Muttoni et al. (2009) sampled the sedimentary sequence of the late Early–late Middle Triassic Alam Formation in the Nakhlak area and the sedimentary sequence of the lower part of the Ashin Formation of late Middle Triassic of Central Iran. The paleomagnetic results suggest considerable European affinity of the sampled units and local vertical-axis tectonic rotations of the eastern part of the Nakhlak structure. The calculated palaeolatitude for tow combined sites of Alam Formation is approximately 21°N ± 4° which shows the sampled locality is close to the European margin in late Early Triassic times.

The lower to middle Jurassic have been much less studied than the other sequences. Besse et al., (1998) worked on Shemshak Formation of Alborz Range but they could isolate only a low-temperature component of single polarity. A comprehensive history of the paleomagnetic investigations of Late Mesozoic-Cenozoic is given in chapter 2.

4. Remaining problems and aims

As previously mentioned, the paleomagnetic researches in Iran have mainly been focused on the reconstruction of the late Paleozoic early Mesozoic northward drift of the Cimmerian blocks (Besse et al., 1998; Muttoni et al., 2009a, 2009b) and the hypothesis of Soffel et al., (1996) that implies a 135° counterclockwise block rotation which has occurred between the internal part of central Iran and Europe since the Middle Triassic, an hypothesis that is based on sparse data from the Triassic sequence of Nakhlak (Muttoni et al., 2009a). In contrast, several open issues regarding the tectonic and stratigraphic evolution of Iran have not been targeted by paleomagnetic researches. These include discrepant views on the Mesozoic paleogeography of the CEIM in Central Iran (compare Stampfli and Borel, 2002; Barrier and Vrielynck, 2008; Wilmsen et al., 2009), lack of paleomagnetic data to determine the exact time of drifting away Iran from Gondwana, the latitudinal drift of Iran and its relationships with the Turan plate after the Cimmerian collision (see Mattei et al., 2014 for a discussion), the debated origin of the curved shape of the Alborz and Kopeh Dagh ranges (Hollingsworth et al., 2010; Cifelli et al., 2015), lack of paleomagnetic data from Jurassic to Cenozoic units (Wensink , 1982; Bina et al., 1986; Soffel et al., 1996; Ballato et al., 2008), leaving the post-Cimmerian history of central Iran poorly constrained (Mattei et al., 2012).

The main objectives of this study are:

- To define the amount of paleomagnetic rotations in Central Iran since Oligocene time, and the relationship between these rotations and the major strike-slip faults kinematics.

- To reconstruct the paleogeographic evolution of the CEIM and Alborz range.
- To give constraints on the origin of the curved shape of the Alborz and Kopeh-Dagh orogens.

5. Outline of the thesis

In chapter two, I revise previously published paleomagnetic data from CEIM and Alborz Mts. and present new paleomagnetic data from the Upper Jurassic Bidou Formation (Fig. 12) from Central Iran (CEIM). I anticipate that these paleomagnetic data are suitable to identify two main episodes of counter-clockwise (CCW) vertical axis rotations that occurred in Central Iran in the Late Jurassic–Early Cretaceous and after the Middle–Late Miocene, and to constrain the timing of Neogene oroclinal bending in the Alborz range. This chapter has been published in Journal of Asian Earth Sciences, vol. 102, 15 April 2015, Pages 92–101 by Massimo Mattei, Francesca Cifelli, Giovanni Muttoni and Hamideh Rashid.

In chapter three, I present preliminary results of paleomagnetic study from Upper Red Formation of eastern Alborz (Jajarm), central Alborz (Semnan) and western Alborz (Alamut nd Manjil) and Shahdad thrust-fold belt (Fig. 12) to constrain the tectonic and kinematic evolution of these curvature belts during the Neogene. The primary results, confirm the orocline bending as an effective mechanism to curvature shape of these to tectonic systems.

In chapter four, to characterize the main intracontinental fault of the Arabia–Eurasia collision zone and to define the deformation style across this tectonic boundary, I combined magnetic fabrics (AMS) and structural data from the Upper Jurassic Garedu Red Beds Fmormation at the western boundary of the northern Shotori Range (Fig. 12). The geometrical relationships are typical of a transected fold and suggest that the Late Cretaceous and Tertiary shortening events of Central Iran were accommodated by a dextral transpressional tectonics along the tectonic boundary between Tabas and Lut blocks. Results from this study underline the importance of the re activation of pre-existing tectonic structures and emphasize the role of the right-lateral transpressional deformation along this main tectonic boundary of Central Iran. This chapter has been published in Geophysical Journal International, vol. 193, pages 1153-1165 by Francesca Cifelli, Massimo Mattei, Hamideh Rashid and Jalil Ghalamghash.

In chapter five, I present new AMS and structural results from the Ferdows active fold–thrust system in the Lut block, Central Iran (Fig. 12), that establish a relationships between the recent tectonics of the area and the evolution of the magnetic fabric. I show that a well-developed magnetic fabric of pure tectonic origin can form also in poorly deformed rocks, which lack evidence of pervasive internal deformation. In particular, I show that the different types of magnetic fabric observed at Ferdows fold–thrust system cannot be explained simply using different degrees of LPS, and that late folding internal strain has to be considered. The implication for the tectonic evolution of the Ferdows fold and thrust system are also discussed. This chapter has been published in Journal of Asian Earth Sciences, vol. 108, 15 August 2015, Pages 48–57 by Hamideh Rashid, Francesca Cifelli and Massimo Mattei.

Chapter six, I present a synthesis of the work, summarizes conclusions reached in each chapter and develop a comprehensive evolutionary paleogeographic map of Iran since Upper Jurassic.

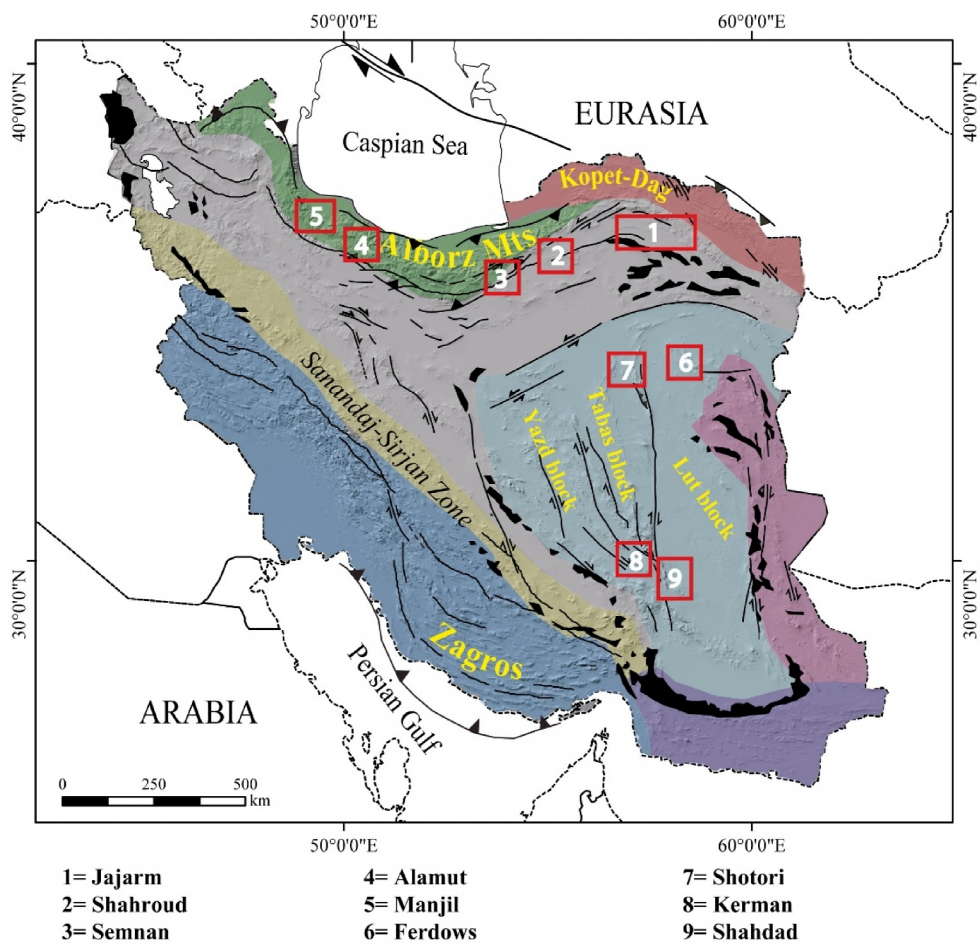

Fig. 12. Tectonic map of Iran showing the main tectonic provinces and the main active faults. The red squares with white numbers inside represents the location of the paleomagnetic sites of this study.

Chapter II

Post-Cimmerian (Jurassic–Cenozoic) paleogeography and vertical axis tectonic rotations of Central Iran and the Alborz Mountains

Massimo Mattei, Francesca Cifelli, Giovanni Muttoni and Hamideh Rashid

This chapter has been published in 2015:

Journal of Asian Earth Sciences, vol. 102, Pages 92–101
http://dx.doi.org/10.1016/j.jseaes.2014.09.038

Keywords: Jurassic, Central Iran, Alborz, Paleomagnetism

Abstract:

According to previous paleomagnetic analyses, the northward latitudinal drift of Iran related to the closure of the Paleo-Tethys Ocean resulted in the Late Triassic collision of Iran with the Eurasian plate and Cimmerian orogeny. The post-Cimmerian paleogeographic and tectonic evolution of Iran is instead less well known. Here we present new paleomagnetic data from the Upper Jurassic Bidou Formation of Central Iran, which we used in conjunction with published paleomagnetic data to reconstruct the history of paleomagnetic rotations and latitudinal drift of Iran during the Mesozoic and Cenozoic. Paleomagnetic inclination values indicate that, during the Late Jurassic, the Central-East-Iranian Microcontinent (CEIM), consisting of the Yazd, Tabas, and Lut continental blocks, was located at low latitudes close to the Eurasian margin, in agreement with the position expected from apparent polar wander paths (APWP) incorporating the so-called Jurassic massive polar shift, a major event of plate motion occurring in the Late Jurassic from 160 Ma to 145–140 Ma. At these times, the CEIM was oriented WSW–ENE, with the Lut Block bordered to the south by the Neo-Tethys Ocean and to the southeast by the Neo-Sistan oceanic seaway. Subsequently, the CEIM underwent significant counter-clockwise (CCW) rotation during the Early Cretaceous. This rotation may have resulted from the northward propagation of the Sistan rifting-spreading axis during Late Jurassic–Early Cretaceous, or to the subsequent (late Early Cretaceous?) eastward subduction and closure of the Sistan oceanic seaway underneath the continental margin of the Afghan Block. No rotations of, or within, the

CEIM occurred during the Late Cretaceous–Oligocene, whereas a second phase of CCW rotation occurred after the Middle-Late Miocene. Both the Late Jurassic–Early Cretaceous and post Miocene CCW rotations are confined to the CEIM and do not seem to extend to other tectonic regions of Iran. Finally, an oroclinal bending mechanism is proposed for the origin of the curved Alborz Mountains, which acquired most of its curvature in the last 8 Myr.

1. Introduction

The present-day structural configuration of Iran (Fig. 1) is the result of a complex history of geodynamic events. These include the collision of the Central-East-Iranian Microcontinent (CEIM sensu Takin, 1972), comprised of the Yazd, Tabas, and Lut blocks, with the southern margin of Eurasia during the Late Triassic Cimmerian orogeny (Sengör, 1984; Zanchi et al., 2006, 2009a,b; Muttoni et al., 2009a), the Late Jurassic–Cretaceous opening of small oceanic basins around the CEIM, and the closure of these basins during Late Cretaceous, in connection with the northward motion of the Arabian Plate and closure of the Neo-Tethys Ocean (Stöcklin, 1974; Dercourt et al., 1986; Sengör et al., 1988; McCall, 1997; Stampfli and Borel, 2002; Bagheri and Stampfli, 2008; Rossetti et al., 2010). Since the Cenozoic, shortening related to the Arabia–Eurasia convergence has been taken up mainly by tectonic displacements in the Zagros, Alborz, and Kopeh Dagh thrust-andfold belts, whereas the intervening, fault-bounded crustal blocks of the CEIM seem to show little internal deformation (Fig. 1).

The Alborz and Kopeh Dagh Mountains in north Iran constitute a system of strongly curved, mostly double-verging orogens (Fig. 1). In particular, the Alborz range is a ca. 100-km-wide, sinuous orogenic belt that stretches E–W for ca. 600 km (e.g., Allen et al., 2003; Guest et al., 2006), and comprises Late Triassic Cimmerian structures (Zanchi et al., 2006) reactivated during the Late Cenozoic Arabia–Eurasia convergence and associated relative motion between the stable and rigid South Caspian Basin in the north and the CEIM in the south (e.g., Jackson et al., 2002; Allen et al., 2003).

The most peculiar feature of the CEIM (to the south of the Alborz–Kopeh Dagh range) is the occurrence of an Upper Mesozoic ophiolitic 'ring', the so-called 'Coloured Mélange', which bounds its most internal part (Fig. 1). This ophiolitic ring is a remnant of Mesozoic peri-Tethyan oceanic basins that formed in the upper plate of the Neo-Tethyan subduction, and document a polyphase tectonic evolution during its Mesozoic–Cenozoic consumption along the Sanandaj–Sirjan Zone (Stöcklin, 1974; Sengör et al., 1988). The CEIM is affected by a complex system of N–S-trending dextral faults, which separate the Yazd, Tabas and Lut blocks causing intensive N–S dextral shearing in the whole area (Walker and Jackson, 2004)(Fig. 1). The left-lateral Great Kavir–Doruneh fault system, crossing the northern part of the CEIM, currently bounds this deformational system to the north.

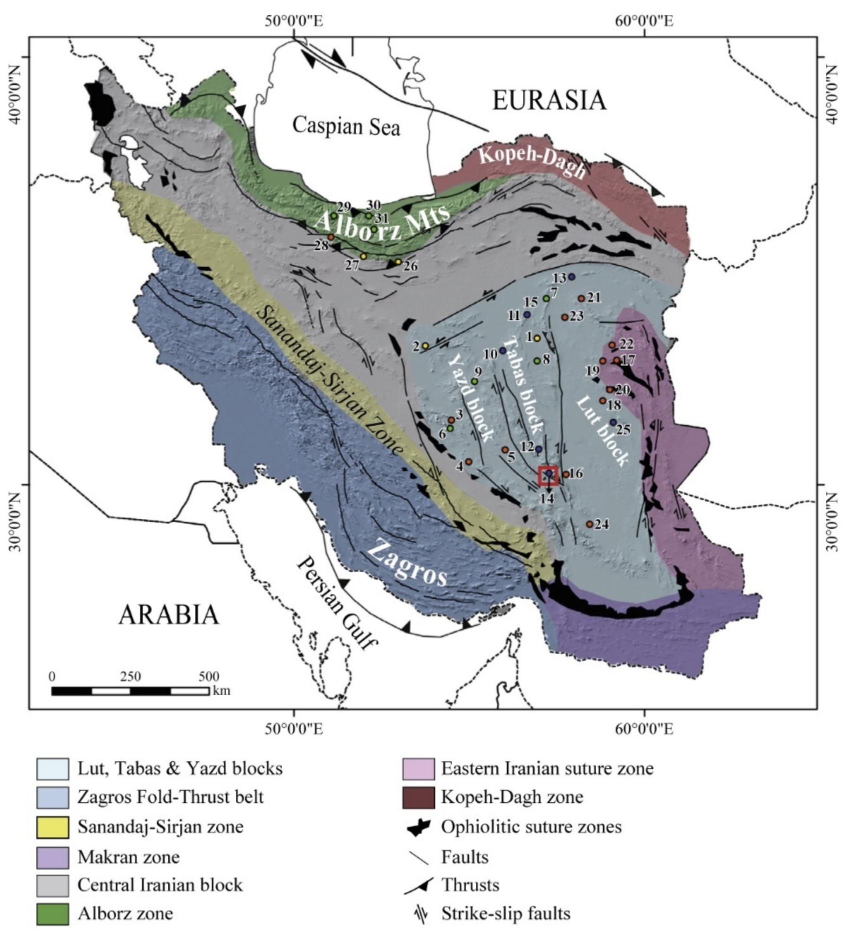

Fig. 1. Tectonic map of Iran showing the main tectonic provinces and the main active faults. Numbers represent sampling localities from the literature discussed in the text (see also Table 1). The red square represents the location of the paleomagnetic sites of this study from the siliciclastic member of the Bidou Formation from the Kerman area.

Despite this complex tectonic history, paleomagnetic data from Iran are very sparse and have been mainly used to unravel its preCimmerian tectonic evolution (Muttoni et al., 2009a, b; see also Besse et al., 1998). These data show that the Iranian block(s) was (were) located close to the Arabian margin of Gondwana in the Paleozoic, drifted off this margin attaining subequatorial palaeolatitudes in the Late Permian-early Early Triassic, and approached the Eurasian margin by the late Early Triassic. In contrast, several open issues regarding the tectonic and stratigraphic evolution of Iran have not been targeted by paleomagnetic research. These include discrepant views on the Mesozoic paleogeography of the CEIM in Central Iran (compare Stampfli and Borel, 2002; Barrier and Vrielynck, 2008; Wilmsen et al., 2009), the debated origin of the curved shape of the Alborz and Kopeh Dagh ranges (Hollingsworth et al., 2010; Alimohammadian et al., 2013), and the latitudinal drift of Iran and its relationships with the Turan plate after the Cimmerian collision (see Mattei et al., 2014 for a discussion).

In this paper, we revise previously published paleomagnetic data from CEIM (Conrad et al., 1981; Wensink, 1982; Bina et al., 1986; Soffel et al., 1989, 1996; Mattei et al., 2014) and Alborz Mts. (Wensink and Varenkamp, 1980; Cifelli et al., submitted to Tectonics) and present new paleomagnetic data from the Upper Jurassic Bidou Formation from Central Iran (CEIM). We anticipate that these paleomagnetic data are suitable to identify two main episodes of counter-clockwise (CCW) vertical axis rotations that occurred in Central Iran in the Late Jurassic–Early Cretaceous and after the Middle–Late Miocene, and to constrain the timing of Neogene oroclinal bending in the Alborz range. A brief summary of previous results (Muttoni et al., 2009a, b; Mattei et al., 2014) is also provided on the post Cimmerian latitudinal drift of Iran and the long-term evolution of climate-sensitive sedimentary facies deposition during the Late Paleozoic–Mesozoic.

2. Previous paleomagnetic results

2.1. Jurassic paleomagnetic data

2.1.1. CEIM

Table 1 – Paleomagnetic directions from CEIM and Alborz Mts.

REGION Age Locality (with number)	n	Lat(°)	Long(°)	Age P (Ma)	D(°)	I(°)	K	α_{95}	S_0	Rot(°)	Err(±)	Ref
YAZD-TABAS												
Neogene												
Tabas (1)	14	33°33'N	57°00'E	10	346.1	46.1	33.3	7	var	-19.8	8.4	1
Anarak (2)	4	33°22'N	53°47'E	25	333.2	29.9	24.1	19.1	var	-35	15.6	1
Eocene												
Mehriz (3)	10	31°33'N	54°32'E	50*	147.4	-37	45.9	7.2	var	-32.5	8.0	2
Jowazm (4)	6	30°31'N	55°02'E	50*	343.7	42	26.5	13.2	var	-26.1	14.0	2
Khan-e-Sork (5)	6	30°49'N	56°05'E	50*	346.6	41	36.9	11.2	var	-23.3	12.0	2
Cretaceous												
Shirku Pass (6)	8	31°21'N	54°30'E	100*	350.1	41.1	21.4	12.2	var	-17.8	13.0	2
Garedu (B) (7)	9	34°30'N	57°16'E	100*	321.2	39.7	19.7	11.9	var	-47.1	12.7	5
Dehuk (8)	4	33°00'N	57°00'E	100	326.1	38.5	19	21.4	var	-42.1	22.0	3
Saghand (9)	33^	32°30'N	55°12'E	120	338.5	25.2	-	5.2	sub-hor	-30	5.0	4
Jurassic												
Robat Khan (10)	8^	33°15’E	56°01’N	145*	135.3	-22	11.2	-	232/13	-53.4	11.0	2
Shirgesht (11)	12^	34°07’E	56°43’N	145*	313	25.7	6.9	9.3	200/40	-55.7	11.2	2
Bidou (12)	5	30°50'N	57°03'E	145	326.4	16.4	10.1	25.3	var	-48.2	21.9	2
Bardaskan (13)	4	35°01'N	58°00'E	145	300.7	13.8	55.6	12.4	205/25	-59.6	13.0	2
Kerman (14)	**6**	**30°14'N**	**57°21E**	**150**	**105.7**	**-19.6**	**12.0**	**20.1**	**var**	**-73.1**	**18.0**	**§**
Garedu (15)	8	34°30'N	57°16'E	145	296.8	24.5	18.8	13.1	var	-72.1	13.0	5
LUT												
Paleogene												
Shahdad (16)	5^	30°12'N	57°42'E	30*	347.8	19.3	60	-	250/23	-19.8	9	2
Hadgiabad (17)	7	33°01'N	59°18'E	50	151.1	-30	77	6	105/32	-39.2	6.0	6
Hamand (18)	11^	32°02'N	58°54'E	50*	306.8	42	144.5	-	115/23	-66.1	12	2
Khusf-Gal-e-Sari (19)	8^	33°00'N	58°54'E	50*	168.1	-22.2	94	-	190/22	-22.1	9	2
Basiran (20)	10^	32°18'N	59°06'E	50*	118.5	-35.6	505.3	-	223/25	-71.6	10	2
Bajest.-Gonabad (21)	24^	34°30'N	58°17'E	60	166	-54.4	78	7.1	53/43	-22.1	10	6
She Deh (22)	9	33°23'N	59°10'E	60	343.3	59.6	59	6	235/19	-24.8	10.0	6
Robat-e-Chah-e-Gonbad (23)	12^	34°03'N	57°48'E	60*	126.1	-48.4	201.4	-	215/12	-61.2	11	2
Bam (24)	17^	28°57'N	58°31'E	80	90	-43	11	18	var	-91	20	7
Jurassic												
Rakhneh (25)	7^	31°30'N	59°12'E	150*	107.2	-8.7	6.5	-	348/74	-82.4	14.0	2
ALBORZ												
Neogene												
Abdolabad (26)	26^	35°20'N	53°00'E	10	328.9	32.4	19.5	6.7	var	-36.7	7.0	10
Eyvanekey (27)	216^	35°30'N	52°00'E	10	16.9	44.1	-	3.3	var	11	5.0	8
Oligocene												
Karaj (28)	2	35°57'N	51°04'E	30	57	58	-	10	var	50	15	6
Cretaceous												
Chalus (29)	5	36°27'N	51°09'E	90	42.8	44.1	22	16.6	var	35.1	18.0	9
Chalus (30)	9	36°27'N	52°09'E	110	22.2	48.7	36	8.6	var	12.4	11.0	9
Haraz River (31)	6	36°09'N	52°18'E	130	41.3	46.8	15	18.1	var	31.4	0.9	9

n = number of sites (or specimens when ^ is added). D, I = site mean declinations and inclinations calculated after tectonic correction. K and α_{95} = statistical parameters after *Fisher* [1953]. S_0 = bedding attitude. Err (±): error for rotations values. Age P = Age of Paleopole (when the age is not certain * is added). Ref. numbers are: § = unpublished data; 1 = Mattei et al., 2012; 2 = Soffel et al. (1989); 3 = Wensink (1982); 4 = Soffel et al. (1996); 5 = Mattei et al. (2014); 6 = Bina et al. (1986); 7 = Conrad et al. (1981); 8 = Ballato et al. (2008); 9 = Wensink & Varekamp (1980); 10 = Cifelli et al., (in press). Reference Eurasia paleopoles are from Besse and Courtillot (2002) for 80-10 Ma and from Irving and Kent (2010) rotated to European coordinates by Mattei et al. (2014) for 200-90 Ma. N = reference number in figure 5.
The ages of paleomagnetic sites have been defined using stratigraphic constraints; reliable ages are available for the Jurassic Garedu (Kimmeridgian–Tithonian) and Bidou (Kimmeridgian–Berriasian) formations, the Cretaceous Dehuk Formation (Albian–Cenomanian) and Alborz volcanics (age) (Wensink and Varenkamp, 1980), and the Miocene Upper Red Formation (Ballato et al., 2008; Mattei et al., 2012; Cifelli et al., submitted). Radiometric ages have been reported for the Paleogene volcanic rocks (Conrad et al., 1981; Bina et al. 1986). For all the other sites, the stratigraphic ages has been calculated on the base of the stratigraphic age suggested in the original papers (Soffel et al., 1989; 1996).

Mattei et al. (2014) report paleomagnetic results from Kimmeridgian–Tithonian red beds of the Garedu Red Bed Formation cropping out in the Garedu syncline of the western Shotori Mountains (#15 in Fig. 1 and Table 1) (see also Cifelli et al., 2013). A welldefined ChRM component direction, stable at temperatures from 580–620 °C to ~670 °C, was isolated, and based on the presence of normal and reversed magnetic polarities and a positive fold test, it was considered primary in origin and acquired during (or shortly after) the deposition of the Garedu Red Bed Formation (Mattei et al., 2014). Soffel et al. (1989) isolated, at sites located near Bardeskan, ChRM directions of dual polarity that are similar to the pre-folding, low inclination ChRM directions of Mattei et al. (2014) (#13 in Fig. 1 and Table 1). In contrast, the ChRM directions of high inclination obtained by Wensink (1982), interpreted as prefolding in age (albeit with inconclusive fold test; Wensink, 1982), most probably represent a record of the post-folding, high inclination B component directions as isolated by Mattei et al. (2014). Soffel et al. (1989) reported paleomagnetic directions from 5 sites sampled from Jurassic sandstones and red sandstones from the Bidou area north of Kerman. Results show ChRM component directions of normal and reverse polarities that, after correction for bedding tilt, cluster either to the northwest or southeast with shallow inclination (#12 in Fig. 1 and Table 1), and are similar to the ChRM directions of the Garedu Red Bed Formation (Mattei et al., 2014). In the Tabas Block, Soffel et al. (1989) report results from two sites of Jurassic age that have ChRM directions oriented to the northwest and down or southeast and up (#10,11 in Fig. 1 and Table 1). In the Lut Block, one site of Jurassic age reported by Soffel et al. (1989) shows ChRM directions oriented southwest and up (#25 in Fig. 1 and Table 1).

2.2 Cretaceous paleomagnetic data

2.2.1 CEIM

Paleomagnetic directions from Cretaceous units of the CEIM are very few and limited to the Tabas and Yazd blocks. Wensink (1982) sampled 6 sites from middle Cretaceous red sandstones and red limestone from the Dehuk village, to the east of the Shotori Range in the Tabas block (#8 in Fig. 1; Table 1). The mean ChRM direction for the analysed sites is oriented northwest and up, and is better grouped after than before tectonic correction, suggesting that the ChRM has a pre-folding origin. Soffel et al. (1989) reported results from Cretaceous volcanic and sedimentary rocks from the Shirkuh Pass area with a mean ChRM direction, calculated from 8 sites, oriented northwest and down (#6 in Fig. 1; Table 1). Soffel et al. (1996, also reported in Besse et al., 1998) sampled Cretaceous limestone from the Saghand area in the eastern Yazd block. The ChRM mean direction, calculated from 33 specimens, is oriented northwest and down (#9 in Fig. 1; Table 1). Mattei et al. (2014) observed an intermediate B component direction oriented northwest and down in in situ coordinates in the Late Jurassic Garedu Red Bed Formation of the Shotori Mountains area (#7 in Fig. 1; Table 1). Site mean B component directions are clustered in in situ coordinates, while after correction for bedding tilt, they become sensibly more scattered, suggesting that they originated from a post-folding magnetic overprinting event of normal polarity, possibly associated with the Cretaceous deformation phase described by Ruttner et al. (1968).

2.2.2 Alborz

Wensink and Varekamp (1980) obtained ChRM directions oriented to northwest and down from 20 sites distributed in 3 different localities from several Cretaceous lava flows from the Chalus and Haraz valleys in the Western Alborz Mountains (#29,30,31 in Fig. 1; Table 1).

2.3 Paleogene paleomagnetic data

2.3.1 CEIM

Conrad et al. (1981) first reported paleomagnetic results from Paleogene volcanics from the southern part of the Lut Block of the CEIM. ChRM directions isolated in 17 samples from different localities are oriented to the east and up (#24 in Fig. 1; Table 1), and are better grouped after than before correction for bedding tilt (Conrad et al., 1981). Bina et al. (1986) reported paleomagnetic directions from Paleocene and Eocene volcanics from 3 different localities of the Lut Block. After correction for bedding tilt, the site-mean ChRM directions cluster either to the northwest and down or to the southeast and up (#17, 21, 22 in Fig. 1; Table 1). Soffel et al. (1989) reported results from a large number of sites sampled from 3 different localities in the Yazd Block (#3, 4, 5 in Fig. 1; Table 1) as well as from 5 localities in the Lut Block (#16, 18, 19, 20, 23 in Fig. 1;

Table 1). The ChRM directions isolated in these sites are oriented either to the northwest and down or southeast and up.

2.3.2 Alborz

Bina et al., (1986) reported data from volcanics from the Karaj area in the Western Alborz. Reliable results have been obtained for 15 samples, which show a mean ChRM direction oriented northeast and down (#28 in Fig. 1; Table 1).

2.4 Neogene paleomagnetic data

2.4.1 CEIM

Mattei et al. (2012) published paleomagnetic results from red marls and siltstones of the Upper Red Formation sampled in 2 localities of the CEIM (Tabas and Anarak, #1 and #2 in Fig. 1, respectively). In these localities, ChRM component directions were isolated and considered as primary in origin on the base of the positive reversal and fold tests. In tilt corrected coordinates, these component directions are oriented either to the northwest and down or southeast and up (#1 and #2 in Fig. 1; Table 1).

2.4.2 Alborz

Ballato et al. (2008) and Cifelli et al. (in press) reported paleomagnetic results from red marls and siltstones of the Upper Red Formation from two localities from the western and eastern sides of the southern Central Alborz. Ballato et al. (2008) isolated ChRM component directions from 216 samples from the Eyvaneikey magnetostratigraphic section, which are oriented either to the northeast and down or southwest and up (#27 in Fig. 1; Table 1). Cifelli et al. (in press) isolated ChRM component directions from 26 samples from the Abdolabad section, which are oriented either to the northwest and down or southeast and up (#26 in Fig. 1; Table 1).

3. PALEOMAGNETIC SAMPLING AND RESULTS

In the Kerman area of Central Iran (as part of the CEIM), we sampled 9 sites in the red marls and siltstones of the Upper Siliciclastic Member (Late Jurassic-Early Cretaceous) of the Bidou Formation (Zamani-Pedram, 2011), a lateral equivalent of the Magu Gypsum Formation and Garedu Red Beds Formation cropping out in the northern Tabas block (Wilmsen et al., 2009; Zamani-Pedram, 2011) (Fig.1). Sampling was carried out along the different flanks of the N–S-oriented Bolbulieh and Hossienabad fold systems, located to the southeast and east of Kerman, respectively (Azizan et al., 2009). The magnetic mineralogy of the sampled sediments was investigated on representative specimens using standard rock magnetic techniques. The stepwise acquisition of an isothermal remanent magnetization (IRM) was imparted using a pulse magnetizer up to 2.0 T fields. A three component IRM was imparted at 2.7 T, 0.6 T, and 0.12 T fields along samples orthogonal axes and thermally demagnetized according to the procedure of Lowrie (1990).

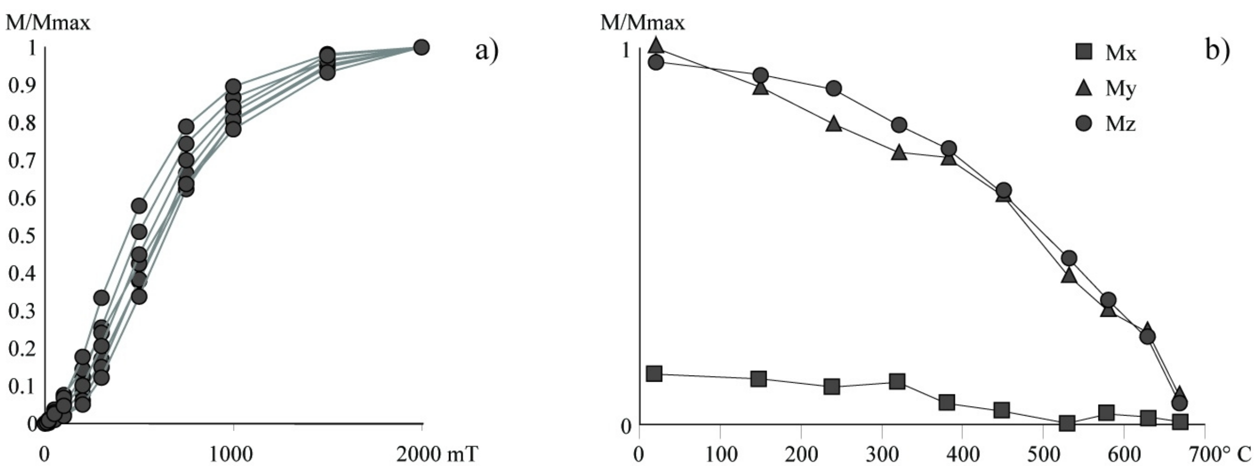

Fig. 2. Isothermal remanent magnetization (IRM) acquisition curves (a) and thermal demagnetization of a three-component IRM (b) from representative hematite-rich samples of the Bidou Formation red beds.

All samples show a progressive increase of IRM that does not reach saturation up to 2.0 T, suggesting the presence of a dominant high coercivity ferromagnetic mineral (Fig. 2a). Thermal demagnetization of a three component IRM confirms these results and helps defining the nature of the magnetic mineral. High-coercivity magnetic phases are prevalent and show maximum unblocking temperatures of about 680°C, which can be attributed to hematite (Fig. 2b).

A total of 84 cylindrical core specimens were subjected to progressive stepwise thermal demagnetization and the natural remanent magnetization (NRM) was measured after each demagnetization step with a 2G Enterprises DC-SQUID cryogenic magnetometer. The low-field magnetic susceptibility was measured after each heating step to monitor thermally induced alterations of the magnetic mineralogy. Heating steps of 100°C, reduced to 15-20 °C close to critical unblocking temperatures, were carried out from room temperature to a maximum of 670°C. The least-square analysis (Kirschvink, 1980) was applied to determine magnetic component directions. The maximum angular deviation (MAD) of the isolated magnetic components was generally <10°. Site-mean paleomagnetic directions were calculated using Fisher (1953) statistics.

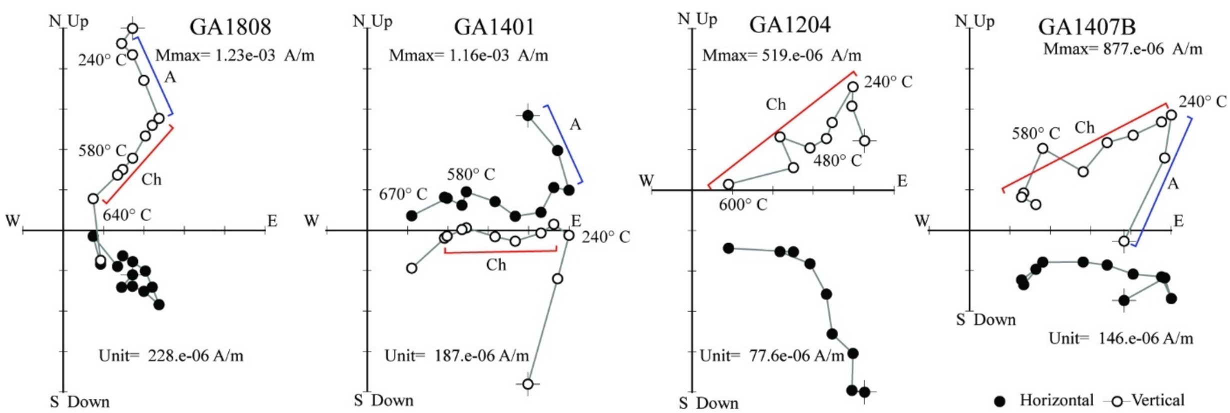

Fig. 3. Vector component diagrams for the progressive demagnetization of representative samples from Bidou Formation red beds. Open and solid symbols represent projections on the vertical and horizontal planes, respectively.

Most of the samples show the presence of an initial A component isolated between room temperature and 180-240 °C, occasionally up to 400 °C (Fig. 3). This A component is generally oriented north and steeply down in in situ coordinates (Fig. 3), whereas upon correction for bedding tilt, it becomes more scattered. The A component, with an in situ overall mean direction of Dec. = 356.0° E, Inc. = 40.3° ($\alpha 95$ = 24.2°), is within error range aligned along a recent geocentric axial dipole field direction (GAD inclination = 54°), and is therefore interpreted as a recent viscous overprint.

After removal of the low-temperature A component, a well-defined characteristic remanent magnetization (ChRM) component is observed in 40% (34/84) of the samples at higher temperatures between average values of c. 580–620°C or occasionally up to 670°C (Fig. 3). Demagnetization diagrams indicate stable behavior with demagnetization vectors aligned along linear paths directed toward the origin of vector component diagrams. Reliable site mean directions have been obtained from seven out of nine sampled sites (Table 2). Site mean directions are scattered in in situ coordinates, while after correction for bedding tilt, they cluster east and southeast and up (sites GA12, GA14, GA15, GA18) or southeast with a subhorizontal inclination (sites GA10-11) (Table 2; Figure 4). Site GA16 shows ChRM component directions broadly aligned along the present-day GAD magnetic field in in situ coordinates or oriented northeast and up in tilt-corrected coordinates; these component directions have been excluded from further analysis as possibly overprinted during recent times.

The overall mean ChRM component direction based on 6 site-mean directions is Dec. = 111.7°E, Inc. = -21.1° (k = 6, α95 = 29.6°) in in situ coordinates, whereas in tilt corrected coordinates, it becomes Dec. = 105.7°E, Inc. = -19.6° (k = 12, α95 = 20.1°) (Fig. 4; Table 1).

Table 2 – Paleomagnetic directions from Bidou Formation

Site	Location		Fm	Litholog y	n/N	S_0	BTC				ATC			
	Lat (°N)	Lon(°E)					D°	I°	K	α_{95}	D°	I°	K	α_{95}
GA10	30°08'49"	57°23'48"	GA	siltstones	3/10	variable	115.3	-9.9	12.5	36.4	110.5	2.5	13.7	34.6
GA11	30°11'35"	57°26'16"	GA	marls	4/9	variable	142.1	-43.6	13.8	25.6	117.8	-3.6	14.4	25.1
GA12	30°10'30"	57°24'46"	GA	siltstones	3/10	218,55	146.4	-16.2	46.8	18.2	127.1	-22.7	47.1	18.2
GA14	30°15'58"	57°17'47"	GA	siltstones	6/9	256,22	93.6	-40.4	18.6	15.9	90.1	-19.2	18.6	15.9
GA15	30°16'12"	57°16'44"	GA	marls	5/10	60,48	71.6	11.1	45.8	11.4	74.1	-35.8	45.8	11.4
GA16*	30°21'58"	57°17'58"	GA	siltstones	7/9	94,70	38.1	35.9	6.2	26.3	50.5	-13.1	6.2	26.3
GA18	30°17'17"	57°18'14"	GA	siltstones	6/8	85,20	105.5	-15.3	39.1	10.8	109.0	-33.9	39.1	10.8
Mean (6 sites)							**111.7**	**-21.1**	**6.1**	**29.6**	**105.7**	**-19.6**	**12.0**	**20.1**

Notes: Abbreviations: n/N—total number of stable directions at a site/number of demagnetized samples; S_0—bedding attitude (azimuth of the dip and dip values). D°, I°— site mean declinations and inclinations calculated before tectonic correction (BTC) and after tectonic correction (ATC); K—precision parameter; α_{95}—confident limit (statistical parameters after Fisher, 1953).

Site-mean directions show declination scattering that persists after tectonic correction (from 74.1° E at site GA15 to 127.1° E at site GA12), and that is possibly related to local tectonic rotations. A tilt-corrected overall mean inclination of -19.6° (±17.2°, k = 16), calculated using the inclination-only statistics of McFadden and Reid (1982), confirms the result obtained with the Fisher statistics (see above). Acknowledging these complexities, and based on a fold test that is positive at 99% level of confidence (McFadden, 1990), we consider this high-temperature ChRM component as primary in origin and acquired during (or shortly after) deposition of the Bidou

Formation.

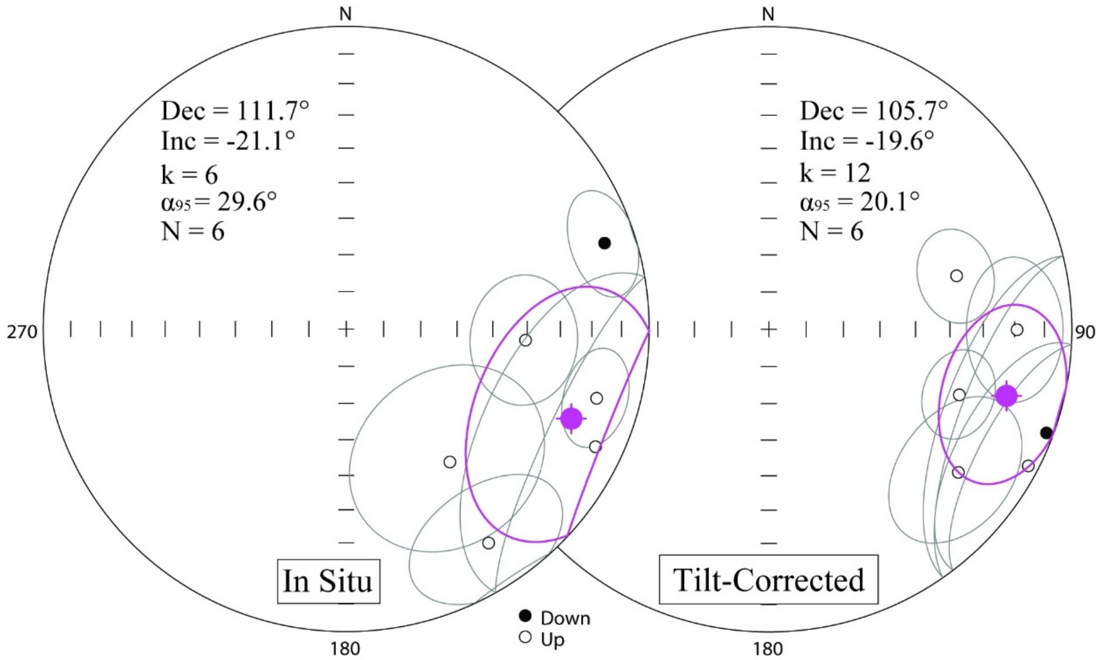

Paleomagnetic directions obtained from the Bidou Formation sites are similar to those obtained from the coeval Garedu Red Beds Formations from northern Tabas Block (Mattei et al., 2014), reinforcing the finding of a low-latitude position of Central Iran during Late Jurassic and the large amount of CCW rotation experienced by Central Iran since that time.

4. CHOICE OF REFERENCE PALEOMAGNETIC POLES

Previous paleomagnetic analyses indicate that the CEIM was located close to the Arabian margin of Gondwana in the Paleozoic, drifted off this margin attaining subequatorial palaeolatitudes in the Late Permian-Earliest Triassic, and approached the Eurasian margin by the late Early Triassic, to then maintain Eurasian affinity as deduced from Late Triassic and Cretaceous data (Muttoni et al., 2009a,b and references therein; see also Besse et al., 1998). Mattei et al. (2014) reported a low paleolatitude (~12° N ± ~5°) for the deposition of the Kimmeridgian–Tithonian (Late Jurassic) Garedu Red Bed Formation from the northern Tabas Block, which was found to be in good agreement with the low paleolatitudes predicted for Eurasia by the apparent polar wander paths (APWPs) of Kent et al. (2010) and Muttoni et al. (2013). These APWPs show the occurrence of a major and rapid shift in pole position of major plates (referred to as Jurassic massive polar shift;

Mattei et al., 2014) during the Middle to Late Jurassic that alternative curves from the literature tend to underestimate, and, for our purposes here, confirm an Eurasian affinity of Iran during the Jurassic (see Mattei et al., 2014 for a discussion). Therefore, Jurassic-Cenozoic paleomagnetic data from the CEIM and the Alborz Mountains have been compared to the Eurasian reference APWP curves to determine the amount of vertical axis rotations for each locality. In particular, we use the Kent and Irving (2010) North America APWP migrated into Eurasian coordinates for the time interval comprised between 200 and 90 Ma (Mattei et al., 2014), whereas for ages comprised between 80 and 10 Ma, we use the Besse and Courtillot (2002) Eurasian APWP.

5. VERTICAL AXIS ROTATIONS OF THE CEIM AND ALBORZ RANGE

Rotation values and associated 95% confidence limits, calculated according to the method of Demarest (1983), are reported in Table 1. In Figure 5, paleomagnetic rotations are displayed according to age of sampled rocks.

Jurassic paleomagnetic directions have been obtained for the CEIM at six localities in the Tabas and Yazd blocks (Fig. 5, #10-15) and one locality in the Lut block (Fig. 5, #25). All Jurassic sites from the CEIM show significant amounts of counter-clockwise (CCW) rotations, ranging between 45° (± 11°) and 82° (± 14°), with a mean value of 66° (± 13°).

Cretaceous paleomagnetic directions have been obtained at four localities in the CEIM (Fig. 5, #6-9) and three localities in the Western Alborz (#29-31). Paleomagnetic directions from the CEIM show CCW rotations comprised between 18° (± 13°) and 47° (± 13°), with a mean value of 34° (± 15°). In the Western Alborz, three paleomagnetic site-mean directions indicate CW rotation, comprised between 12° (± 11°) and 35° (± 18°), with a mean value of 28° (± 15°).

Paleogene paleomagnetic directions have been obtained at twelve localities in the CEIM (Fig. 5, #3-5 and #16-24) and one locality in the Western Alborz (#28). Paleomagnetic directions from the CEIM show CCW rotations ranging between 91° (± 20°) and 20° (± 9°), with a mean value of

43° (± 14°), whereas the single locality from the Western Alborz (# 28) is rotated CW by 50° (± 15°).

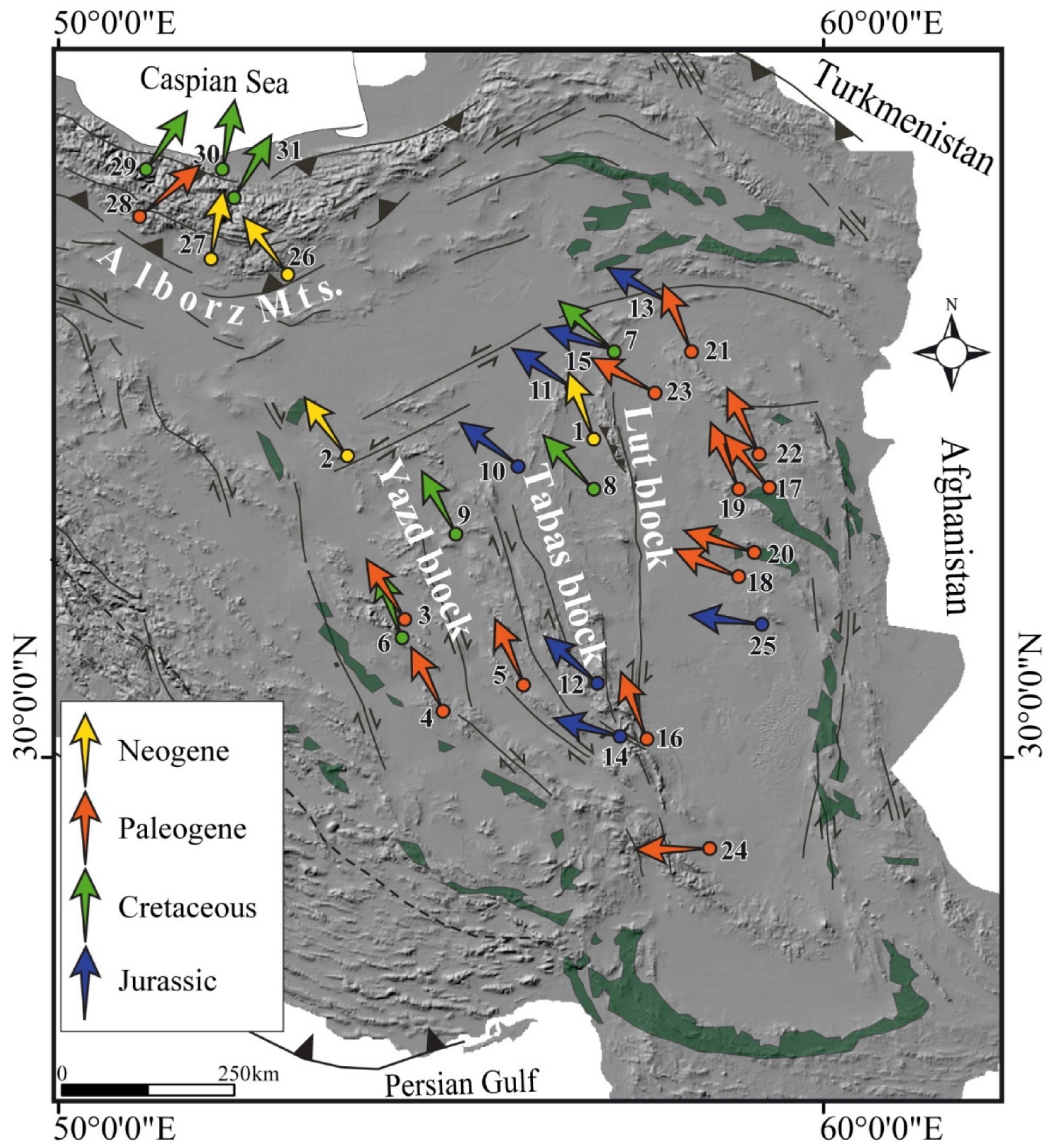

Fig. 5. Paleomagnetic rotation from the Central-East Iranian Microcontinent (CEIM) and the Alborz Mountains, calculated relative to the Kent et al., 2010 North America Apparent Polar Wonder Path (APWP) migrated into Eurasian coordinates for the time interval comprised between 200 and 90 Ma, and the Besse and Courtillot (2002) Eurasian APWP for the time interval comprised between 80 and 10 Ma. Numbers refer to data listed in Table 1.

Neogene results have been obtained from the Upper Red Formation of the CEIM (Fig. 5, #1-2) and in southern Central Alborz (#26-27). In the CEIM, paleomagnetic directions are rotated CCW (#1–2), whereas in southern Central Alborz, paleomagnetic directions from the Eyaneykey and Abdolabad sections (#26-27) indicate CW and CCW rotations, respectively.

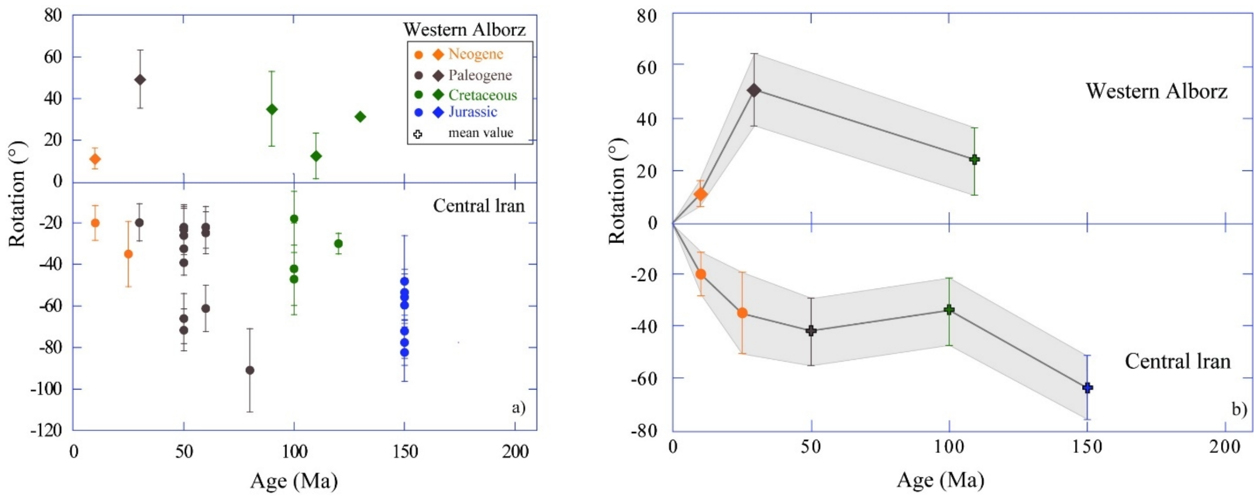

Fig. 6. Rotation (a) and age-mean rotations (b) values (in °) plotted versus age for the Central-East Iranian Microcontinent (CEIM) and the Alborz Mountains. See text for explanation about data processing. The illustrated paleomagnetic data are the same as those reported in Fig. 5 and Table 1.

A summary of the mean paleomagnetic rotations versus age is shown separately for the CEIM and Western Alborz in Figure 6. In the CEIM, we observe two distinct phases of CCW vertical axis rotations: an older phase, which occurred during the Early Cretaceous with an average amount of ≈30° CCW, and a more recent phase, which accomplished an additional ≈35° CCW, ≈20° of which occurred in the last 10 Myr (see also Mattei et al., 2012). In contrast, in the Western Alborz, no significant vertical axis rotations occurred in the time interval comprised between the Cretaceous and Paleocene, whereas opposite vertical axis rotations have been recorded in the Middle-Upper Miocene units cropping out along the two arms of the curved Alborz orogen (Fig. 6; see also Fig. 5).

6. PALEOGEOGRAPHIC EVOLUTION OF THE CEIM AND ALBORZ RANGE

Paleomagnetic results of this study and the literature give some new constraints on the tectonic and paleogeographic evolution of Iran. In particular, we focus our attention on the tectonic and paleogeographic evolution of the CEIM during Middle Jurassic-Late Cretaceous, taking into account latitudinal drifting events, vertical axis rotations, facies distribution, and main geodynamic processes in the area.

6.1 CEIM

Paleomagnetic results from upper Jurassic units of the CEIM confirm the latitude drop predicted for Eurasia by APWPs incorporating the Jurassic massive polar shift (Mattei et al., 2014; see also discussion above). In particular, during the Middle Jurassic (170 Ma, Fig. 7a), the CEIM, attached to Eurasia, was stationed in the mid-latitude (≈ 40°N) temperate belt, whereas during the Late Jurassic (145 Ma, Fig. 7b), it shifted to the low latitude tropical arid belt (≈ 15°N). This latitude shift explains the switch from coal-bearing sedimentation to carbonate platform deposition in the late Middle Jurassic (e.g. Fürsich et al., 2003), which appears to coincide with the drop to arid tropical latitudes during the Jurassic massive polar shift (see Mattei et al., 2014 for a detailed discussion on this issue). Paleomagnetic data from Upper Jurassic units also show that the CEIM rotated ≈ 65° CCW since the Late Jurassic, without significant differences among the Yazd, Tabas, and Lut blocks. These results are coherent with facies analyses and stratigraphic relationships (Dercourt et al., 1986; Fürsich et al., 2003; Wilmsen et al., 2003; 2009; 2010), which suggest that, during the Late Jurassic, the Yazd, Tabas, and Lut blocks of the CEIM were oriented east-northeast/west-southwest, and had the same lateral arrangement with respect to each other as they have today, arguing against significant horizontal displacement and differential vertical axis rotations along the block-bounding faults (Fig. 7b). The stratigraphy and facies distribution show that the Yazd Block was emergent for most of the Jurassic period and that marine influence increased from the Tabas to the Lut blocks. On this basis, the Lut Block should represent an area close to the oceanic basin and should therefore face the Neo-Tethys Ocean to the south and southeast (Fig. 7a).

The first episode of vertical axis rotation of the CEIM occurred during the Late Jurassic-Early Cretaceous. This event is suggested by the difference of ≈ 30° between the large CCW rotations measured in Late Jurassic red beds from different localities of the Tabas, Yazd and Lut blocks of

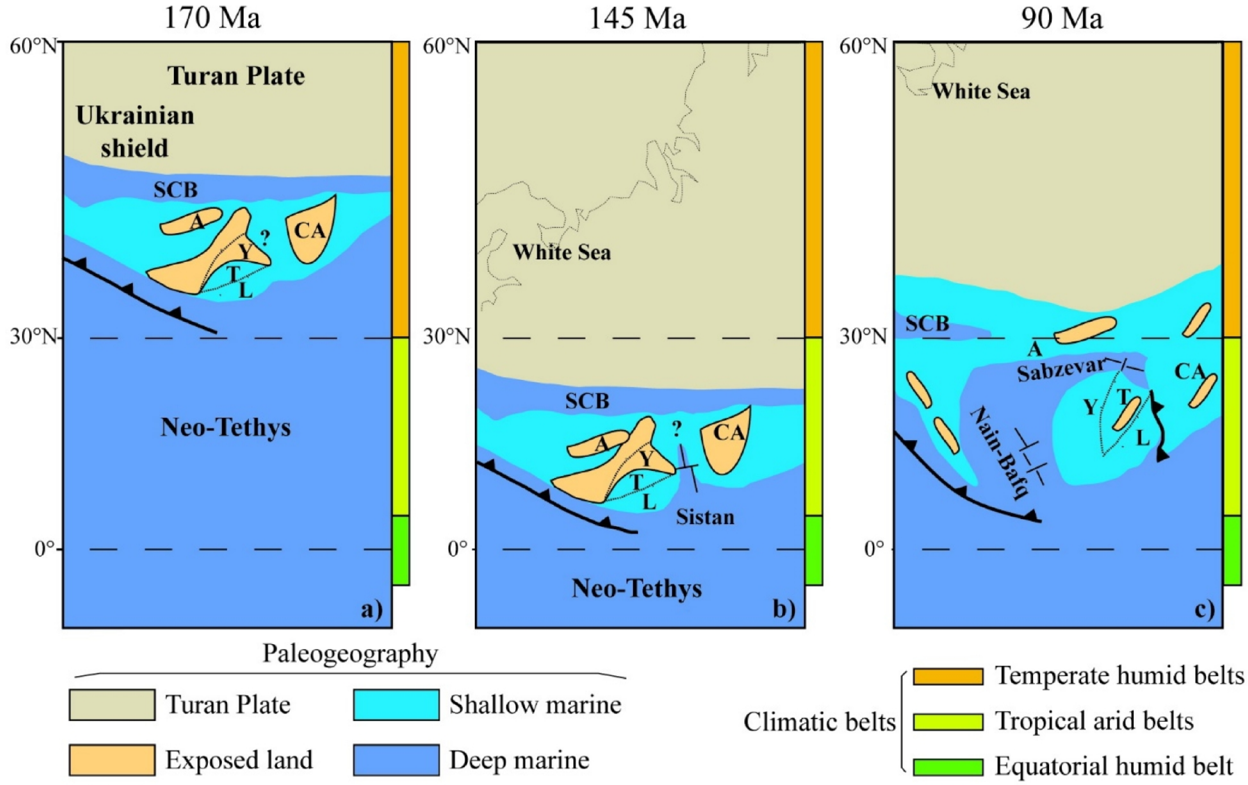

Fig. 7. Paleogeographic reconstructions of the Central-East Iranian Microcontinent (CEIM) – comprised of the Yazd, Tabas, Lut blocks – during the Middle Jurassic-Late Cretaceous time interval. Paleolatitudes are derived from paleomagnetic data from Iran (b, c) in conjunction with paleolatitudes expected for the CEIM from different apparent polar wander paths (APWPs) from the literature (a). Standard zonal climate belts (columns in the right side of paleogeographic reconstructions) are also reported to visualize the influence of continental drift on the distribution of climate-sensitive sedimentary facies of Iran. The Neo-Tethys Ocean (a, b, c) and the Sistan oceanic subduction and subsequent closure (c) are also reported, together with the inferred position of the rift axis in the Sistan, Sabzevar, and Nain-Baft marginal basins. The orientation of the CEIM is derived by paleomagnetic data and by facies distribution of Middle–Late Jurassic carbonate platform-to-basin depositional system (Dercourt et al., 1986; Fürsich et al., 2003; Wilmsen et al., 2003, 2009, 2010). Y = Yazd; T = Tabas; L = Lut; A = Alborz; SCB = Southern Caspian Basin; CA = Central Afghanistan.

the CEIM, and the smaller CCW rotation measured in Late Cretaceous units of the same areas. On the basis of its timing and regional distribution, we relate the ≈ 30° CCW rotation of the CEIM to the Early Cretaceous opening and subsequent closure of oceanic seaways, relics of which are preserved in the Nain-Baft, Sabzevar, and Sistan ophiolitic domains surrounding the CEIM (Fig. 7c). In particular, several pieces of evidence suggest that the oceanic seaways that faced the southeastern side of the CEIM were already formed during the Early Cretaceous. Babazadeh and De Wever (2004 a,b) suggested that the Sistan Ocean was already open at the beginning of the Aptian (121 Ma), based on the presence of Early Cretaceous (Albian-Aptian) radiolarian faunas in pelagic cherts within the Sistan ophiolitic assemblage. In the Makran accretionary prism of southeast Iran, geochronological studies on igneous rocks from ophiolite complexes have yielded 40Ar/39Ar hornblende cooling ages of 156-139 Ma (Kananian et al., 2001) and 143–141 Ma (Ghazi et al., 2004), indicating formation of oceanic crust around the CEIM in Late Jurassic to early Early Cretaceous times. Furthermore, radiometric ages on high-pressure metamorphic rocks suggest that subduction of oceanic lithosphere along the eastern margin of the Sistan Ocean had begun prior to 125 Ma (Early Cretaceous) (Fotoohi Rad et al., 2009), whereas high-pressure granulites in the Sabzevar units seems to suggest the occurrence of early (106 Ma) subduction of the Sabzevar oceanic seaway (Rossetti et al. 2010). Our data are not conclusive for indicating if the measured CCW rotation of the CEIM resulted from the northward propagation of rifting-spreading in the Sistan basin during Late Jurassic to Early Cretaceous times (Fig. 7b), or to the subsequent (late Early Cretaceous?) eastward subduction and closure of the Sistan oceanic basin underneath the continental margin of the Afghan Block (Fig. 7c, Rossetti et al., 2010).

From the Late Cretaceous to the Oligocene, no significant paleomagnetic rotations have been observed in Central Iran. Late Cretaceous–Oligocene data from Central Iran show similar amounts of CCW rotations (comprised between ≈30° and ≈40°). Most of these CCW rotations occurred after the Middle–Late Miocene and accommodated NNE–SSW shortening related to the Arabia-Eurasia convergence: the CEIM became and area dominated by CCW-rotating crustal blocks bounded by N–S oriented right-lateral faults, whereas CW rotations occurred north of the Great-Kavir fault where ENE–WSW oriented left lateral strike-slip faults prevail (Mattei et al., 2012) (Fig. 1).

6.2 Alborz

Paleomagnetic data from the Alborz Mountains show a very different pattern with respect to the CEIM. Data from Cretaceous volcanic rocks from the Western Alborz are characterized by CW rotations comprised between ≈ 10° and ≈ 35°, without significant trends with age. Data from the sedimentary units of Middle–Late Miocene age from the Eyvanekey section and the Abdolabad area, located along the western and eastern arms of the Alborz curved orogen, show rotations of about 11° (±5°) CW and 37° (±7°) CCW, respectively. Taken altogether, these paleomagnetic data indicate that the western arm of the central southern Alborz, oriented ESE–WNW (Fig. 1), rotated CW, whereas the eastern arm, oriented WSW-ENE, rotated CCW. Hence, the Alborz orogen resulted from secondary bending, with most of its curvature acquired after about 8 Ma (Late Miocene), which is the upper age of the Upper Red Formation (Ballato et al., 2008).

7. CONCLUSIONS

Our new paleomagnetic results from Upper Jurassic Bidou Formation integrated with published paleomagnetic data from Iran, lead us to the following conclusions:

(1) During the Late Jurassic, the CEIM was located at low latitudes close to the Eurasian margin, in agreement with the position predicted for Eurasia from the Kent and Irving (2010) APWP during the so-called Jurassic massive polar shift (Mattei et al., 2014).

(2) The Jurassic latitudinal drift of Eurasia fully explains the sedimentary facies evolution of Iran under the assumption of standard zonal climate belts (see Mattei et al., 2014 for details).

(3) During the Late Jurassic, the different blocks forming the CEIM (Yadz, Tabas, Lut) were oriented WSW–ENE, with the Lut block facing the Neo-Tethys Ocean in the south and the Sistan oceanic seaway in the southeast.

(4) Large CCW rotations characterized the CEIM; these rotations occurred in two distinct phases, during the Early Cretaceous and after the Middle–Late Miocene. These rotations are confined to the CEIM and do not extend to the other tectonic provinces of Iran (e.g., Alborz).

(4) No detectable vertical axis rotations of, or within, the CEIM occurred during the Late Cretaceous–Oligocene time interval.

(5) The origin of the curved shape of the Alborz Mountains is due to an oroclinal bending mechanism, with most of its curvature acquired after about 8 Ma (Late Miocene).

Chapter III

Oroclines in the Alborz and Central Iran

The results in this chapter are shown in a preliminary fashion and without a complete discussion. These chapter will published as two papers separately in the future.

1. Introduction

Carey (1955), introduced the term orocline to represent an originally linear orogenic system that acquired curvature during a second phase of tectonic deformation (Weil and Sussman, 2004). Consequently, in an orocline, a one-to-one relationship exists between vertical-axis rotation and the total curvature in structural features (Weil and Sussman, 2004). Since Paleomagnetism has the capability to record rotations about vertical axes and tilts about horizontal-axes (Weil and Sussman, 2004), by comparing paleomagnetic declinations and structural data, the mauntans belt can be distinguished as primary and secondary arcs. (e.g. Weil and Sussman, 2004; Cifelli et al., 2008). In primary arcs, paleomagnetic declinations remain parallel along the arc and do not correlate with changes in thrust and fold axis trend. In secondary arcs, paleomagnetic declinations change direction along the arc and follow changes in thrust and fold-axis trend (Cifelli et al., 2008).

In this chapter, we present preliminary results of paleomagnetic study from Upper Red Formation of eastern, central and western Alborz Mountain and Shahdad thrust-fold belt to constrain the tectonic and kinematic evolution of these curvature belts during the Neogene.

2. Alborz Mountan

2. 1. Samling

Paleomagnetic sampling was carried out in the Alborz curved orogen, from longitude ≈ 49°E to ≈ 58°E (Fig. 1). Seventy-six sites were sampled and in each site 9 to 15 cores were taken from different stratigraphic levels in order to average secular variation of the geomagnetic field and to check for the occurrence of polarity reversals. In the Western Alborz, between longitude ≈49°E and ≈50°30’E (Fig. 1), we sampled 24 sites from marls and siltstones of Upper Red Formation in the Manjil and Alamut basins. In the Central Alborz twenty-five sites have been sampled between longitude ≈53°E and ≈55°20’E (Fig.1) from red marls, gray marls and siltstone of Lower Red, Qom and Upper Red formations. In the Eastern Alborz, the area between Jajarm and Mashkan, comprised between ≈ 56°29’E and ≈ 58°E (Fig.1), we sampled 27 sites from Neogene marls of the URF (25 sites) and from Eocene marls and siltstone (2 sites).

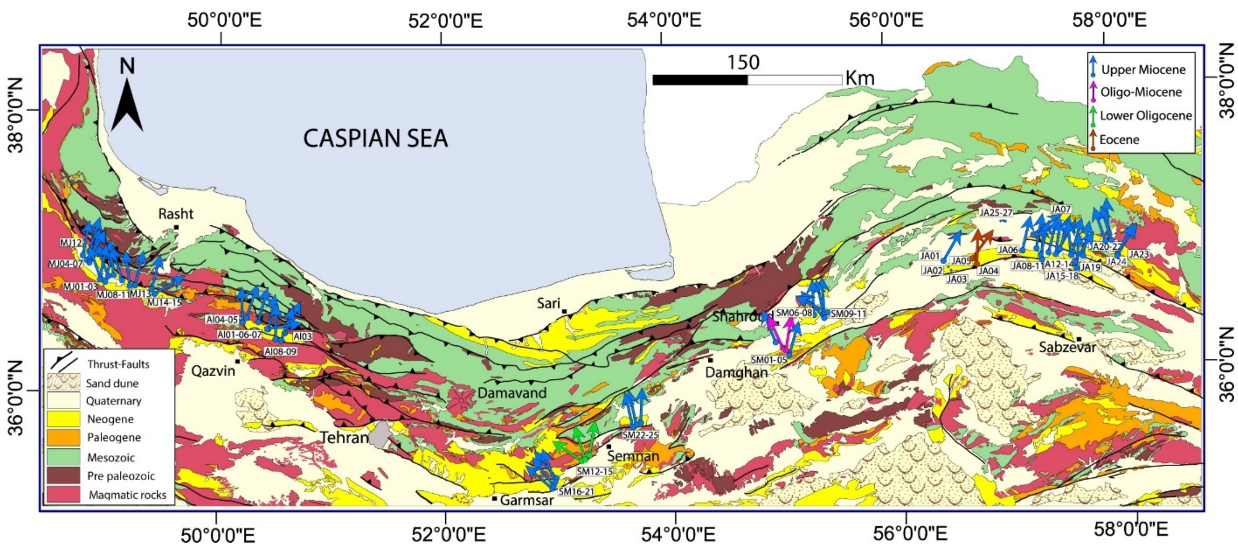

Fig.1. Paleomagnetic directions from the weastern, Central and eastern Alborz Mountains. Rotation is calculated relative to the Besse and Courtillot [2002] European APWP for the 40 to 10 Ma time interval.

2.2. Methods and results

Samples were demagnetized using a 2G Enterprises dc SQUID (superconducting quantum interference device) cryogenic magnetometer located in a shielded room at the INGV Laboratory of Paleomagnetism (Rome, Italy). Data analyses was carried out using the Remasoft 3.0 software. The natural remanent magnetization (NRM) of one specimen per core was measured by means of progressive stepwise thermal demagnetization using small temperature increments (80-100 °C up to 300 °C and 30–50 °C above 300 °C) until the NRM decreased below to the limit of the instrument sensitivity or random changes of the paleomagnetic directions appeared.

Thermal demagnetization defines two types of magnetic behaviour. The first one, recognized in

100 samples (17.2%), is characterized by a single magnetization component with only normal polarity (Fig. 3a). These samples undergo a sharp decrease of NRM intensity between 20°C and 300°C and are completely demagnetized between 580° C and 670°C. In geographic coordinates, the mean paleomagnetic direction for this normal polarity component is Dec. = 3.8°, Inc. = 52.6°, with α_{95} = 2.3° and k = 38.7 (Fig. 2a). This direction is almost coincident with that of the expected present-day geocentric axial dipole (GAD) field for the study area (Dec. = 0, Inc. = 54.5). When the tectonic tilt correction is applied, the mean direction is less grouped and becomes Dec. = 11.0°, Inc. = 46.2°, with α_{95} = 6.3° and k = 6.0 (Fig. 2b), suggesting that these samples were recently overprinted. On this basis, we do not consider them further for tectonic interpretations.

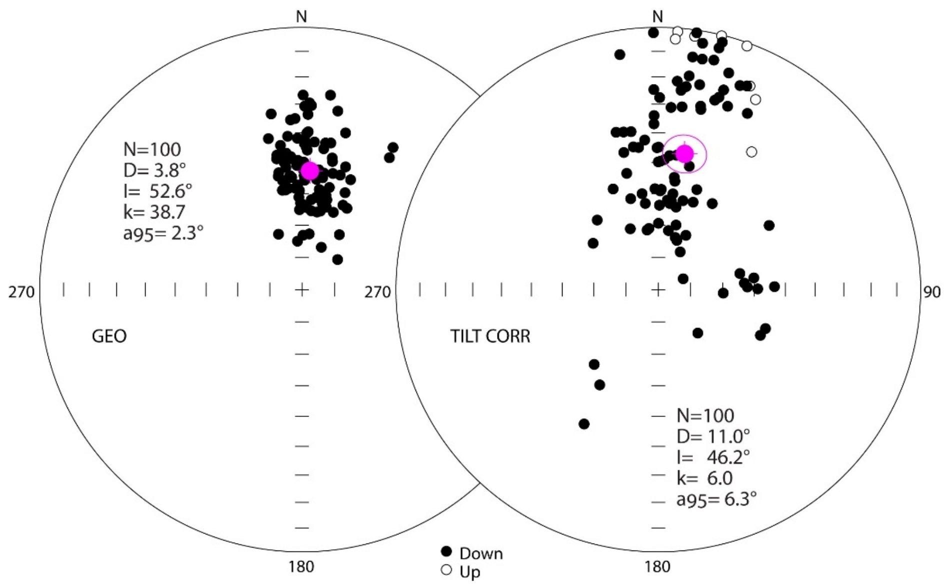

Fig. 2. Equal-area projection of sample characteristic remanent magnetization (ChRM) directions from the Alborz Mountain. The 95% confidence ellipse for the normal and reversed directions is indicated.

The second type of behavior was observed in the remaining samples (~87%), where a ChRM has been isolated. After removal of a viscous low temperature normal polarity component at 180°/240° C, in most of the samples the vectors aligned along a single linear path oriented towards the origin of the diagrams for both normal and reverse polarities. The ChRM directions were computed by fitting the linear component between 230/320°C and 580/640°C (Fig. 3b-d). In some other cases a linear path to the origin has been observed, after the removal of a middle temperature component at 360/480°C. In these samples the ChRM directions were computed by fitting the linear component between 440/610°C and 580/670°C (Fig. 3e, f).The least-square analysis (Kirschvink, 1980) was applied to determine characteristic remanent magnetization (ChRM) directions. The characteristic remanent magnetization (ChRM) was determined by principal component analysis [Kirschvink, 1980] in 479 specimens. The maximum angular deviation (MAD) of the isolated magnetic components was generally <10°. The site-mean paleomagnetic directions from 56 sites were calculated using Fisher (1953) statistics and are reported in Tables 1, 2 and 3. Bedding corrections were performed by progressively untilting bedding to horizontal using the Remasoft 3.0 software (Chadima and Hrouda, 2009). When a fold plunging was observed in the tectonic structures, we applied a double tilting correction to restore the bedding to the horizontal.

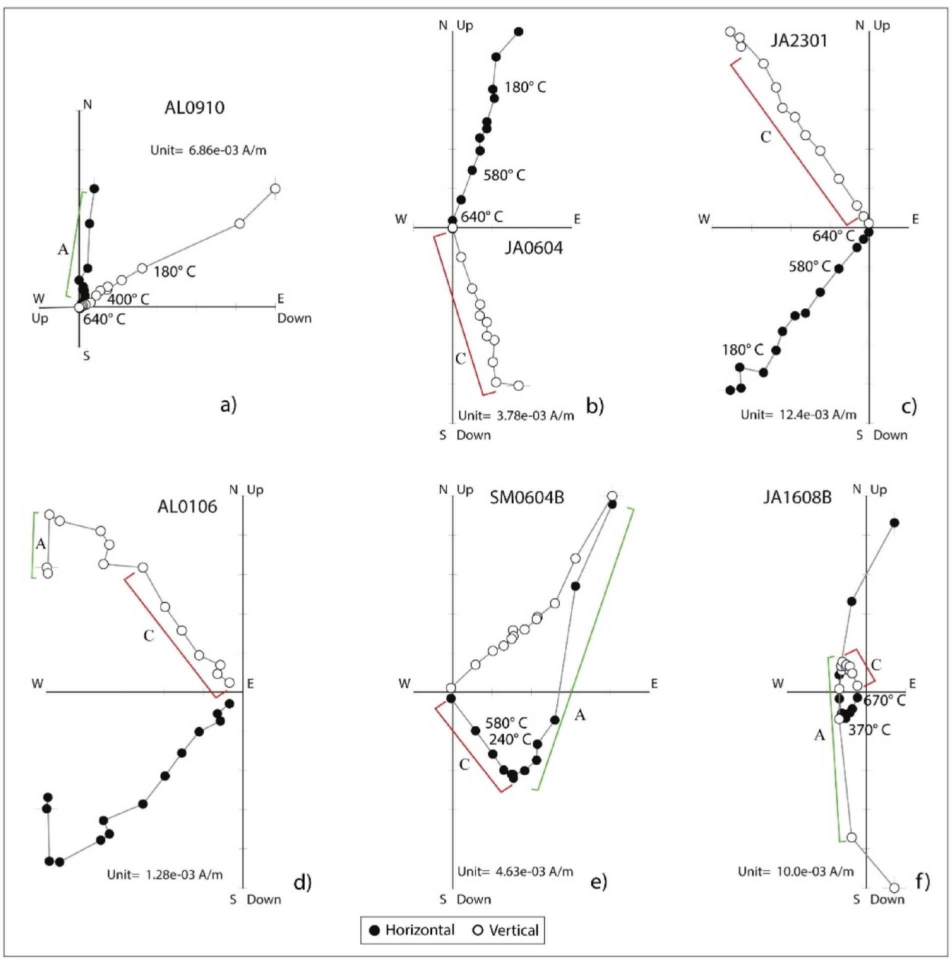

Fig.3. Vector component diagrams for the progressive thermal demagnetization. Open and solid symbols represent projections on the vertical and horizontal planes, respectively.

Table 1. Paleomagnetic rotations from western Alborz

Location							AFC					
Site	**Lat (°N)**	**Lon(°E)**	**Fm**	**Lithology**	**N/n**	**S0**	**D°**	**I°**	**K**	**α_{95}**	**R (°) ± Err (°)**	**F (°) ± Err (°)**
Al01	36°26'41.34"	50°24'42.78"	URF	Red marls	10/8	52,15	196.8	-42.1	13.6	15.6	12.8±17.0	13.0±12.4
Al03	36°24'49.62"	50°30'30.36"	URF	Red marls	10/8	6,45	212.1	-48.2	15.7	14.4	28.1±17.3	6.9±11.0
Al04	36°29'29.04"	50°16'44.52"	URF	Red marls	9/3	198,18	202.9	-23.6	28.1	23.7	18.9±20.5	31.5±18.6
*Al05	36°28'36.18"	50°16'14.40"	URF	Red marls	9/4	338,20	358.5	47.9	56.3	6.9	-	-
Al06	36°27'56.52"	50°21'33.90"	URF	Red marls	10/7	25,22	21.1	33.6	60.4	7.8	17.1±7.4	21.5±6.5
*Al07	36°26'53.34"	50°24'32.88"	URF	Red marls	11/7	266,10	266.2	-40.9	23.2	12.8	-	-
Al08	36°26'41.34"	50°24'42.78"	URF	Red marls	9/8	194,63	10.7	45.0	31.5	10	6.7±11.5	10.1±8.1
Al09	36°24'49.62"	50°30'30.36"	URF	Red marls	10/6	194,63	206.4	-25.4	9.0	23.6	22.4±21.3	29.7±18.6
Mean					6		21.8	36.5	47.2	9.8	17.8±10	18.6±8
MJ01	36°47'51.06"	48°59'40.92"	URF	Red marls	9/6	12,15	20.2	36.6	35.0	11.5	16.2±11.0	18.6±9.0
MJ02	36°48'9.60"	48°58'42.30"	URF	Red marls	7/5	344,27	16.1	34.6	7.0	31.2	12.1±30.1	20.6±24.4
MJ03	36°48'34.62"	48°58'37.62"	URF	Red marls	8/7	16,17	357.4	48.0	35.2	10.3	−6.6±12.2	7.2±8.4
MJ04	36°56'19.14"	48°50'29.94"	URF	Red marls	12/8	52,84	218.0	-68.0	28.3	9.9	34.0±21.0	−12.7±7.8
MJ05	36°55'33.90"	48°51'41.88"	URF	Red marls	10/8	26,89	204.6	-53.6	27.2	10.8	20.6±14.6	1.6±8.5
MJ06	36°55'48.36"	48°51'46.92"	URF	Red marls	10/3	32,57	212.4	-57.5	18.6	29.4	28.4±51.6	−2.2±22.9
MJ07	36°57'22.32"	48°49'11.40"	URF	Red marls	10/5	48,78	16.4	20.0	48.6	11.1	12.4±9.7	35.2±9.0
MJ08	36°45'53.82"	49°12'47.10"	URF	Red marls	10/7	286,13	360.0	40.3	169.0	4.7	−4.0±5.6	14.9±4.4
MJ09	36°47'17.46"	49° 8'23.28"	URF	Red marls	9/8	210,28	351.8	36.8	50.2	7.9	−12.2±7.9	18.5±6.3
MJ10	36°49'6.18"	49° 4'54.90"	URF	Red marls	10/6	227,28	173.8	-29.0	37.0	11.2	−10.2±10.4	26.2±9.1
MJ11	36°48'56.88"	49° 3'56.88"	URF	Red marls	11/9	29,28	163.5	-38.0	23.4	10.9	−20.5±11.2	17.2±9.0
MJ12	36°58'18.96"	48°51'50.94"	URF	Red marls	11/11	75,14	19.4	39.0	26.0	9.1	15.4±9.1	16.3±7.5
MJ13	36°46'16.44"	49°14'32.64"	URF	Red marls	10/6	32,33	194.9	-27.2	15.1	17.8	10.9±16.0	28.1±14.1
MJ14	36°44'12.00"	49°24'20.76"	URF	Red marls	9/6	172,9	196.1	-27.5	37.6	11.1	12.1±10.2	27.8±8.8
Mean					**14**		**10.2**	**40.6**	**22.1**	**8.7**	**6.2±9.2**	**14.7±7.3**

Notes: Abbreviations: URF=Upper Red Formation; N/n=number of specimens/ number of used speciments in calculations; S0 = bedding plane (mean value for each site); site; D°, I°=site mean declinations and inclinations calculated after tectonic correction (ATC); K=precision parameter; α_{95}=confident limit (statistical parameters after Fisher, 1953); R (°) ± Err (°)=rotation and respective error; F (°) ± Err (°)=flattening and respective error. R and F values (and associated error) were calculated according to the method by Demarest (1983) using the coeval European pale poles from Torsvik et al., (2012).

2.2.1. Western Alborz

In the Manjil basin a ChRM has been isolated in fourteen sites (MJ01-14), whereas site MJ15 show scatter directions and has been not considered for further tectonic interpretations (Table 1). Most of the sites show well defined ChRM direction, with α_{95}<12. Sites MJ02, MJ06, and MJ13 show higher values of α_{95}, but directions of ChRM component similar to the other sites from the basin and have been also considered for tectonic interpretations (Table 1). Among the fourteen

sites, seven record normal polarity and seven sites show a reverse polarity. After tectonic correction, normal and reversed polarity site-mean directions group into two antipodal clusters, and the reversal test is positive (type Rc with γo=7.4° and γc=18.5°) according to McFadden and Mc Elhinny (1990). The regional tilt test of McFadden (1990) is also positive at 99% level of confidence ($\xi_{in\ situ}$= 6.716; $\xi_{unfolded}$= 0.837 with a $\xi_{99\%}$= 6.087), suggesting a pre-tilt origin of the isolated ChRM in these sites. When reported to normal polarity, sites located in the northwest and southeast part of the basin are consistently oriented NNE, whereas sites located in the central part of the basin are oriented NNW. When the fourteen ChRM directions are considered together the mean direction for the Manjil Basin is declination (Dec.) = 10.2°, inclination (Inc.) = 40.6°, k = 22.1, α_{95} = 8.7° (Table 1 and Fig. 4).

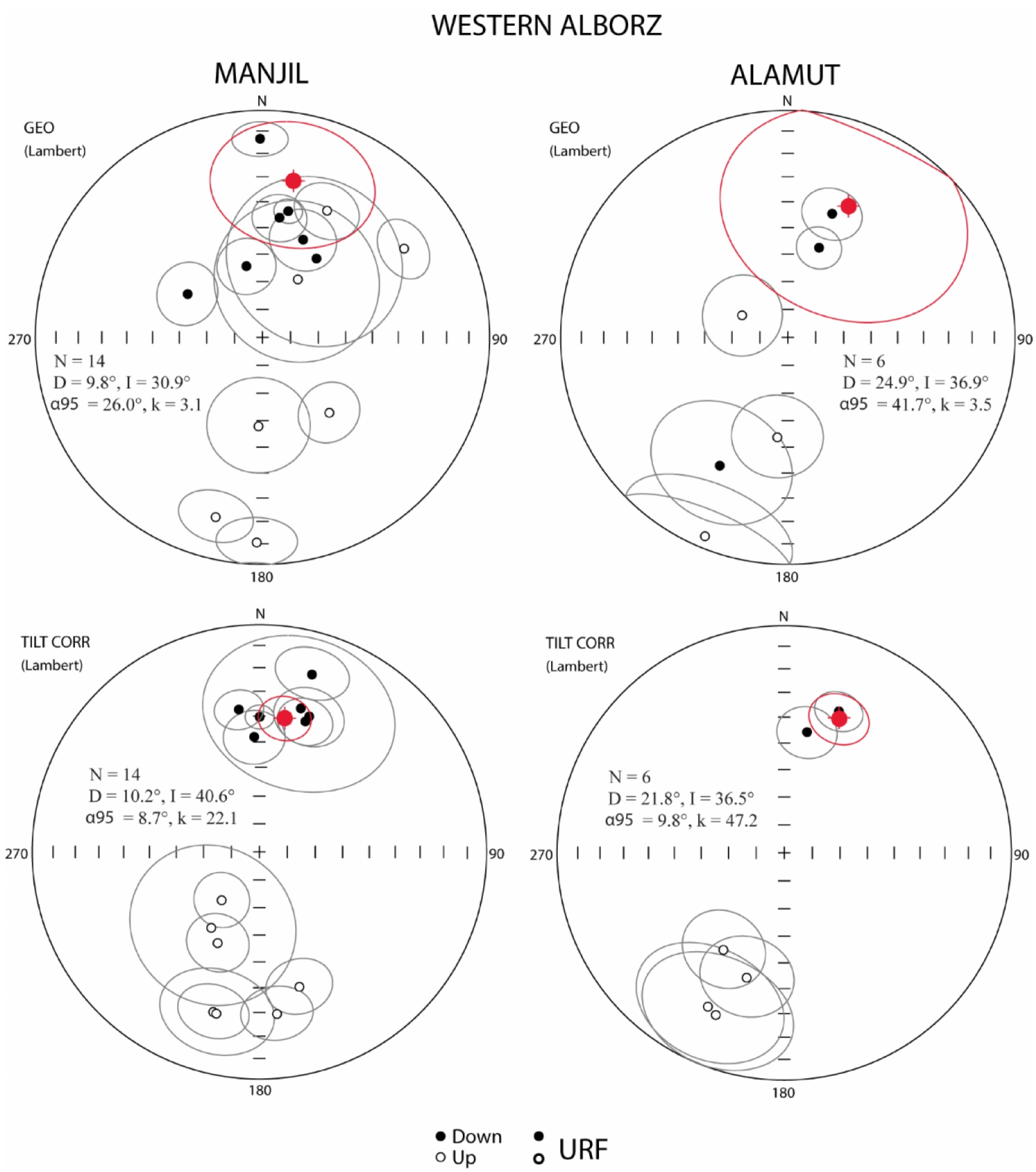

Fig. 4. Equal-area projection of the site-mean directions from the Western Alborz (Manjil and Alamut), respectively. The 95% confidence ellipse for the normal and reverse directions is indicated.

In the Alamut basin ChRM component directions have been isolate in all the sites but AL02 which shows scattered directions among the different samples. Site AL05 bears a normal polarity component direction oriented close to the present day GAD field direction in geographic coordinates. The ChRM isolated at site AL07 is oriented up to the east and is far from the ChRM component directions isolated in all the other sites, suggesting a possible influence of local tectonics. These two sites have been not further considered for tectonic interpretations. Among the other six sites, four bear reverse polarity and two normal polarity magnetization. After tectonic correction, normal and reversed polarity site-mean directions group into two antipodal clusters, and the reversal test is positive (type Rc with γo=7.8° and γc=22.6°) according to McFadden and Mc Elhinny (1990). The regional tilt test of McFadden (1990) is also positive at 99% level of confidence ($\xi_{in\ situ}$= 3.936; $\xi_{unfolded}$= 1.853 with a $\xi_{99\%}$= 3.919), suggesting a pre-tilt origin of the isolated ChRM in these sites. When all the sites are transposed to normal polarity they show a NNE orientation of the ChRM and the mean direction for the Alamut basin is declination (Dec.) = 21.8°, inclination (Inc.) = 36.5°, k = 47.2, α_{95} = 9.8° (Table 1 and Fig. 4).

2.2.2. Central Alborz

In the area between longitude ≈53°E and 55°20'E, ChRM component directions have been isolated in nineteen sites. These sites also include paleomagnetic results from sites SM16-21, named as Abdolabad section by Cifelli et al., (2015). Five sites (SM03, SM15, SM16, SM17, and SM23) bear normal polarity component directions oriented along the present day GAD field direction in geographic coordinates and after tilt correction their mean directions diverge from the rest of the Central Alborz sites (Table 2). These sites are affected by some later magnetic overprint, which was not removed during stepwise demagnetization, which formed after tectonic tilting of bedding. Sites SM07, SM12 and SM24 show well defined ChRM component in most of the samples but they show a scatter distribution (α_{95} > 32.0) when they are considered all together. These sites have been not considered for further tectonic interpretation. In the remaining 17 sites, 8 sites recorded strictly reverse polarity magnetization, 9 sites recorded strictly normal polarity magnetization. All these sites show well-grouped magnetic directions, with α_{95} values between 4.1° and 13.4°, but site SM21 with α_{95}=20.8°. When the 9 normal and 8 reversed single polarity sites are considered together, the reversal test of McFadden and

Table 2. Paleomagnetic rotations from western Alborz

Location							AFC					
Site	***Lat (°N)***	***Lon(°E)***	***Fm***	***Lithology***	***N/n***	***S0***	***D°***	***I°***	***K***	α_{95}	***R (°) ± Err (°)***	***F (°) ± Err (°)***
SM01	36°14' 41.7"	55°01'06.4"	Qom	Red marls	11/10	222,54	343.6	30.9	16.0	12.5	-23.2±11.7	23.8±9.9
SM02	36°14' 54.7"	55°00'53.1"	Qom	Red marls	15/12	321,63	3.4	30.1	27.3	8.5	-3.4±8.1	24.6±6.9
*SM03	36°16' 26.9"	54°59'21.2"	URF	Red siltstones	15/12	132,45	81.9	61.8	51.0	6.1	-	-
SM04	36°16'42.3"	54°58'48.4"	URF	Red siltstones and marls	9/8	165,67	162.5	-37.2	39.1	9.0	-21.6±9.3	18.1±7.4
SM05	36°13'30.4"	55°01'48.1"	URF	Red marls	11/10	282,12	20.9	35.2	55.0	6.6	16.8±6.4	20.1±5.2
SM06	36°28'53.8"	55°20'53.5"	URF	Red marls	13/13	18,76	144.2	-33.9	34.4	7.2	-39.9±7.0	21.4±5.8
SM08	36°29'08.0"	55°19'1.1"	URF	Gr./red marls	11/11	357,52	7.4	33.9	31.5	8.3	3.3±8.0	21.5±6.6
SM09	36°29'08.0"	55°20'55.8"	URF	Gr./red marls	13/12	164,59	352.6	45.9	18.8	10.3	-11.5±11.7	9.5±8.1
SM10	36°29'30.7"	55°21'19.3"	URF	Gr./red marls	13/13	28,10	181.3	-39.0	15.3	11.0	-2.7±11.2	16.4±8.7
SM11	36°29'47.8"	55°21'50.7"	URF	Gr./red marls	12/10	342,69	121.2	-45.2	143.0	4.1	-62.9±4.9	10.2±3.5
SM13	35°30'37.5"	53°13'08.7"	LRF	Red siltstones	12/12	161,86	171.2	-55.1	20.8	9.7	-17.2±13.6	-1.±7.8
SM14	35°30'44.6"	53°12'55.9"	LRF	Red siltstones	11/11	288,33	132.5	-25.9	35.1	7.8	-55.8±7.2	28.2±6.4
*SM15	35°31'16.5"	53°14'54.9"	LRF	Red siltstones	10/6	24,64	12.0	5.3	59.3	88.0	-	-
*SM16	35°20'32.5"	52°55'54.7"	URF	Red siltstones	13/8	156,73	149.1	33.6	36.9	9.2	-	-
*SM17	35°20'12.5"	52°56'7.4"	URF	Red marls and siltstones	12/8	144,64	92.9	54.0	12.5	16.3	-	-
SM18	35°20'7.8"	52°56'42.6"	URF	Red marls	12/5	148,64	150.6	-12.0	37.0	12.7	-33.9±10.1	42.2±10.0
SM19	35°20'38.4"	52°56'57.2"	URF	Red marls and siltstones	12/7	142,51	343.5	38.1	63.4	7.6	-20.5±7.7	16.1±6.1
SM20	35°21'18.3"	52°57'8.9"	URF	Red marls and siltstones	11/8	145,30	326.3	37.3	44.2	8.4	-37.7±8.4	16.9±6.7
SM21	35°19'29.2"	52°56'31.7"	URF	Red marls and siltstones	11/6	163,59	315.9	59.5	11.3	20.8	-48.1±34.7	-5.3±16.3
SM22	35°43'45.7"	53°39'17.0"	URF	Gr./red marls	13/10	65,43	352.6	42.6	13.9	13.4	-11.4±14.4	11.9±10.5
*SM23	35°45'06.0"	53°42'8.4"	URF	Red marls and siltstones	13/12	183,19	7.3	46.9	66.4	5.7	-	-
SM25	35°44'01.4"	53°39'48.7"	URF	Red and grey marls	12/6	45,38	172.4	-39.4	70.2	8.1	-11.6±7.9	11.6±5.7
Mean					**17**		**342.6**	**39.5**	**17.4**	**8.8**	**-21.4±9.1**	**14.8±7.0**
Mean			URF		**13**		**342.9**	**40.2**	**17.6**	**10.2**	**-21.1±10.6**	**14.8±8.1**

Notes: Abbreviations: Qom= Qom Formation; URF=Upper Red Formation; LRF= Lower Red Formation; N/n=number of specimens/ number of used speciments in calculations; S0 = bedding plane (mean value for each site); site; D°, I°=site mean declinations and inclinations calculated after tectonic correction (ATC); K=precision parameter; α_{95}=confident limit (statistical parameters after Fisher, 1953); R (°) ± Err (°)=rotation and respective error; F (°) ± Err (°)=flattening and respective error. R and F values (and associated error) were calculated according to the method by Demarest (1983) using the coeval European pale poles from Torsvik et al., (2012).

McElhinny (1990) is positive (type Rc with γo=12.5° and γc=17.6°). The tilt test of McFadden (1990) is also positive at 99% level of confidence ($\xi_{in\ situ}$=15.105; $\xi_{unfolded}$=2.250 with a $\xi_{99\%}$=6.721).These results demonstrate that the ChRM for the Central Alborz area was acquired prior to folding and can be considered as a primary component of magnetization. ChRM direction, when reported to normal polarity, are generally oriented NNW and the mean directions for the Central Alborz is declination (Dec.) = 342.6°, inclination (Inc.) = 39.5°, k = 17.4, α_{95} = 8.4° (Table 2 and Fig. 5).

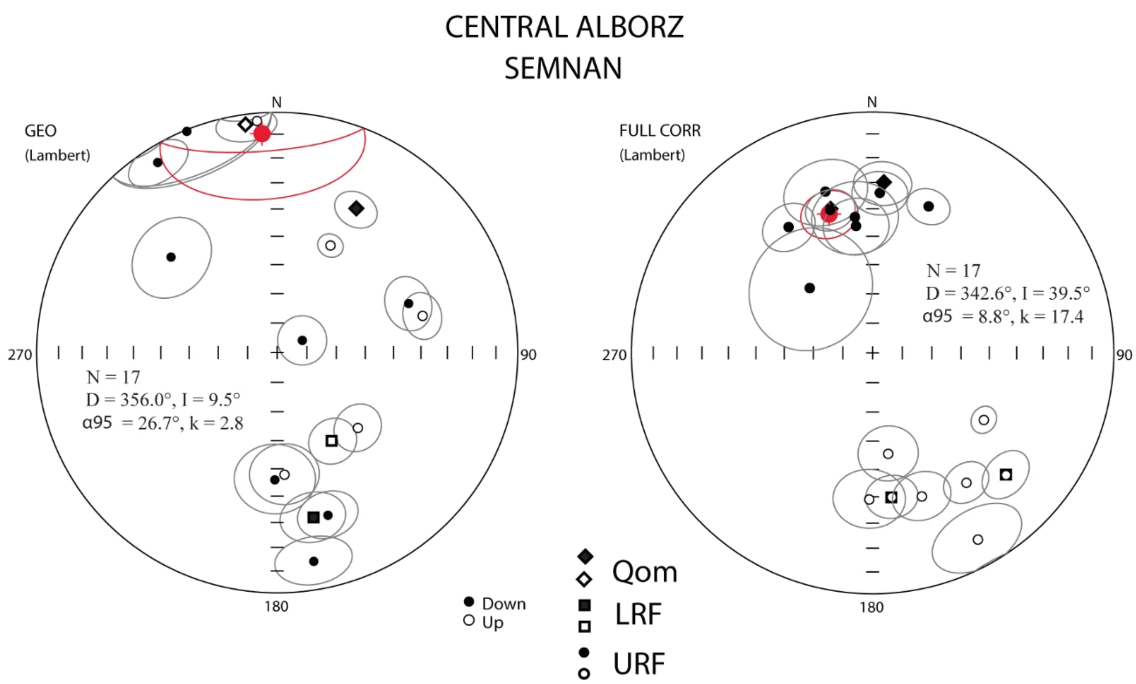

Fig. 5. Equal-area projection of the site-mean directions from the Central Alborz (Semnan). The 95% confidence ellipse for the normal and reverse directions is indicated.

2.2.3. Eastern Alborz

In the area between Jajarm and Mashkan, comprised between ~ 56°29'E and ~ 58°E, we obtained reliable ChRM in all the 27 sampled sites. Sites JA02, JA03 and JA19 bear normal polarity component directions oriented along the present day GAD field direction in geographic coordinates, which could indicate a recent magnetic overprint (Table 3). Therefore these 3 sites have been excluded from further analyses. In the remaining 24 sites, 13 sites recorded strictly reverse polarity magnetization, 8 sites recorded normal polarity magnetization, and the remaining 3 sites recorded mixed polarities. 23 of 24 these sites show well-grouped magnetic directions, with α_{95} values between 5.4° and 14.2° whereas site JA07 has α_{95} value= 20.2°.The reversal test of McFadden and McElhinny (1990) and the regional tilt test of McFadden (1990) have been performed for the twenty-one sites located in the tectonic structures comprised between the Samghan uplift and Rivand folds (Fig 7). Sites JA20, JA21 and JA22, which have been sampled along the prosecution of the E-W oriented left-lateral Farhadan fault, are considered separately. After tectonic correction, normal and reversed polarity site-mean directions group

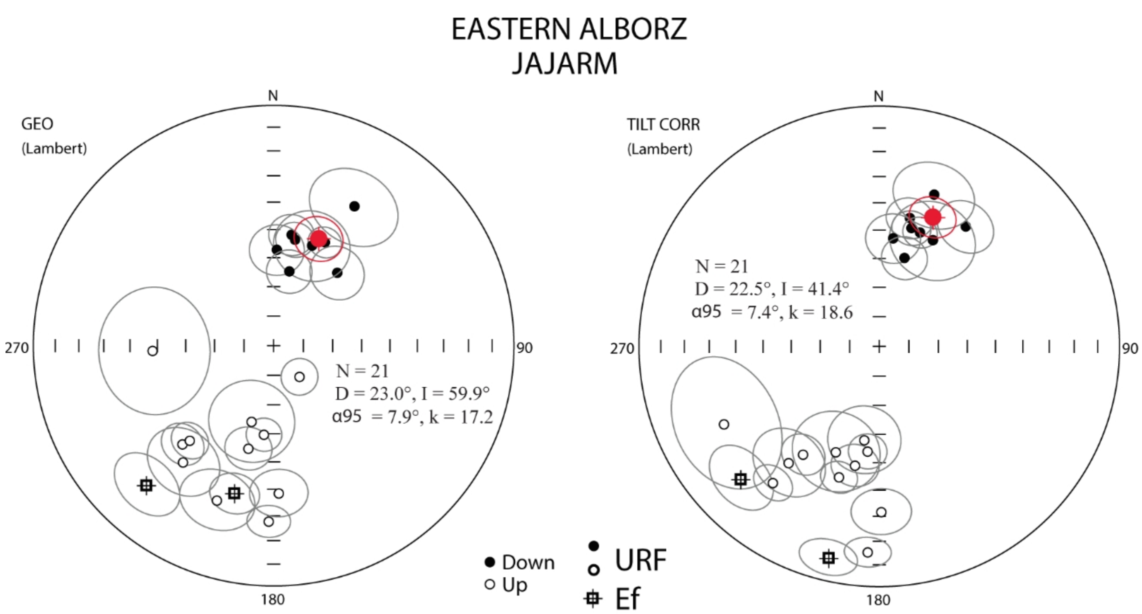

Fig. 6. Equal-area projection of the site-mean directions from the Eastern Alborz (Jajarm). The 95% confidence ellipse for the normal and reverse directions is indicated.

into two antipodal clusters, and the reversal test is positive (type Rc with γo=8.9° and γc=12.5°) according to McFadden and Mc Elhinny (1990). The regional tilt test of McFadden (1990) is also positive at 99% level of confidence ($\xi_{in\ situ}$= 8.193; $\xi_{unfolded}$= 0.368 with a $\xi_{99\%}$= 7.483), suggesting a pre-tilt origin of the isolated ChRM in these sites. The 21 ChRM direction, when reported to normal polarity, are generally oriented NNE and the mean directions for the Samghan uplift and Rivand folds area is declination (Dec.) = 22.5°, inclination (Inc.) = 41.4°, k = 18.6, α_{95} = 7.4° (Table 3 and Fig. 6).

Table 3. Paleomagnetic rotations from eastern Alborz													
Location							***AFC***						
Site	**Lat (°N)**	**Lon(°E)**	**Fm**	**Lithology**	**N/n**	**S0**	**D°**	**I°**	**K**	**α95**	**R (°) ± Err (°)**	**F (°) ± Err (°)**
JA01	36°49'42.7’’	56°26'36.9"	URF	Red-marls	13/8	304/8	215.1	-44.1	61.7	7.1	31.0±7.9	11.6±5.7
*JA02	36°47'18.0"	56°28'49.3"	URF	Red silty marls	12/9	300/4	358.5	42.7	25.2	10.4	-	-
*JA03	36°45'40.6"	56°29'55.9"	URF	Red silty marls	10/9	158/15	16.7	57.1	22.2	11.2	-	-
JA04	36°48'5.10"	56°42'31.3"	*Ef*	Sandstones and marls	11/7	8/26	193.6	-10.5	63.1	7.7	2.5±6.7	45.3±6.4
JA05	36°48'42.7"	56°41'45.3"	*Ef*	Sandstones and marls	10/7	128/10	226.4	-21.4	34.3	10.5	35.3±9.2	34.4±8.5
JA06	36°53'4.80"	57° 8'32.8"	URF	Red marls	14/11	39/8	13.4	44.3	39.5	7.4	9.3±8.3	11.4±5.9
JA07	36°58'44.7"	57°14'14.5"	URF	Red marls	11/4	18/35	243.3	-28.5	21.7	20.2	59.2±18.1	27.2±15.8
JA08	36°51'35.1"	57°16'45.0"	URF	Red marls	11/10	45/6	15.4	47.7	62.4	6.2	11.3±7.4	8.0±5.0
JA09	36°50'10.4"	57°18'4.8"	URF	Red silty marls	12/11	354/6	191.5	-48.0	37.1	7.6	7.4±9.1	7.7±6.1
JA10	36°48'40.2"	57°17'55.3"	URF	Red marls	12/9	28/29	186.3	-53.7	69.6	6.2	2.2±8.4	2.0±5.0
JA11	36°51'18.2"	57°22'6.1"	URF	Red marls	11/9	312/6	19.7	48.3	90.0	5.5	15.6±6.7	7.4±4.5
JA12	36°50'2.40"	57°26'26.9"	URF	Red silty marls	12/9	24/19	35.8	38.4	33.2	9.1	31.7±9.2	17.3±7.2
JA13	36°50'22.0"	57°27'7.5"	URF	Red silty marls	11/9	39/10	193.2	-50.6	79.1	5.8	9.1±7.3	5.1±4.7
JA14	36°51'2.20"	57°28'29.2"	URF	Red marls	14/11	37/13	202.3	-50.6	11.3	14.2	18.2±17.8	5.1±11.2
JA15	36°41'54.6"	57°35'55.4"	URF	Red marls	12/9	220/25	189.1	-57.5	19.6	11.9	5.0±17.7	-1.7±9.3
JA16	36°43'48.8"	57°35'35.5"	URF	Red silty sandstones	10/7	0/0	217.8	-38.4	27.1	11.8	33.7±11.9	17.3±9.3
JA17	36°46'35.4"	57°35'18.8"	URF	Red silty marls	13/8	17/20	19.9	33.3	20.8	12.4	15.8±11.7	23.4±9.8
JA18	36°48'32.9"	57°34'26.2"	URF	Red marls	10/8	14/7	179.3	-31.6	39.8	8.9	-4.8±8.3	24.1±7.1
*JA19	36°44'51.3"	57°39'28.5"	URF	Red marls	10/10	28/35	15.8	21.5	82.2	5.4	-	-
JA23	36°49'56.9"	58° 0'48.4"	URF	Red silty marls	13/7	25/18	217.9	-28.7	96.9	6.2	33.8±5.8	27.1±5.0
JA24	36°47'24.7"	57°58'39.0"	URF	Red marls	14/9	222/16	26.8	49.0	14.6	13.9	22.7±16.8	6.8±10.9
JA25	37° 4'32.6"	56°58'38.2"	URF	Red marls	14/10	44/6	7.3	52.6	30.9	8.8	3.2±11.5	3.6±7.0
JA26	37° 4'37.0"	57° 0'25.7"	URF	Red marls	11/9	35/6	15.9	58.6	48.5	7.5	11.8±11.4	-2.4±6.0
JA27	37° 4'13.2"	57° 1'39.4"	URF	Red silty marls	9/7	20/13	183.2	-15.2	93.8	6.3	-1.0±5.4	41.0±5.1
JA01	36°49'42.7’’	56°26'36.9"	URF	Red-marls	13/8	304/8	358.5	42.7	25.2	10.4	-	-
*JA02	36°47'18.0"	56°28'49.3"	URF	Red silty marls	12/9	300/4	16.7	57.1	22.2	11.2	-	-
*JA03	36°45'40.6"	56°29'55.9"	URF	Red silty marls	10/9	158/15	193.6	-10.5	63.1	7.7	2.5±6.7	45.3±6.4
Mean					**21**		**22.5**	**41.4**	**18.6**	**7.4**	**18.4±7.9**	**14.8±5.9**
Mean			**URF**		**19**		**21.5**	**43.9**	**24.7**	**6.9**	**17.4±7.7**	**12.3±5.5**
JA20	36°54'22.7"	57°53'20.6"	URF	Red silty marls	10/7	319/20	166.1	-47.9	68.5	7.3	-18.0±8.7	6.8±5.9
JA21	36°54'47.4"	57°54'24.1"	URF	Red silty marls	9/8	24/25	167.8	-62.3	15.4	14.6	-16.3±25.7	-6.5±11.5
JA22	36°55'25.6"	57°54'11.9"	URF	Red silty marls	12/12	35/27	1.1	59.3	46.8	6.4	-3.0±10	-3.5±5.2

Notes: Abbreviations: Ef=Eocene sediments; URF=Upper Red Formation; N/n=number of specimens/ number of used speciments in calculations; S0 = bedding plane (mean value for each site); site; D°, I°=site mean declinations and inclinations calculated after tectonic correction (ATC); K=precision parameter; α_{95}=confident limit(statistical parameters after Fisher, 1953); R (°) ± Err (°)=rotation and respective error; F (°) ± Err (°)=flattening and respective error. R and F values (and associated error) were calculated according to the method by Demarest (1983) using the coeval European pale poles from Torsvik et al., (2012).

Two of the 3 sites (JA20-22) located along the prosecution of the E-W oriented left-lateral Farhadan fault have a reversed polarity, whereas 1 site has a normal polarity magnetization (Table 3). ChRM directions, when all the sites are translated to normal polarity, are oriented N to

Table 4.

Age P (Ma)	λ (°N), ϕ (E), A95
10 (URF)	-86.7°, 330.0°, 1.8°
20 (QOM)	-84.4°, 332.1°, 2.6°
30 (LRF)	-83.1°, 326.5°, 2.6°
40 (Ef)	-81.1°, 324.3°, 2.9°

Note: Abbreviations: Qom= Qom Formation; URF=Upper Red Formation; LRF= Lower Red Formation; (λ (°N), ϕ (E), A95) = latitude of the paleopole (°N), longitude of the paleopole (°E), and confi dence limit on the paleopole at the 95% level, respectively.

NNE. Clustering, as measured by the Fisher k parameter, improved from k = 31.9 for in-situ site means to k = 84.5 for unfolded directions, indicating ChRM was acquired prior to folding.

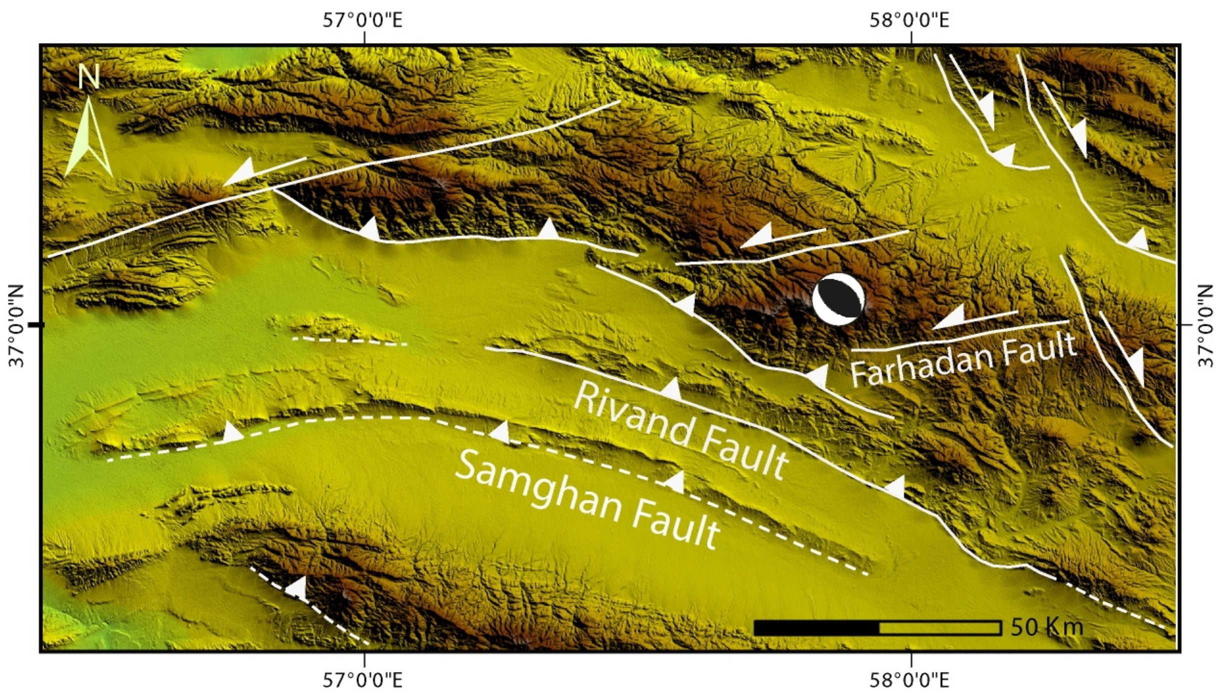

Fig. 7. Shaded-relief topographic map (SRTM data) of the eastern part of Alborz Mauntain, and the main faults of the area. Focal mechanisms of Esfarayen earthquakes (1969) is also reported.

2.3. Analysis of Paleomagnetic rotations in Alborz

Since no APWP is available for Iran, the observed paleomagnetic directions have to be compared with those expected for the Eurasian plate. Paleomagnetic rotations were then computed in relation to the fixed Eurasian plate using the coeval European paleopoles from Torsvik et al., (2012). Rotation values and associated 95% confidence limits were calculated according to the method of Demarest (1983) (Table 1, 2, 3).

In the Western Alborz all the paleomagnetic sites are from lower-middle Miocene URF and their paleomagnetic directions have been compared with the 10 Ma reference pole. Among the sites, nine show statistically significant CW rotations, and six sites show mean declinations rotated clockwise respect to the reference poles, but with error greater than rotation values. Only one site (MJ05) shows mean declination rotated CCW, whereas four more sites from the Manjil basin show mean declination rotated CCW, with errors greater than rotation values. At the basin scale the mean declination for the Alamut Basin is rotated 17.8° CW (±10°) (Fig. 8, Table 1), whereas the Manjil basin shows a limited and statistically not significant CW rotation (R=6.2° ±9.2°) (Fig. 8, Table. 1).

In the Central Alborz we calculated declination respect to the coeval reference poles for thirteen Lower Middle Miocene sites from the URF, two sites (SM01, SM02) from Upper Oligocene-Lower Miocene Qom Formation and two sites (SM13, SM14) from Oligocene Lower Red Formation (Table. 2, Fig. 1). Declinations from eleven of the seventies sites show significant CCW rotations, whereas six sites are statistically not rotated. CCW rotations are comprised between -11° (SM09 and SM22) and -63° (SM11), whereas at the regional scale the Central Alborz show a mean CCW rotation R= -21.4°(± 9.1°). When only the 13 sites from Lower-Middle Miocene URF are considered together the regional direction is declination (Dec.) = 342.9°, inclination (Inc.) = 40.2°, k = 17.6, α_{95} = 10.2°, and the calculated rotation respect to the coeval reference pole is R=-21.1° ± 10.6° (Figg. 8, Table 2).

Fourteen sites show statistically significant CW rotations (comprising the Eocene site JA05), whereas seven sites are statistically not rotated respect to the reference directions (which include the Eocene site JA04). When the 19 sites from Lower-Middle Miocene URF are considered together the regional direction is declination (Dec.) = 21.5°, inclination (Inc.) = 43.9°, k = 24.7, α_{95} = 6.9°, and the calculated rotation is R=17.4° ± 7.7° (Fig. 8, Table 3). Conversely, the three sites located along the prosecution of the Farhadan fault, show CCW rotation (JA20) or are not statistically rotated respect to the expected direction (JA21 and JA22) (Fig.2).

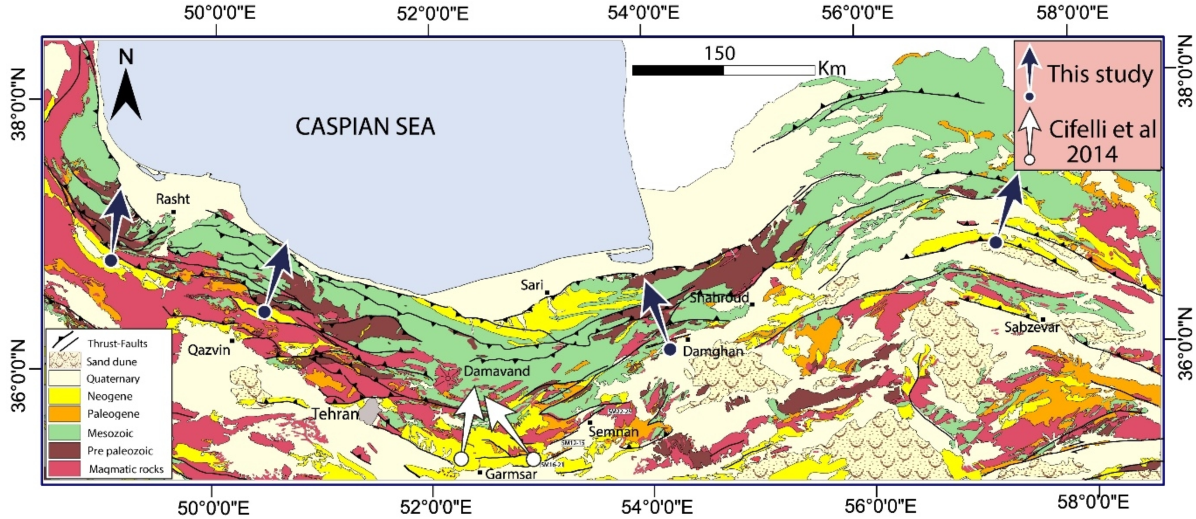

Fig. 8. Paleomagnetic directions from the Alborz Mountains, Rotation is calculated relative to Torsvik et al., (2012). European APWP for the 40 to 10 Ma time interval.

Taken together, these paleomagnetic data show that the western arm of the Alborz, oriented NW-SE (Fig. 8), rotated CW, whereas the Central part, oriented SW–NE, rotated CCW and eastern arm, oriented NW-SE, rotated CW. Hence, the Alborz orogen resulted from orocline bending with most of its curvature acquired after about 7.6 Ma (Cifelli et al, 2015), which is the upper age of the Upper Red Formation (Ballato et al., 2008). In eastern Alborz the orogenic curvatures seems to follow the shape of the continental blocks located to the south (Fig.9), like Central Iran and the Eastern Iranian blocks (Hollingsworth et al., 2010, Robert et al., 2014, Cifelli et al., 2015). For the central and western Alborz, it seems suitable to attribute the development of the Alborz Mountains orocline, to bending processes associated with the presence of the South Caspian Basin (Fig. 9), which acted as back stop of orogenic deformation (Robert et al., 2014, Cifelli et al., 2015). Cifelli et al., 2015 suppose that the interaction between the different crustal blocks within the collision zone caused oroclinal bending in northern Iran.

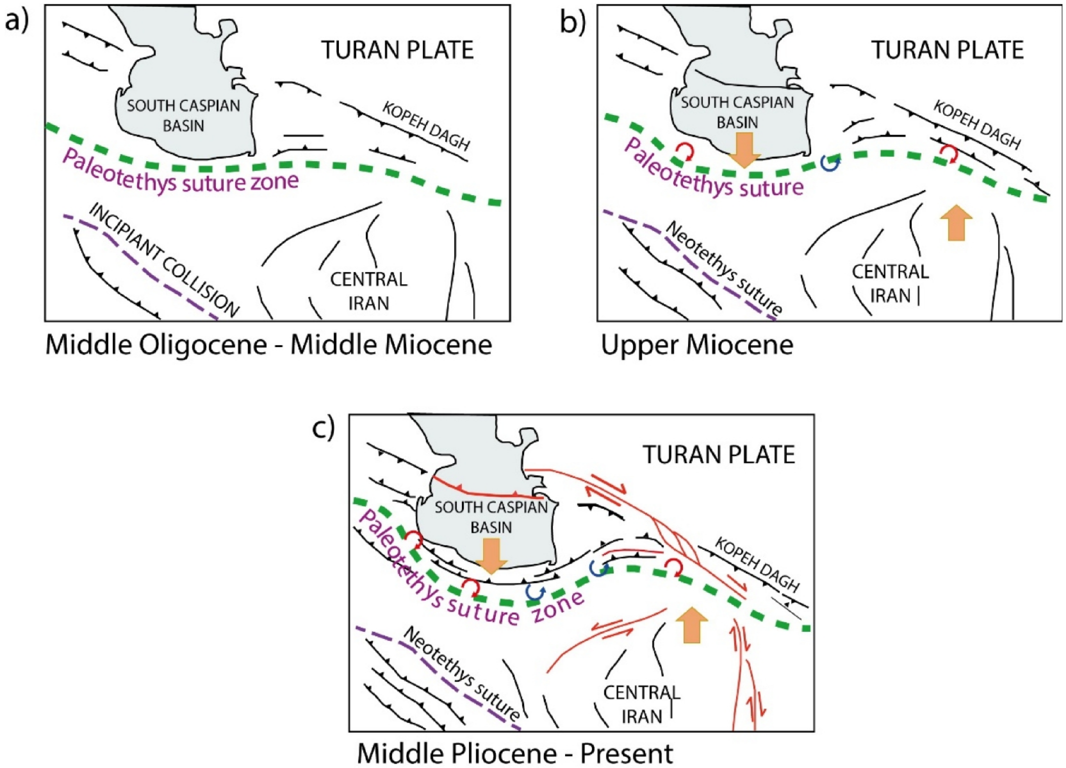

Fig. 9. Schematic reconstructions of the evolution of the Southern Alborz Mountains during a) the Middle Oligocene-Middle Miocene; b) the Upper Miocene and c) the Middle Pliocene to the present-day. Modifide from Robert et al., 2014 and Hollingsworth et al., 2010.

3. Shahdad Thrust- fold belt

Paleomagnetic samples have been taken from the Neogene red marls and siltstones of the Upper Red Formation of Shahdad fold-thrust belt located in the southwest of Lut block. Sampling has been done along the convex shape of this thrust belt from North to South. Paleomagnetic data show CCW rotations of 22.8 (±18.6) in Northern part, 13.8 (±7.9) CCW in North-Center, 16 (±17.9) CCW in South-Center and 5.4 CW in Southern part (Fig. 11, Table 5). These paleomagnetic data represent that the Northern part of Shahdad Fold and Thrust Fault, oriented NNW-SSE, rotated relatively large CCW, Central part, oriented N-S, rotated CCW and Southern part, oriented NNE-SSW, rotated CW. By preliminary results and the positive orocline test (Fig. 10), we suggest the secondary nature for the Shahdad Fold and Thrust Fault arc (Fig. 11), which at least obtained part of its curvature after the Late Miocene which is the upper age of the Upper Red Formation.

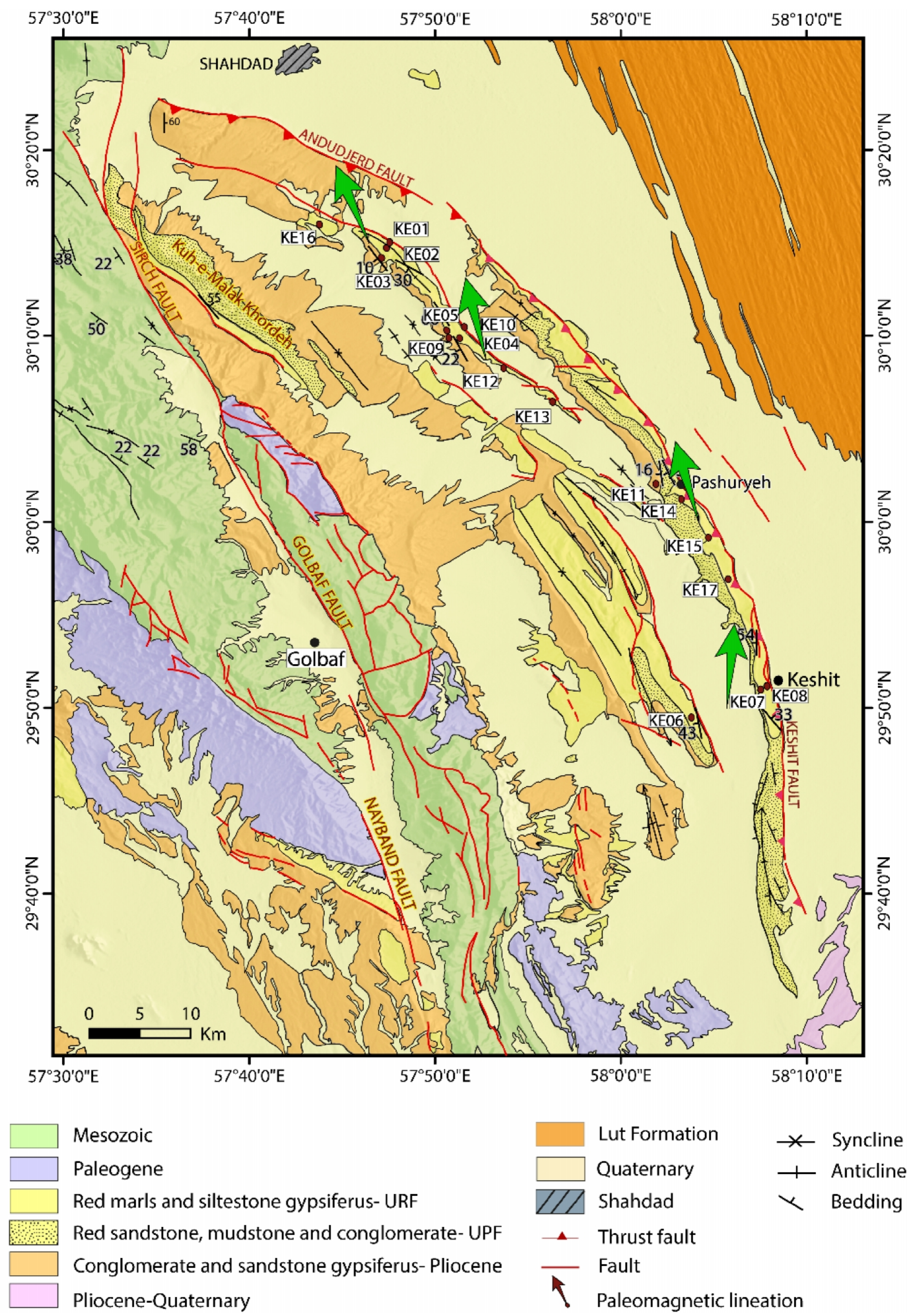

Fig. 11. Paleomagnetic directions from the Shahdad Thrust-Fold belt, Rotation is calculated relative to the Besse and Courtillot (2002) Eurasian APWP for the time interval comprised 10 Ma.

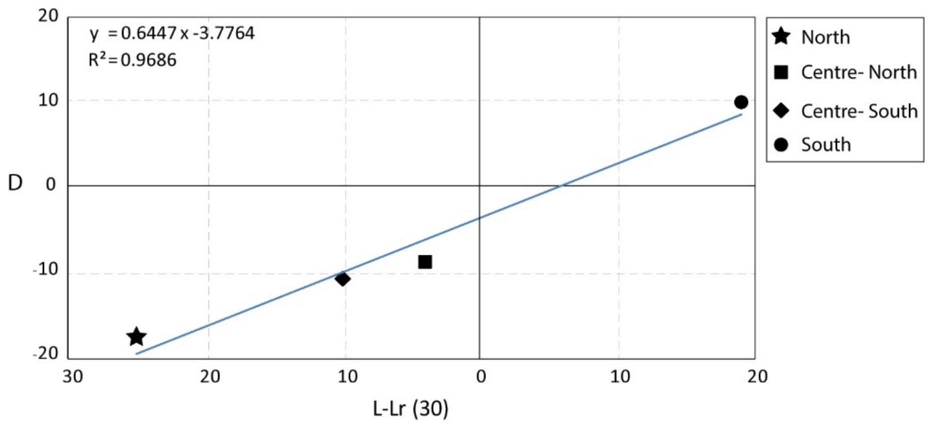

Fig.10. Oroclinal test for the Shahdad Thrust-Fold Belt.

Table 5. Paleomagnetic rotations from Shahdad Thrust-Fold belt

Region	**Lat(°)**	**Long(°)**	**Fm**	**N**	**D(°)**	**I(°)**	**K**	**α_{95}**	**R (°) ± Err (°)**	**F (°) ± Err (°)**
North	30°15'	57°46'	UPR	4	342.3	41.8	27.88	17.7	-22.8±18.6	-13.8±7.9
Center	30°8'	57°53'	UPR	6	351.3	37.2	47.8	7.8	-13.8±7.9	-13.8±7.9
Center-South	30°00'	58°03'	UPR	4	349.1	57.7	35.3	15.7	-16±17.9	-13.8±7.9
South	29°5'	58°06'	UPR	3	10.5	35.7	25.8	24.8	5.4	-13.8±7.9

Notes: Abbreviations: URF=Upper Red Formation; N =number of sites; D°, I°=site mean declinations and inclinations calculated after tectonic correction; K=precision parameter; α_{95}=confident limit (statistical parameters after Fisher, 1953); R (°) ± Err (°) =rotation and respective error; F (°) ± Err (°) =flattening and respective error. R and F values (and associated error) were calculated according to the method by Demarest (1983) using the coeval European paleopoles from Besse and Courtillot, (2002).

Chapter IV

Right-lateral transpressional tectonics along the boundary between Lut and Tabas blocks (Central Iran)

Francesca Cifelli, Massimo Mattei, Hamideh Rashid and Jalil Ghalamghash

This chapter has been published in 2013:

Geophysical Journal International, vol. 193, Pages 1153–1165
http://dx.doi.org/10.1093/gji/ggt070

Keywords: Magnetic fabrics, transpressional tectonics, inversion tectonics, Late Jurassic, transected folds, Central Iran.

Abstract:

One of the major issues for understanding the tectonic evolution of continental regions is how pre-existing discontinuities influence the style and distribution of deformation, which is often not obviously and uniquely connected to the plate-boundary kinematics. Iran represents one of the most instructive regions to study continental deformation, as here the present-day Arabia-Eurasia convergence is accommodated in a very wide area over a range of structures. The tectonic boundary between the Lut and the Tabas blocks of Central Iran currently accommodates part of the Arabia-Eurasia convergence by right-lateral strike-slip faults, associated with NNW-SSE oriented fold-related thrust. During Middle-Late Jurassic, this boundary was the location of a large-scale shelf-lagoon carbonate platform-slope-to-basin depositional system, mainly controlled by the activity of a N-S oriented normal fault system. In this study, the geometry and the kinematics of the deformation at the tectonic boundary between the Lut and the Tabas blocks, are reconstructed from an integrated AMS (Anisotropy of Magnetic Susceptibility) and structural analysis in the Upper Jurassic Garedu Red Beds Fm., outcropping at the core of a NNE-SSW oriented syncline in the northern Shotori Range. AMS and structural results indicate that the Upper Jurassic Garedu Red Beds Fm. syncline can be defined as a transected fold, where the mismatch between fold hinge and magnetic fabric/cleavage is about 15° counterclockwise, suggesting that this fold system formed as a consequence of right-lateral transpressional tectonics. Results from this study thus document the evolution of Jurassic normal faults to a transpressional tectonic boundary between the Tabas and Lut crustal blocks sometime between the Lower Cretaceous and Paleocene.

1. Introduction

Transpressional tectonics has been recognized as a main deformation feature in many orogenic belts and oblique convergent plate boundaries which are characterized by a very long history of deformation and where the main deformation features are influenced by the geometry and orientation of preexisting tectonic structures rather than by plate boundary kinematics (Holdsworth *et al.* 1998 and references therein). Therefore, the identification of structures involved in transpressional tectonics is essential to understand how shortening due to plate convergence is accommodated within continental regions.

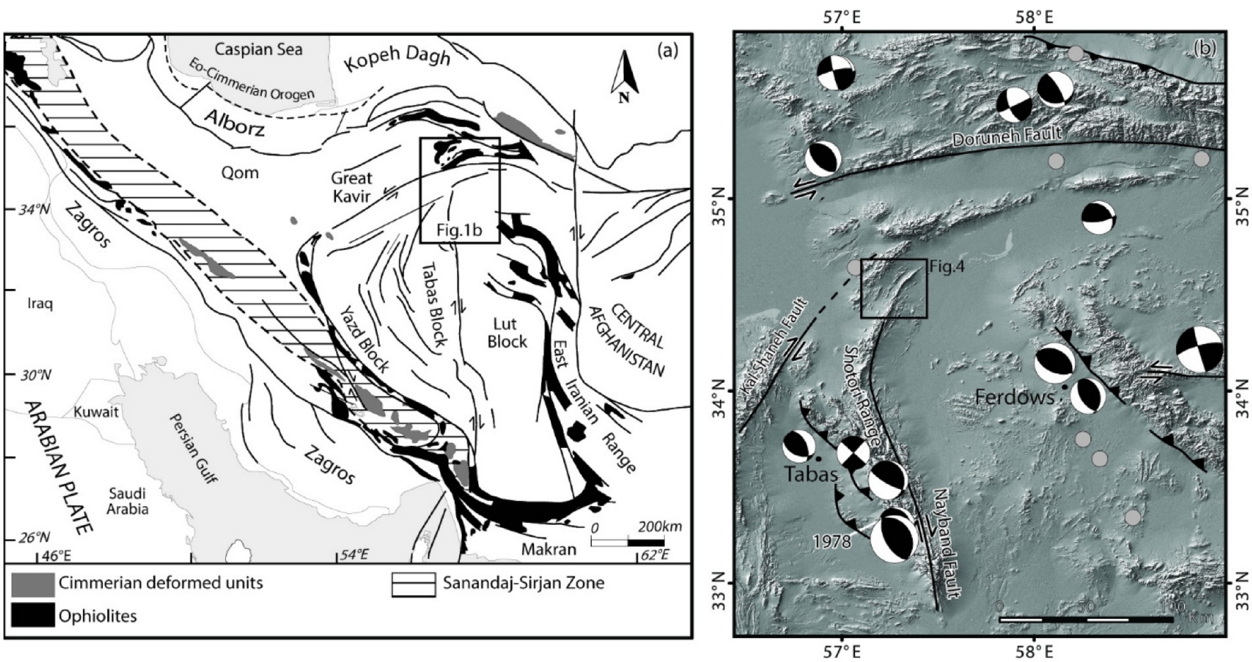

Fig. 1. (a) Tectonic scheme of the Iranian region. (b) Shaded-relief topographic map (SRTM data) of the Tabas and Lut blocks area, and main active faults of the area. Focal mechanisms and epicentres of earthquakes with Ms= 5.7 are also reported (modified from Jackson 2001).

Central Iran is a suggestive example of geological areas that underwent long-lived tectonic deformation, being its present-day position and structural configuration the result of different geodynamic events (Fig. 1a). These events include the collision of different continental blocks, forming the CEIM (Central and East Iranian Microcontinent, *sensu* Takin 1972), during the Late Triassic Eo-Cimmerian orogeny (Sengor 1984; Zanchi *et al.* 2006; Zanchi *et al.* 2009; Muttoni *et al.* 2009), the Cretaceous opening of small oceanic basins around the CEIM, and the closure of these basins at the end of Late Cretaceous, in connection with the motion of the Arabian Plate and the closure of Neotethys (Stöcklin 1974; Tirrul *et al.* 1983; Dercourt *et al.* 1986; Sengör *et al.* 1988; McCall 1997; Stampfli & Borel 2002; Bagheri & Stampfli 2008; Rossetti *et al.* 2010). Today, Central Iran is characterized by N-S right-lateral (e.g., the Nayband fault) and E-W left-lateral oriented strike-slip fault systems (e.g., the Doruneh fault) that accommodate the present-day Arabia-Eurasia convergence in a way that cannot be easily predicted by plate tectonics kinematics (Tchalenko & Ambraseys, 1970; Jackson & McKenzie 1984; Jackson *et al.* 1995; Berberian & Yeats 1999; Vernant *et al.* 2004; Walker & Jackson 2004; Allen *et al.* 2004, Allen *et al.* 2011) (Fig. 1b).

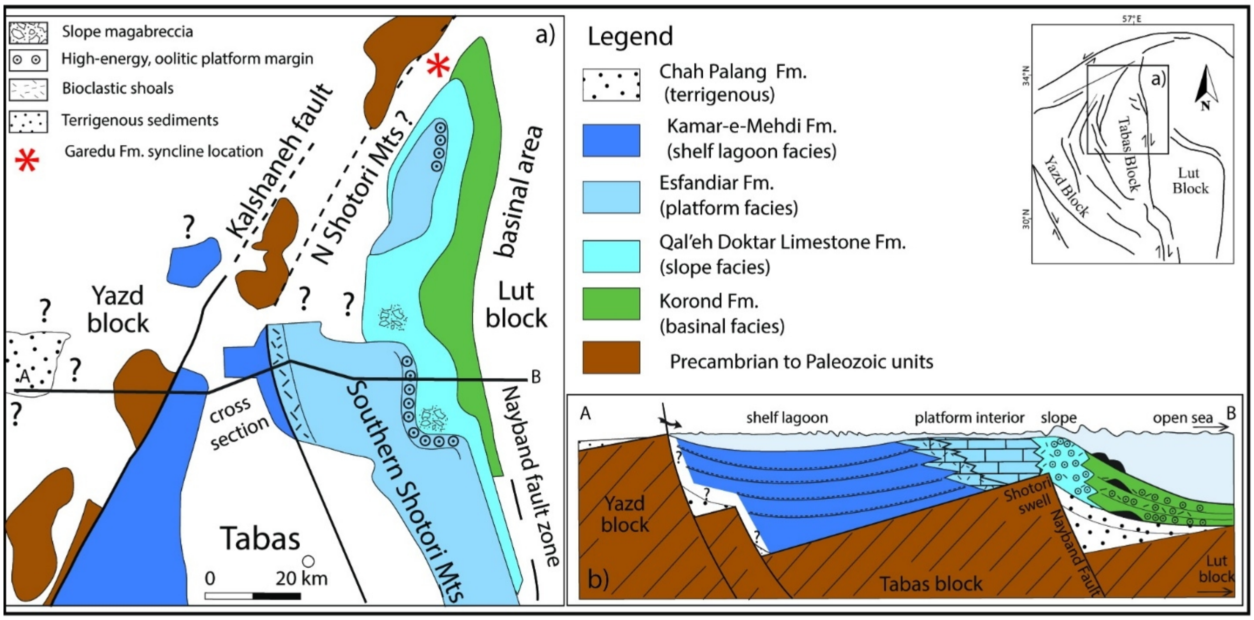

Fig. 2. (a) Early-Middle Oxfordian palaeogeography of the northern Tabas Block; (b) simplified geological section along the Late Jurassic carbonate platform-to-basin structures across the Tabas and Lut blocks of Central Iran (redrawn and modified from Wilmsen et al. 2010).

In Central Iran, N-S right-lateral strike-slip faults define the boundary between the Yazd, Tabas and Lut blocks (Fig. 1a). The Shotori Range, a prominent mountain chain mainly formed by Jurassic sediments, dominates the region at the boundary between Tabas and Lut blocks. During the Middle and Late Jurassic, this area was characterized by a carbonate platform-to-basin depositional system, whose evolution was mainly controlled by tectonic activity of N-S oriented (in present-day coordinates) normal faults (e.g. Nayband fault) (Fursich *et al.* 2003; Wilmsen *et al.* 2009a; Wilmsen *et al.* 2009b; Wilmsen *et al.* 2010) (Fig. 2). During Late Cretaceous and Tertiary, such pre-existing tectonic structures were reactivated and the Shotori Range units were deformed by folds and thrust faults and dissected by N-S to NNE-SSW oriented right-lateral strike-slip faults, which show evidence of present-day activity (Ruttner *et al.* 1968a; Ruttner *et al.* 1968b; Berberian, 1979). In the Shotori Range structural studies have been mainly focused on active tectonics in the Tabas fold system, where in 1978 a destructive earthquake occurred (Berberian, 1979; Walker *et al.* 2003, Fig. 1b). Conversely, no specific studies have been published so far on the deformation history of the northern Shotori Range, and on the geometry and kinematics of the main tectonic structures affecting the region.

In order to characterize this main intracontinental fault of the Arabia-Eurasia collision zone and to define the deformation style across this tectonic boundary, in this work we combined magnetic fabrics (AMS) and structural analysis. We present AMS and structural data from the Upper Jurassic Garedu Red Beds Fm., cropping out in a NNE-SSW oriented syncline core, at the western boundary of the northern Shotori Range. Results show a well-defined magnetic fabric, which is oriented parallel to the cleavage planes system and shows a systematic mismatch with the main fold trend. These geometrical relationships are typical of a transected fold and suggest that the Late Cretaceous and Tertiary shortening events of Central Iran were accommodated by a dextral transpressional tectonics along the tectonic boundary between Tabas and Lut blocks. Results from this study underline the importance of the re–activation of preexisting tectonic structures and emphasize the role of the right-lateral transpressional deformation along this main tectonic boundary of Central Iran.

2. Geological setting

Central Iran is the result of the assemblage of the Cimmerian microplates (CEIM, *sensu* Takin, 1972), which drifted from Gondwana during the Permian and collided with Eurasia in the Late Triassic (e.g. Sengor 1984; Muttoni *et al.* 2009), giving place to the Eo-Cimmerian orogeny (Sengor 1979; Stampfli *et al.* 1991; Van der Voo 1993; Zanchi *et al.* 2006; Zanchi *et al.* 2009). Since that time Central Iran has been the place of several episodes of opening and closure of back arc basins, related to the consumption of the Neo-Tethys Ocean and the collision of the Arabia plate (e.g., Berberian & King 1981; Dercourt *et al.* 1986). These episodes caused the Late Cretaceous emplacement of the ophiolite mélange belts, which surround Central Iran and are associated to an important deformation phase, well documented in the numerous mountain chains dominating the area (e.g., Tirrul *et al.* 1983; Rossetti *et al.* 2010). During Tertiary, shortening related to the Arabia-Eurasia collision has been – and is at present being – taken up mainly by deformation in the Zagros, Alborz, and Kopeh Dag thrust-and-fold belts (Fig. 1a). Today, the fault-bounded crustal blocks of Central Iran (Yazd, Tabas and Lut blocks) show little internal deformation, and active convergence is mainly accommodated by NE–SW left-lateral and N–S right-lateral strike-slip faults, which can adjust the NNE–SSW Arabia-Eurasia convergence if they are allowed to rotate clockwise (CW) and counterclockwise (CCW), respectively (Walker & Jackson 2004; Allen *et al.* 2011; Mattei *et al.* 2012).

The Shotori Range is one of the most prominent mountain chains in Central Iran (Fig. 1b). Its length is more than 200 km and elevations reach 2800 m above sea level. The Shotori Range separates two very flat areas, the Lut desert to the east, and the Tabas and Great Kavir plains to the west (Fig. 3a), which correspond to different crustal blocks, characterized by different stratigraphy and tectonic evolution (e.g., Stöcklin *et al.* 1965). The Shotori Range itself is formed by two sectors with different orientation, elevation, and width. The southern branch, which develops to the east of the Tabas plain between latitude 33°N and 34°N, is NNW-SSE oriented. It is characterized by the highest elevations and width, which gradually decreases moving southward. Along the southern branch of the Shotori range, the foothills that extend toward the Tabas plain are interested by active thrust-related folding process testified by the destructive 1978 Tabas earthquake (Berberian 1979). The northern branch (Kuh-e-Bam and Kuh-e-Masafer in Fig. 3a), which extends north of 34°N, is NNE-SSW oriented, shows lower altitudes, and is only 10 km wide.

The stratigraphy of the northern Shotori range is mostly characterized by Jurassic units, organized in several sedimentary cycles bounded by angular unconformities (Fig. 3b). Following a phase of mostly continental siliciclastic sedimentation in the Early and Middle Jurassic (Shemshak Fm.), mixed siliciclastic–calcareous units deposited (Middle Jurassic Parvadeh and Baghamshah Fms.), marking a pronounced transgression and a progressive trend toward a deep marine deposition.

This evolution was mostly controlled by tectonic subsidence of the Tabas block related to the activity of N-S oriented normal faults, e.g. Nayband and Kal Shaneh faults (Fig. 2). Starting from

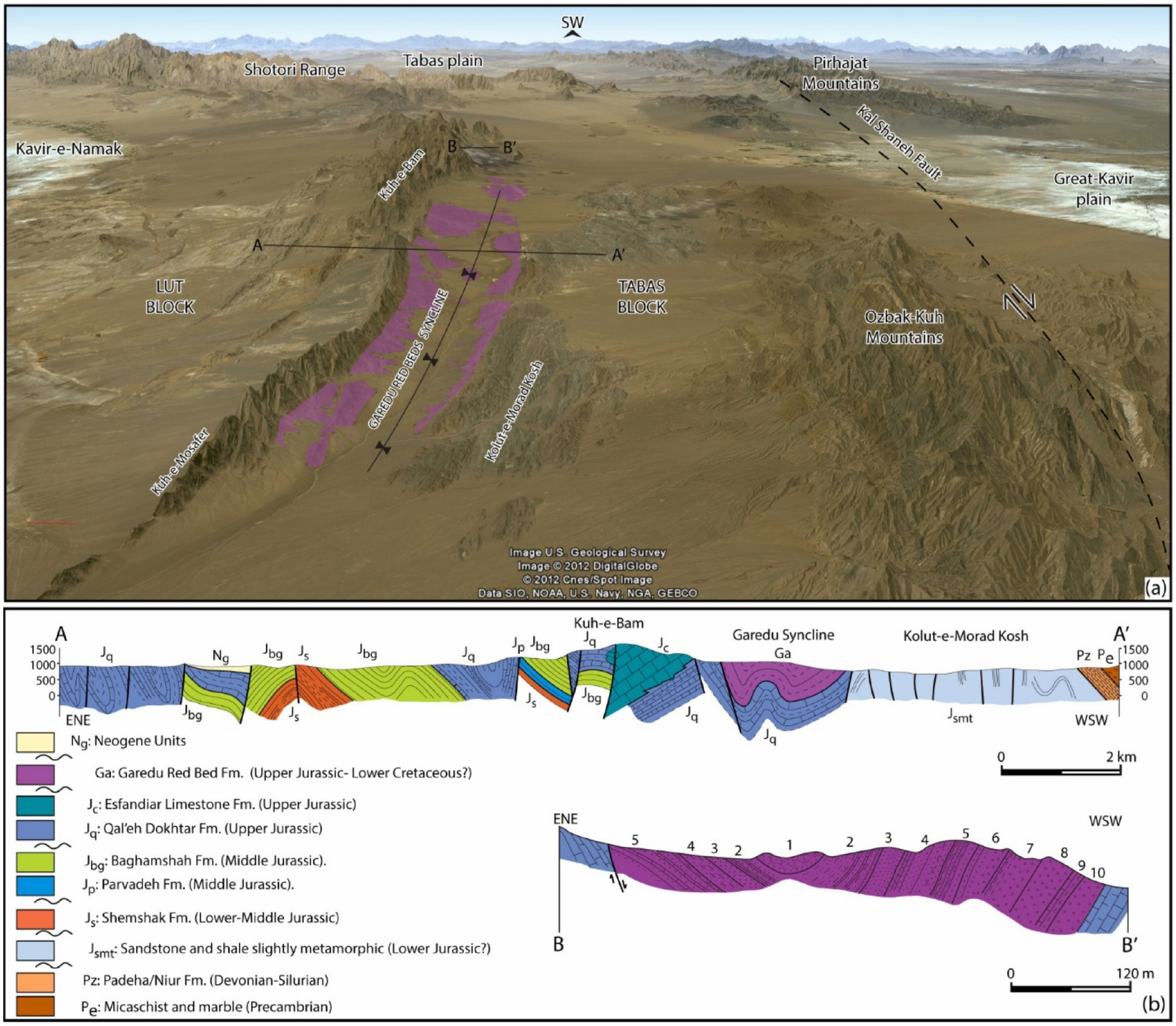

Fig. 3. (a) Google map view of the Garedu syncline and surrounding areas. A-A' and B-B' are the location of the two cross sections drawn in Fig. 3b. b) A-A': regional geological section across the Garedu syncline (modified from Ruttner *et al.* 1968a). B-B': geological section of the Garedu syncline close to the Garedu mine, where the stratigraphy of the Garedu syncline close to the Garedu mine, where the stratigraphy of the Garedu Red Beds Fm. is also described. 1) red sandstones and shales alternating with oolitic limestones; 2) limestones alternating with red sandstones; 3) red sandstones; 4) limestones alternating with red sandstones and shales; 5) red sandstones and shales alternating with limestones; 6) conglomerates, sandstones and shales; 7) conglomerates and red shales; 8) coarse-bedded conglomerates; 9) limestones and shales; 10) coarse conglomerates (redrawn from Ruttner *et al.* 1968b).

the uppermost Middle Jurassic (Callovian) a low-latitude carbonate depositional system was established. This depositional system persisted until the latest Oxfordian/Early Kimmeridgian (Esfandiar and Qal'eh Dokhtar limestone formations) and represents a large-scale shelf-lagoon carbonate platform-slope-to-basin system that developed across the present-day boundary between the Tabas and Lut blocks (Wilmsen *et al.* 2009a) (Fig.2). The Esfendiar Fm. consists of medium-bedded to massive carbonates, which were sedimented on an extensive carbonate platform. Towards the east, at the junction of the Tabas and Lut blocks, the platform sediments of the Esfandiar Limestone Fm. interfinger with deeper-water sediments of the Qal'eh Dokhtar Limestone Fm. (Fig. 2b), formed by oolitic–bioclastic limestone intercalated with marl and marly limestone. The carbonate platform-to-basin depositional system ceased during the Late Jurassic as a consequence of renewed tectonic activity along the Nayband fault (Wilmsen *et al.* 2010). During this period the strata of the Esfandiar and Qal'eh Dokhtar Limestone formations were partly eroded, and subsequently covered by Kimmeridgian–Tithonian limestone conglomerates and red siliciclastic sediments of the Garedu Red Bed Fm., which mark the evolution of the northern Shotori Range area toward a fluvial and flood-plain depositional system (Wilmsen *et al.* 2009a). The Mesozoic succession of the Shotori range is covered, via an angular unconformity, by conglomerate deposits overlaid by Eocene volcanic units, which have been attributed at the Kerman Fm., Paleocene in age (Ruttner *et al.* 1968a; Ruttner *et al.* 1968b).

Folds and low-angle thrust faults, represent the main structural features of the axial part of the chain (Fig. 3b). Conversely, the eastern and western borders of the Shotori Range are characterized by the occurrence of high-angle faults (e.g. Nayband Fault), parallel to the general trend of the chain, which show evidence of recent tectonic activity (Ruttner *et al.* 1968b). The western boundary of the northern Shotori Range is formed by a NNE oriented syncline, extending over about 80 km. The core of the syncline, which represents the boundary between the Shotori Range tectonic structure, to the west, and the eastern margin of the Ozbak-Kuh Mountains, to the east, is formed by the Late Jurassic Garedu Red Beds (Fig. 3a). The Garedu syncline can be described as an open fold with a smooth and rounded hinge, with an almost vertical axial plane (Fig. 3b). Sideways most of the flanks of the fold, the boundary between the Garedu Red Beds Fm. and the underlying units is stratigraphic (Ruttner *et al.* 1968b) (Fig. 4). A NNE-SSW oriented sub-vertical fault dismembers the eastern flank of the fold in its southern part, whereas along the northern part, the contact is mostly tectonic, and a high-angle fault omits the basal conglomerates of the Garedu Red Beds Fm.

The stratigraphy of the Garedu Red Beds Fm. has been described in previous papers (Ruttner *et al.* 1968a; Wilmsen *et al.* 2009a). In particular, Ruttner *et al.* (1968a) have measured a detailed stratigraphic section of the Garedu Red Beds in a small syncline located 2.5 km east-southeast of the Garedu Mine (see location in Fig. 3a). In this area the Garedu Red Beds stratigraphically overlie the Qal'eh Dokhtar Fm. limestone and reach a stratigraphic thickness of about 470 m. The base of the Garedu Red Beds Fm. is formed by about 8 m of red coarse-grained conglomerates, which pass upward to alternation of red sandstones, siltstones and shales, and rare marine grey limestones levels (see the B-B' geological section in Fig. 3b for further details). The age of the Garedu Red Beds Formation is poorly constrained by biostratigraphic data. South of the Tabas plain, they overlie the Callovian–Lower Kimmeridgian Esfandiar Limestone Formation, suggesting a post-Early Kimmeridgian age (Wilmsen *et al.* 2009a). Ruttner *et al.* (1968a) reported rare calcareous algae of inferred Kimmeridgian–Tithonian age from the Garedu Red Beds Formation of the northern part of the Shotori Mountains.

3. Methods and sampling

In the last decades, numerous studies have shown that the anisotropy of magnetic susceptibility (AMS) can be related to mineral and tectonic fabrics and that it can be successfully employed in the field of structural geology as a powerful tool for fabric analysis in different rock types (e.g., Jackson & Tauxe 1991; Rochette *et al.* 1992; Tarling & Hrouda 1993; Borradaile & Henry 1997; Mattei *et al.* 1997; Cifelli *et al.* 2005). The principal axes of AMS ellipsoid are usually close to the strain ellipsoid axes, indicating that the magnetic fabric is a strain-induced phenomenon, and suggesting that magnetic fabric measurements are at least qualitatively significant with respect to the strain history of rocks (e.g. Goldstein & Brown 1988). The AMS is a second-rank symmetric tensor that can be geometrically expressed in terms of three principal susceptibilities axes (maximum, intermediate and minimum, $K_1 \geq K_2 \geq K_3$). In sedimentary rocks, an evolution of the magnetic fabric has been observed with the increasing of deformation (Fig. 5). In undeformed sediments the magnetic foliation is parallel to the bedding plane; this fabric is attributed to depositional and/or compaction processes (Lowrie & Hirt 1987; Lee *et al.* 1990; Paterson *et al.*

1995) (Fig. 5a). If these sediments undergo tectonic deformation, progressively a tectonic AMS subfabric will develop modifying the primary sedimentary magnetic fabric, according to the nature and extent of deformation. When the deformation is low to moderate, the principal maximum axis K_1 (magnetic lineation) will align perpendicular to the shortening direction (Kissel *et al.* 1986; Mattei *et al.* 1997; Sagnotti *et al.* 1998; Pares & Van der Pluijm 2002; Aubourg *et al.* 2004; Cifelli *et al.* 2009; Oliva-Urcia *et al.* 2009, Aubourg *et al.* 2010, among many others) (Fig. 5b).

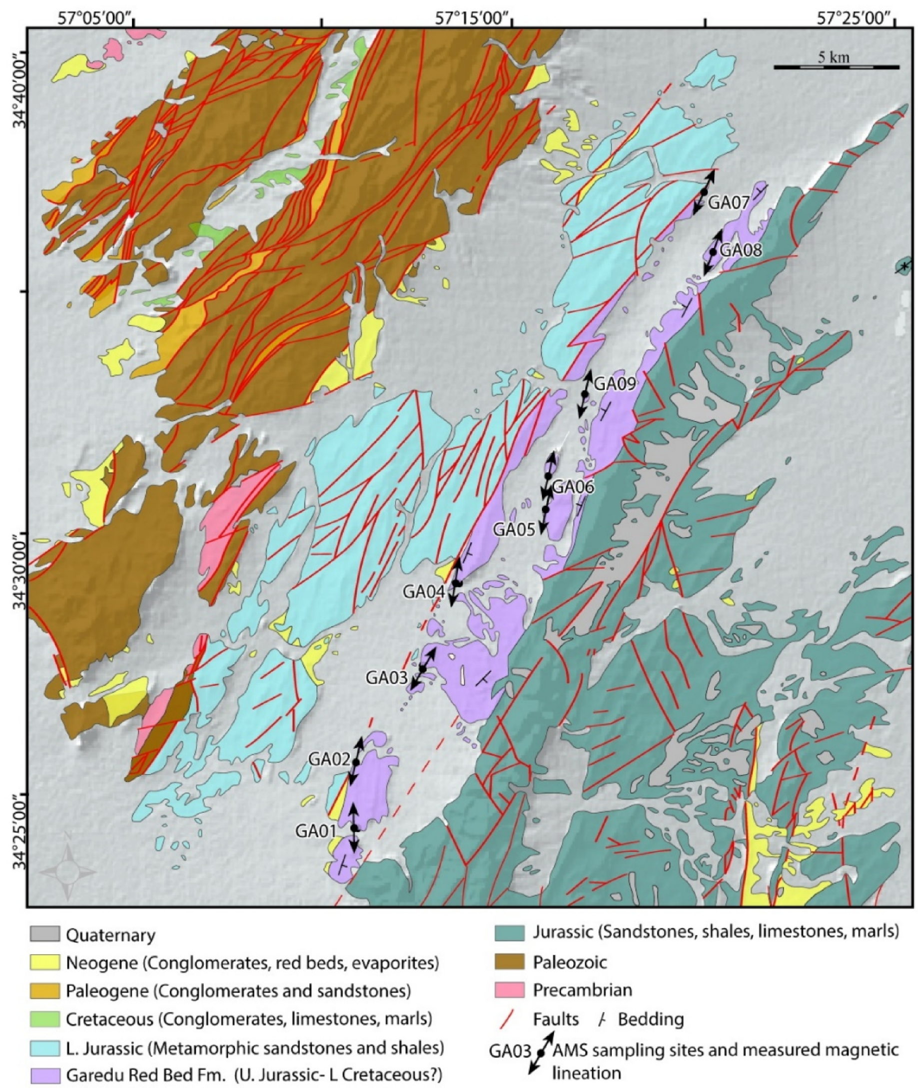

Fig. 4. Simplified geological map of the Garedu Red Beds syncline. (Redrawn and simplified from Aghanabati 1994a, Aghanabati 1994b and Ruttner *et al.* 1968b). AMS sampling sites and directions of *in situ* magnetic lineations from this study are also reported.

K_3 remains perpendicular to the bedding plane, still marking the primary magnetic fabric acquired during compaction. If shortening increases, the K_3 becomes distributed along a girdle that is parallel to the tectonic shortening direction, and the magnetic ellipsoid is prolate (Pares & Van der Pluijm 2002) (Fig. 5c). Additional shortening returns the magnetic ellipsoid to the flattening field and the magnetic foliation becomes parallel to the flattening plane and mesoscopic cleavage (Lowrie & Hirt 1987; Housen & Van der Pluijm 1991; Hirt *et al.* 1995; Luneburg *et al.* 1999; Debacker *et al.* 2009) (Fig. 5d), whereas the magnetic lineation is aligned parallel to the stretching direction, with the development of a purely tectonic magnetic fabric (Fig. 5e-f). For this reason the orientation of K_1 (magnetic lineation) represents a useful structural information that can be integrated with the classic strain markers in order to define the deformation pattern in sedimentary sequences (Fig. 5 g-h).

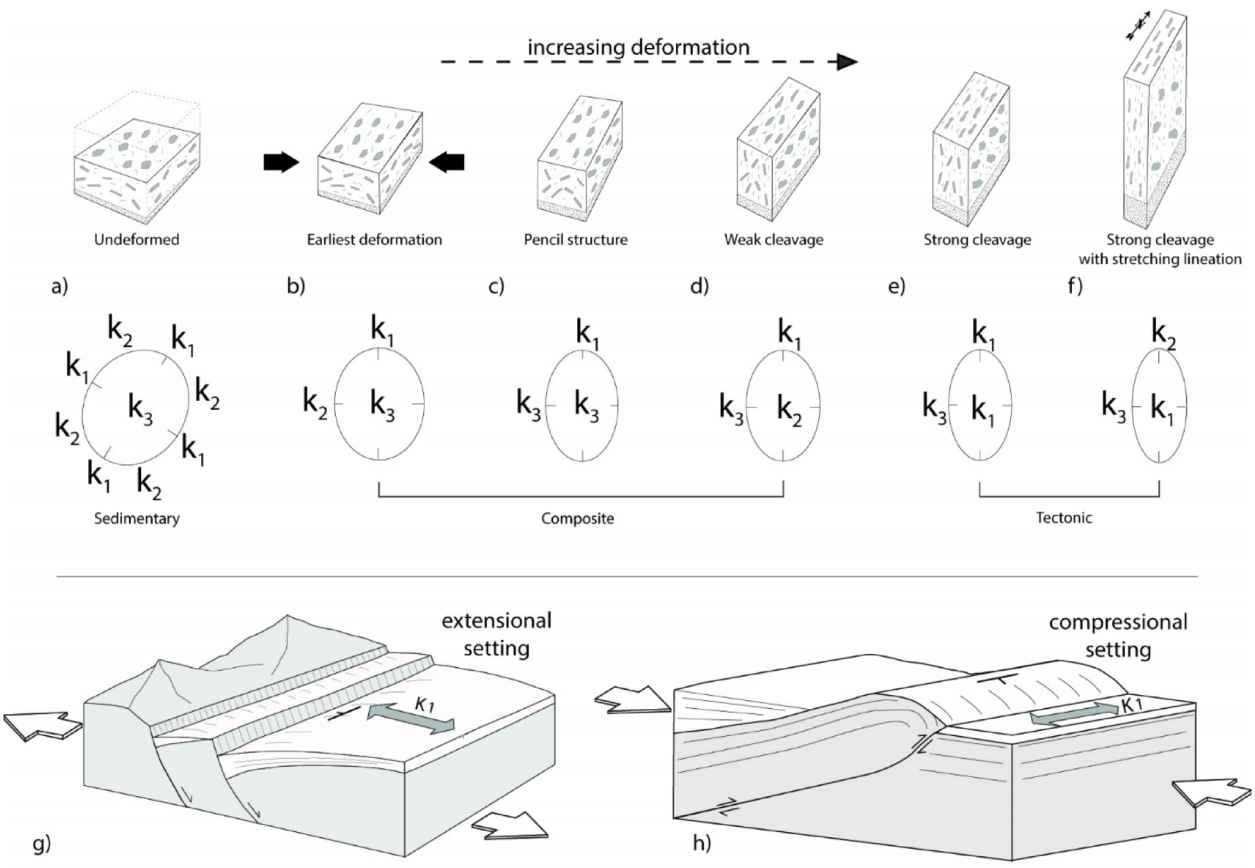

Fig. 5. Evolution of the directional and shape characteristics of AMS and strain ellipsoids during progressive deformation (panels a–f; modified from Graham 1966). If deformation is low-to-moderate, the magnetic maximum principal axis K_1 (magnetic lineation) shows strict correlation with the tectonic structures in extensional (g) and (h) compressional settings.

In the Garedu Red Beds 9 sites (103 samples) were sampled in red marls, marly-siltstones, and siltstones distributed in different stratigraphic levels in the two limbs of the Garedu Red Beds syncline (Fig. 4). At each site, cores were drilled with an ASC 280E petrol powered portable drill and oriented in situ by a magnetic compass. From each core standard cylindrical specimens were cut. The magnetic mineralogy of the sampled sediments was investigated on representative specimens using standard rock magnetic techniques. The stepwise acquisition of an isothermal remanent magnetization (IRM) was applied using a pulse magnetizer up to 0.9 T fields. A three component IRM was imparted at 1.7 T, 0.6 T, and 0.12 T fields along samples' orthogonal axes and thermally demagnetized following the Lowrie's (1990) procedure. The low-field AMS at room temperature was measured with an AGICO KLY-3S susceptibility bridge in the paleomagnetic laboratory of the Department of Geological Sciences of the University of Roma Tre. The anisotropy measurements at the site levels were evaluated using Jelínek's (1977) statistics. Structural analysis was carried out in AMS sites where deformation was detectable at the outcrop scale, in order to directly compare fabric analyses and mesoscale deformation. The collected data are mostly cleavage planes and extensional veins, which have been elaborated and plotted using the DAISY 4.15 software (Salvini, 2004).

4. Results

4.1. Structural analyses results

The Garedu Red Beds syncline is almost cylindrical. Bedding planes are distributed along a well-defined great-circle girdle whose normal plunges gently to the NNE (Fig. 6a). Cleavage planes are oriented NNE-SSW (Fig. 6b), are generally very steep, and show a variable angle to bedding, which ranges between 10° and 30°. Only at one location (GA08) two cleavage systems have been measured: a very steep system, dipping toward WNW, which forms a very small angle to bedding, and a more gentle system, dipping to the ESE, which is almost orthogonal to bedding (Fig. 6b and Fig. 9i). The steep dipping cleavage system formed during a late stage of fold growth, whereas the gently dipping cleavage planes, which are almost orthogonal to bedding, formed as a consequence of layer parallel shortening and have been later passively rotated during fold growth.

Individual planar calcite-filled veins and en echelon arrays of planar to sigmoidal veins occur in sites GA02, GA03, and GA04 (Fig. 6c). Planar veins typically have very large length-to-width ratios, whereas veins in en echelon arrays have length-to-width ratios that approach 2:l. The orientation

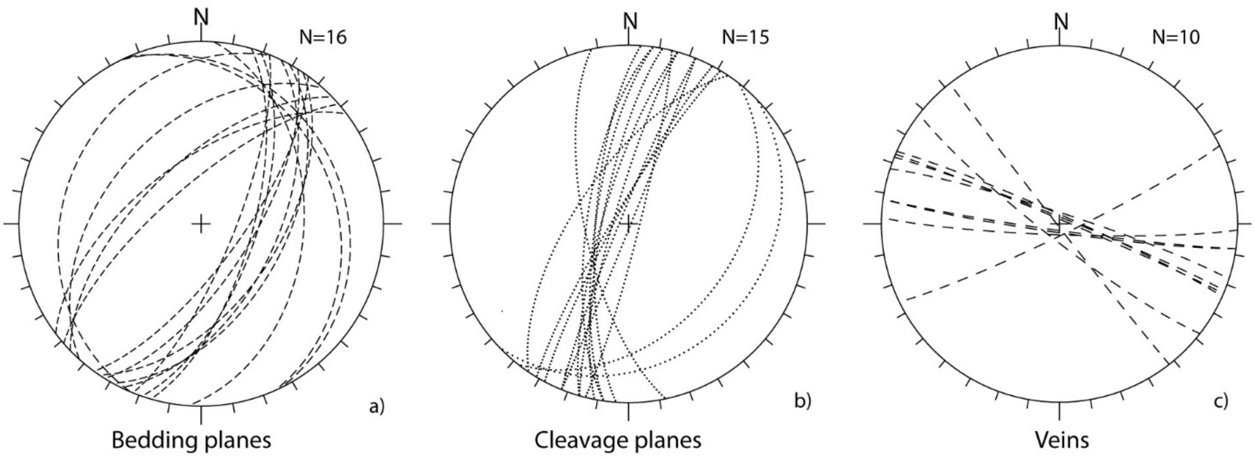

Fig. 6. Structural data from the Garedu syncline. (a) Bedding planes; (b) cleavage planes; (c) filled veins planes. Note that cleavage and bedding planes are not coaxial. Data are plotted on lower hemisphere, equal-area projections.

of the calcite filled veins ranges between WSW-ENE to NW-SE, with a mean direction WNW-ESE, which is almost orthogonal to the cleavage plane systems (Fig. 6). This relationship suggests that cleavage and calcite veins formed at the same time.

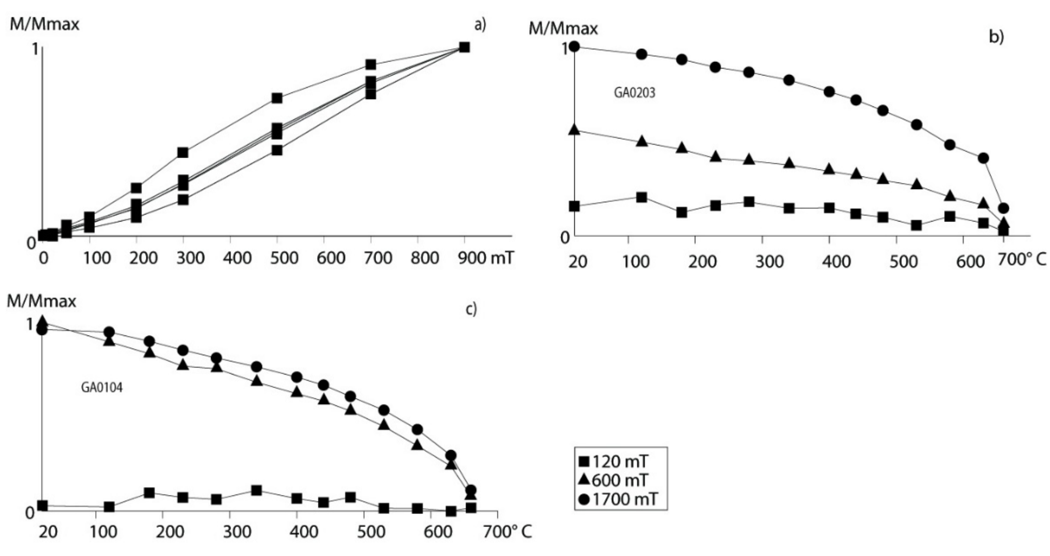

Fig. 7. Magnetic mineralogy of the analysed samples in the Garedu sites. (a) IRM acquisition curves showing the prevalence of high-coercivity minerals in the analysed samples. (b and c) Thermal demagnetization curves of a three-component (hard, medium, soft) IRM (Lowrie 1990) for haematite bearing samples.

4.2. Magnetic mineralogy and AMS results

In the Garedu Red Beds Fm. all the specimens show a progressive increase of the IRM and do not reach the saturation at 900 mT, suggesting that high coercivity ferromagnetic minerals are largely present in the analysed lithology (Fig. 7a). Thermal demagnetization of a three component IRM confirms these results and helps defining the nature of the magnetic minerals. High-coercivity magnetic phases are prevalent and show a maximum unblocking temperatures of about 680° C, which can be attributed to the presence of hematite (Fig. 7b, c).

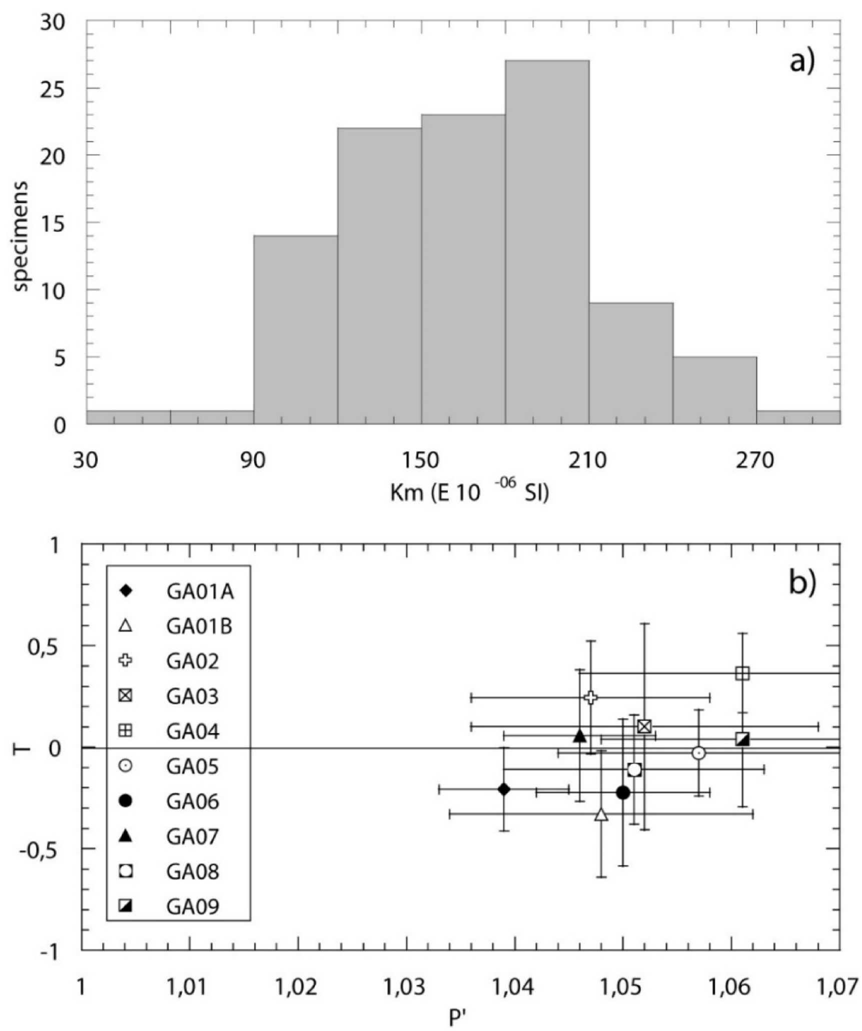

Fig. 8. Magnetic parameters for the entire set of 103 specimens of the Garedu Red Beds. (a) Frequency distribution of the mean susceptibility (Km) values; (b) degree of anisotropy P'versus T diagram, calculated using mean site values.

The mean magnetic susceptibility (K_m) of the analyzed specimens is moderately low, ranging mostly between 90 and 270 * 10^{-6} SI (Fig. 8a and Table 1). These values indicate that paramagnetic minerals significantly contribute to the low-field AMS (Rochette 1987) and that the magnetic fabric may be reasonably interpreted in terms of preferred orientation of the paramagnetic grains, and probably hematite (Fig. 7b,c) (Hounslow 1985; Parès & Van der Pluijm 2002; Cifelli *et al.* 2005;). P' values are generally more than 1.04, the L parameter ranges between 1.017 and 1.032, while the F parameter ranges between 1.015 and 1.040 (Table 1). Ellipsoid shapes generally vary from moderately oblate (T=0.364) to moderately prolate (T=-0.328), with most of the sites showing triaxial ellipsoids (T≈0) (Fig. 8b and Table 1). This variability of AMS ellipsoids shape parameters appears to be controlled mainly by the angular relationships between bedding and cleavage planes. In fact, in sites where oblate fabrics (T>0) are observed (GA02 and GA04), the bedding and cleavage planes, which show both a NNE-SSW direction, are very steep with a small angle between the two planes (Fig. 9c, e). Conversely, prolate shapes (T<0) have been observed at sites where bedding dips gently (GA01b and GA06, Fig. 9b,g), or where two cleavage planes systems, at high angle from each other, have been observed (GA08, Fig. 9i).

Table 1. List of magnetic anisotropy factors computed at each site of the sampled Garedu Fm. sites.

Site	Lat	Lon	So	N	k_m	L	F	Pj	Tj	D,I(K_{max})	D,I(K_{min})	e_{12}
GA01a	34°23'51.6''	57°10'59.1''	26, 56	9	171	1.023(0.005)	1.015(0.005)	1.039(0.006)	-0.207(0.206)	193,3	87,23	5
GA01b	34°23'51.7''	57°10'60.3''	Variable	10	130	1.029(0.007)	1.017(0.011)	1.048(0.014)	-0.328(0.311)	172,7	270,50	11
GA02	34°25'13.6''	57°10'54.7''	22, 75	12	119	1.017(0.007)	1.029(0.009)	1.047(0.011)	0.245(0.277)	14,4	283,11	15
GA03	34°27'11.9''	57°12'40.5''	29, 52	13	198	1.019(0.009)	1.030(0.020)	1.052(0.016)	0.101(0.506)	31,19	290,30	14
GA04	34°28'57.2''	57°13'43.4''	19, 65	10	182	1.018(0.006)	1.040(0.012)	1.061(0.015)	0.364(0.196)	190,4	99,3	10
GA05	34°30'28.2''	57°15'47.3''	222, 46	9	192	1.028(0.006)	1.028(0.010)	1.057(0.013)	-0.027(0.212)	10,18	103,8	10
GA06	34°31'10.3''	57°15'54.9''	203, 25	8	195	1.030(0.011)	1.018(0.008)	1.050(0.008)	-0.223(0.361)	193,3	102,15	11
GA07	34°37'06.9''	57°19'56.4''	Variable	11	125	1.021(0.008)	1.023(0.007)	1.046(0.007)	0.057(0.325)	25,10	116,4	12
GA08	34°36'00.1''	57°20'16.7''	Variable	11	161	1.027(0.003)	1.024(0.012)	1.052(0.012)	-0.109(0.268)	22,15	118,22	13
GA09	34°32'57.9''	57°16'54.1''	Variable	10	213	1.029(0.013)	1.030(0.009)	1.061(0.013)	0.040(0.332)	14,26	106,5	8

Note: For each locality the line shows the arithmetic means of the individual site mean values (standard deviation in parenthesis). So = bedding plane (mean value for each site); N = number of specimens; D,I (K_{max}) = declination and inclination of the maximum susceptibility axis (geographic coordinates); D,I (K_{min}) = declination and inclination of the minimum susceptibility axis (geographic coordinates); $K_m = (k_{max}+k_{int}+k_{min})/3$ (mean susceptibility, in 10^{-6}SI units); L = k_{max}/k_{int} (lineation); $F=k_{int}/k_{min}$ (foliation); $P_j=\exp\{2[(h_1\ h)^2+(h_2-h)^2+(h_3-h)^2]\}^{1/2}$ (corrected anisotropy degree); $T = 2(h_2-h_3)/(h_1-h_3)-1$(shape factor; Jelinek,1981); S_0=bedding attitude (azimuth of the dip and dip values); $h_1 = \ln k_{max}$; $h_2=\ln k_{int}$; $h_3=\ln k_{min}$; $h=(h_1+h_2+h_3)/3$; $e_{1\text{-}2}$ = semi-angle of the 95% confidence ellipses around the principal susceptibility axes.

The main magnetic susceptibility directions for each site are tightly grouped with a well-defined magnetic foliation and magnetic lineation (Fig. 9). The magnetic foliation is well defined in all the sites, and shows no apparent relation to bedding orientation, being very steep to sub-vertical even in sites where bedding planes show gentle to sub-horizontal dip (Fig. 9f,j). Furthermore, where bedding is very steep (Fig. 9b, c, d, h), an obliquity of the magnetic foliation respect to bedding direction has been observed. Where a tectonic foliation has been observed (cleavage) the magnetic foliation is parallel or sub parallel to it (Fig. 9c, e, i, j).

The magnetic lineation (K_1) is well defined in all sites, with e_{1-2} angles (the semi-angle of the 95% confidence ellipse in the K_1-K_2 plane) never exceeding 19°, independently of their position within the syncline (Fig. 9 and Table 1). K_1 is NNE-SSW oriented, sub-horizontal, or slightly plunging northward. As already observed for the magnetic foliation, the magnetic lineation shows a different relationship with bedding in the different sites. Where cleavage is recognizable (site GA02, GA04, GA08 and GA09), the magnetic lineation lies within the cleavage planes (GA02, GA08) or at the intersection between the cleavage planes and bedding (GA04, GA09). On the other hand, when cleavage is not observed, K_1 lies in the bedding plane (site GA01, GA07). At site GA02 and GA03 the magnetic lineation is slightly oblique respect to bedding direction and is oriented orthogonal to the calcite-filled extensional vein system.

5. Discussion

5.1. The origin of magnetic fabric

A good agreement is mostly observed between the axes of the magnetic fabric and those of the tectonic fabric measured in the field. The magnetic fabric of the Garedu Red Beds is characterized by a well-defined magnetic lineation and magnetic foliation. The magnetic foliation shows a NNE-SSW orientation and a sub-vertical dip: the mean direction of the K_3 (pole to magnetic foliation) calculated from all the sites is N108, 2 (e_{1-2} = 11.1°), indicating that magnetic foliation is concordant with cleavage (Fig 10). K_1 is oriented from N-S to NE-SW, with a gentle plunging toward the NNE (the mean direction of the K_1 calculated from all the sites is N18, 7 (e_{1-3}= 9.9°) (Fig. 10a). Both magnetic foliation and magnetic lineation have an orientation slightly rotated toward the north respect to the fold axis of the main syncline (N36, 27), whereas are almost parallel to the main direction of cleavage system (N17, 83) and orthogonal to the main orientation of the filled vein planes (N112, 84), giving strong evidence that the orientation of magnetic fabric has been mainly driven by tectonic processes (Fig. 10b). The magnetic fabric of the Garedu Red Beds, however, is still affected by the influence of the original sedimentary fabric, with the magnetic lineation lying within the bedding plane (Fig. 9).

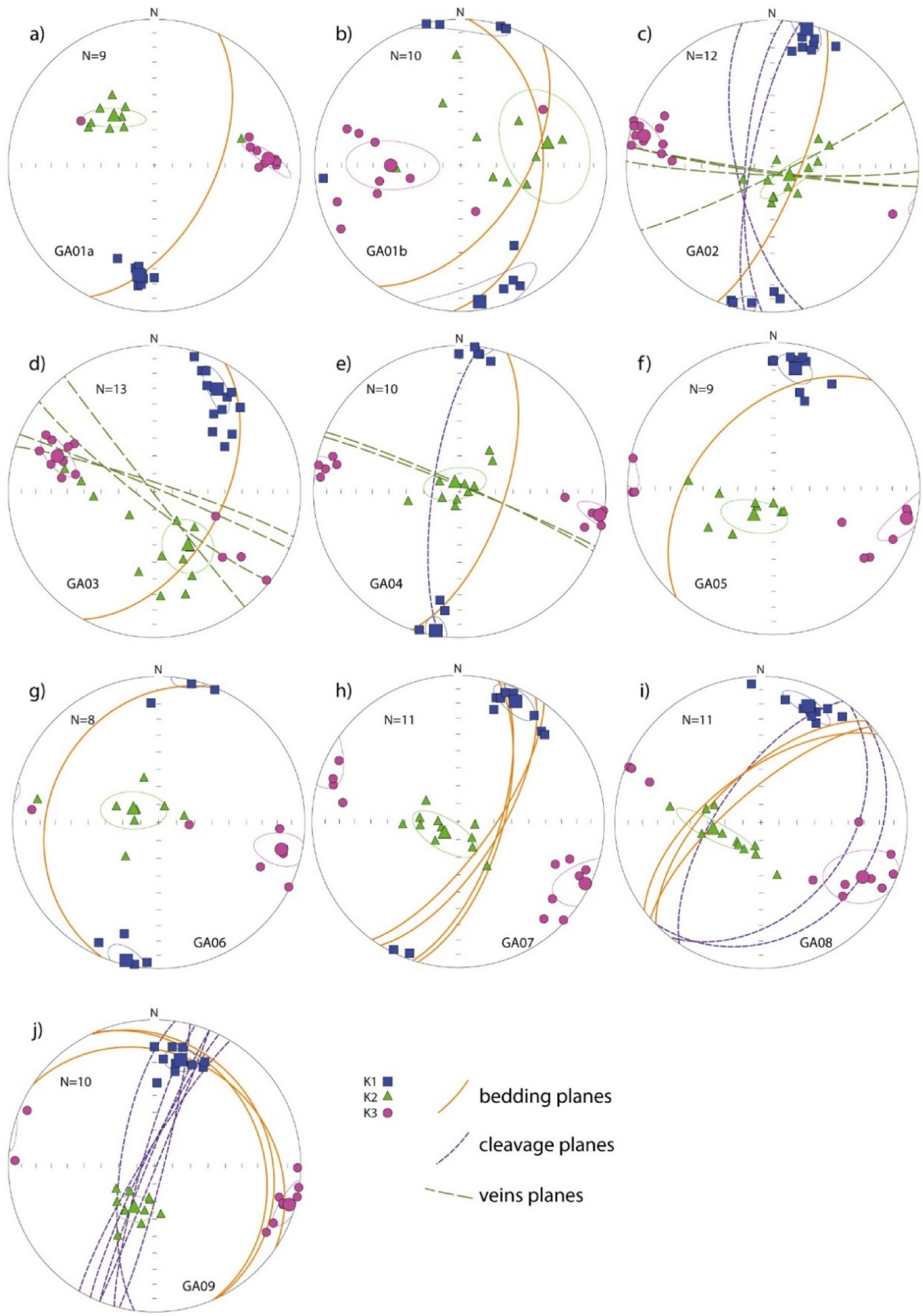

Fig. 9. AMS plots for representative sites analysed in this study. Data are plotted on lower hemisphere, equal-area projections, in geographic coordinates. Squares and circles represent maximum and minimum axes, respectively. Bedding, cleavage and calcite filled veins planes are also represented.

During deformation, the magnetic fabric in sedimentary rocks has a progressive evolution from a pure sedimentary fabric to a purely tectonic fabric, which is marked by a changing in the shape parameters (Graham 1966; Kligfield *et al.* 1981; Hrouda 1982; Housen & van der Pluijm 1991). In the Garedu Red Beds sites, shape parameters are mainly depending from the angular relationships between bedding and cleavage planes. Prolate fabrics have been measured mainly at sites with gently dipping bedding or where two set of cleavage planes, with a high angle between planes systems, were observed (e.g., GA01, GA06, and GA08) (Table 1). Conversely, oblate fabrics have been mainly observed at sites where bedding planes are very steep and where they form a small angle with cleavage (e.g. GA02 and GA04). Furthermore, in some sites (GA04 and GA09) the magnetic lineation lies at the intersection between cleavage and bedding, suggesting a partial influence of original bedding on the orientation of the magnetic fabric. On this basis we suggest that magnetic fabric in the Garedu Red Beds represents an intermediate stage between a purely sedimentary and a purely tectonic fabric (Fig. 5c, d) (Borradaile & Tarling, 1981; Kligfield *et al.* 1981; Housen & van der Pluijm 1991; Richter *et al.* 1993; Parés *et al.* 1999; Parés & van der Pluijm 2002; Luo *et al.* 2009; Aubourg *et al.* 2010). In this stage the orientation of the magnetic fabric is mostly controlled by cleavage, but the original sedimentary planar fabric has not been completely erased and bedding planes still record a preferred orientation of mineral grains. Therefore, in the Garedu Red Beds sites we observe the interaction of two competing sub-fabrics, where the orientation of the magnetic lineation tracks the intersection direction of the two planar fabrics, with the tectonic fabric prevailing on the sedimentary one.

5.2. Fold kinematics

Folds with an associated cleavage that does not parallel the fold axial planes (transected folds) have been documented from a number of areas (e.g. Borradaile 1978; Stringer & Treagus 1980; Gray 1981; Woodcock *et al.* 1988; Johnson 1991). However, the angular transection involved is usually small (<20°) and many transected folds have gone unrecognized using standard structural techniques. Structural and AMS results from the Garedu Red Beds show an obliquity between fold orientation on one hand and cleavage, magnetic foliation and magnetic lineation on the other. This obliquity can be observed both at the scale of single sites (Fig. 9c, d, e, f, i, j) and at

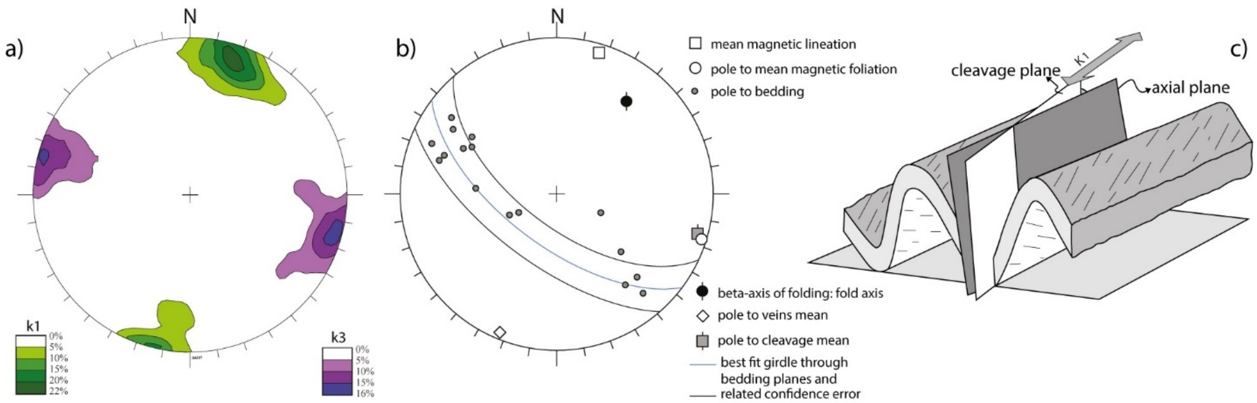

Fig. 10. Mean direction of magnetic foliation and magnetic lineation from the Garedu syncline compared with structural data directions. a) Contouring plots of K_1 (magnetic lineation) and K_3 (pole to magnetic foliation) directions from all the Garedu sites; b) mean direction of K_1, K_3, fold axis, cleavage and filled veins. c) Angular relationship between cleavage, magnetic lineation and axial plane (modified from Borradaile 1978).

the scale of the overall fold (Figs. 4, 10b). On this basis, the Garedu Red Beds syncline can be defined as a transected fold (Fig. 10c). An analogous geometric relationship between tectonic foliations and fold hinge or axial planes has been recognized in Scotland and in the Caledonian-Appalachian orogenic belts (Soper & Hutton 1984; Soper 1986; Woodcock *et al.* 1988; Lafrance & Williams, 1992). In these regions the formation of transected folds has been associated to transpressional tectonics, where folds and cleavages rotate during the deformation and where exists a slight time difference between the onset of folding and cleavage formation. In the Garedu Red Beds syncline the mismatch between fold hinge and magnetic fabric (lineation and foliation), and cleavage is about 15° counterclockwise (Fig. 4 and Fig. 10), which would suggest that this fold formed as a consequence of right-lateral transpressional tectonics.

5.3. Age of deformation and tectonic evolution of the area

N-S to NNE-SSW oriented right-lateral faults, which are parallel to the Garedu Red Beds syncline, represent the main active deformation feature of this sector of Central Iran (Stöcklin *et al.* 1965; Ruttner *et al.* 1968a; Stöcklin & Nabavi 1971; Walker & Jackson 2004). In particular, the Kal Shaneh fault, in the SW of the study area, shows clear evidences of right-lateral movement. Ruttner *et al.* (1968a), on the base of facies correlations in the Permian-Triassic units, have estimated a right-lateral displacement of this fault of about 40-50 kilometers. At the same time this fault also cuts young alluvial fan deposits suggesting its activity until recent time (see Fig. 34 in Ruttner *et al.* 1968a). In the western border of the Shotori Range, focal mechanism, aftershocks distribution, surface deformation, and faulting concordantly showed that the 1978 Tabas earthquake occurred on a previously unrecognised NW- to NNW-oriented thrust fault with a small component of right-lateral strike-slip (Berberian, 1979; Walker *et al.* 2003). Furthermore, toward the south, the whole tectonic border between the Tabas and Lut blocks is characterized by active right-lateral faults, well defined by seismicity and GPS data (Vernant *et al.* 2004; Walker & Jackson 2004).

In the Shotori Range several phases of deformation have been recognized, which could have been responsible of the folding of the Garedu Red Beds syncline. Southwest of the study area, the deformed Garedu Red Beds are unconformably overlain by Paleocene Kerman Fm. conglomerates (Ruttner *et al.* 1968a). In the western side of the Shotori Range, Stöcklin & Nabavi (1971) have demonstrated the existence of two distinct phases of deformation, as the fold and thrusting of the Paleozoic and Jurassic units are directly overlain by Neogene conglomerates and Tertiary red beds, which are also folded and dissected by faults. On this basis Ruttner *et al.* (1968a) suggested a Late Cretaceous age for the older deformation phase, which should be responsible of the first episode of folding of the Garedu Red Beds, followed by a Neogene to Quaternary phase of deformation. These two distinct episodes of deformation can be also observed in the Tabas fold system, to the south of the study area, where the western sector of the Shotori Range is deformed by NNW-SSE thrust related folds. In this area Tertiary sedimentary units, which lie with an angular unconformity on top of strongly folded Jurassic sediments (Stöcklin & Nabavi 1969) are deformed and folded as a consequence of active motion along the Tabas thrust fault (Berberian, 1979; Walker *et al.* 2003). In this area, Mesozoic and Tertiary units outcrop in folded structures that have parallel structural trend, suggesting that the Pre-Tertiary (Late Cretaceous?) and the active episode of folding are coaxial.

Accordingly, the timing of acquisition of magnetic fabric in the Garedu Red Beds syncline is hard to be precisely constrained. In fact, even if well-defined magnetic fabrics have been measured in recent, poorly deformed, sediments as result of tectonic deformation (Cifelli *et al.* 2004; Cifelli *et* *al.* 2007; Porreca & Mattei, 2012, among others), a recent age for the origin of the magnetic fabric in the Garedu Red Beds syncline seems unrealistic. In fact, in the Garedu Red Beds syncline the close relationships between magnetic fabric, cleavage and filled joints demonstrate that they formed during the same deformation event. This deformation phase should have occurred when the Garedu Red Beds were still buried at significant depth, allowing the formation of penetrative cleavage planes system. This tectonic event could be reasonably dated between Lower Cretaceous (possible upper age of the Garedu Red Beds Fm.) and Paleocene (age of the Kerman Fm. conglomerates, which unconformably overlie the Garedu Red Beds Fm.) and is related to the shortening episodes which caused the closure of the small oceanic basins testified by the ophiolitic rim around Central Iran (Fig. 1a), as a consequence of the motion of the Arabian Plate and the closure of the Neotethys oceanic basin (Tirrul *et al.* 1983; Dercourt *et al.* 1986).

Our AMS and structural results suggest that right-lateral transpressional folds accomplished this shortening episode in the northern Shotori range, along the boundary between the Tabas and Lut block. The Shotori Range presents some typical structural and tectonic features of a reactivated tectonic margin, which are favorable conditions for the developing of transpressional tectonics, such as the presence of long-lived tectonic systems that correspond with the present-day boundaries among the main Central Iran crustal blocks. In particular, the N-S to ENE-WSW oriented active faults that bound the Yazd, Tabas, and Lut blocks of Central Iran (Kal-Shaneh and Nayband faults), have reactivated Middle-Late Jurassic normal faults that controlled the tectono-sedimentary evolution of the carbonate platform system developed along the tectonic boundaries of the Tabas block (Wilmsen *et al.* 2010) (Fig. 2).

6. Conclusions

AMS and structural data collected from the Upper Jurassic Garedu Red Beds from Central Iran show a magnetic fabric typical of an intermediate stage of deformation, with a magnetic foliation parallel to cleavage and magnetic lineations often lying at the intersection between cleavage and bedding. Magnetic fabric and cleavage are rotated counterclockwise respect to the fold hinge, suggesting that the Garedu Red Beds syncline is a transected fold, which formed as a consequence of a right-lateral transpressional regime at the boundary between the Tabas and Lut blocks of Central Iran, between the Lower Cretaceous and Paleocene. During Middle-Late Jurassic this boundary was the location of a carbonate platform-slope-to-basin depositional system, mainly controlled by the activity of a N-S oriented normal fault system. Our results thus document that Jurassic normal faults changed to a transpressional tectonic boundary, suggesting that inversion tectonics is a valuable mechanism to explain the style and distribution of deformation in Central Iran.

Chapter V

Late folding-related magnetic foliation in the active Ferdows (northeastern Iran) thrust-fold system

Hamideh Rashid, Francesca Cifelli, Massimo Mattei

This chapter has been published in 2015:

Journal of Asian Earth Sciences, vol. 108, Pages 48–57
http://dx.doi.org/10.1016/j.jseaes.2015.04.023

Keywords: AMS, LPS, cleavage, Central Iran

Abstract:

In this work we present new AMS and structural results from the Ferdows active fold-thrust system (Lut block, Central Iran). AMS analyses show that the Miocene units of the Upper Red Formation have a well-defined magnetic fabric of tectonic origin, with both magnetic lineation and magnetic foliation oriented parallel to the regional fold axes. In most of the cases the magnetic fabric, acquired when the bedding was still horizontal, is related to different degrees of LPS shortening. In some other cases, the magnetic foliation is vertical and oblique to the bedding, suggesting that in the Ferdows thrust-fold structure a cleavage system, not visible at the outcrop scale, has been developed as a consequence of later shortening related to the activity of the thrust system, responsible of the recent earthquakes in the area. Results from this study establish a relationships between the recent tectonics of the area and the evolution of the magnetic fabric and demonstrate that a well-defined magnetic fabric of pure tectonic origin can also develop in poorly deformed rocks lacking field evidence of pervasive internal deformation.

1. Introduction

Anisotropy of Magnetic Susceptibility (AMS) has been often and successfully used as a tectonic marker in poorly deformed sedimentary rocks, which appear to lack evidence of deformation at the outcrop scale (Kissel *et al.* 1986; Mattei et al., 1997; Pares et al., 1999; Kanamatsu et al., 2001; Housen and Kanamatsu, 2003, among many others). When subjected to strain, the magnetic fabric of sedimentary rocks rapidly evolves showing a well-defined magnetic lineation since the early stages of deformation (Kissel et al., 1986; Mattei et al., 1997; Parés, 2004; Cifelli et al. 2007; 2009; Parés and van der Pluijm 2002; Larrasoana et al., 2011). In these poorly deformed rocks it is often observed that the magnetic foliation lies parallel to the bedding plane, implying that it is originated either during sedimentary processes or as a consequence of subsequent compaction, without any influence of tectonic processes (e.g. Kissel et al., 1986; Sagnotti et al., 1998; Pares et al., 1999). When a magnetic foliation of tectonic origin has been observed, the evolution of the magnetic fabric has been attributed to layer parallel shortening (LPS) processes which occurred during the early stages of deformation (Pueyo-Morer et al., 1997; Larrasoana et al., 2004; Weil and Yonkee, 2009). In these cases the magnetic foliation may be cryptic and not necessarily accompanied by its macroscopic equivalent plane in the field, or may be observed in sedimentary rocks where a tectonic foliation (cleavage) is also visible at the mesoscale; in this case the magnetic foliation is dispersed around the bedding planes or, when cleavage becomes stronger, the distribution of minimum axes changes into a cluster that is perpendicular to the cleavage plane (Lowrie & Hirt, 1987; Housen and Van der Pluijm, 1991; Averbuch et al., 1992; Hirt et al., 1995; 2000; Lunemburg et al., 1999; Debacker et al., 2004; 2009; Tavani & Cifelli, 2010; Cifelli et al., 2013). In only few cases, a peculiar orientation of magnetic foliation has been observed, which shows no relationships with LPS deformation, suggesting that it formed as a consequence of internal strain during the late stages of folding (Averbuch et al., 1992; 1995; Saint-Bezar et al., 2002).

In this study we present new AMS and structural results from the Ferdows active fold-thrust system (Lut block, Central Iran), that establish a relationships between the recent tectonics of the area and the evolution of the magnetic fabric. We show that a well-developed magnetic fabric of pure tectonic origin can form also in poorly deformed rocks, which lack evidence of pervasive internal deformation. In particular, we show that the different types of magnetic fabric observed at Ferdows fold-thrust system cannot be explained simply using different degrees of LPS, and that late folding internal strain has to be considered. The implication for the tectonic evolution of the Ferdows fold and thrust system are also discussed.

2. Geological setting

Geodetic and seismic data show that in Iran the present-day deformation related to Arabia-Eurasia convergence is mainly accommodated by displacements in the Zagros, Alborz and Kopeh-Dagh Mountains fold-and-thrust belts, whereas only a minor amount of shortening is taken up in Central Iran (Vernant et al., 2004), which shows a very complex and still not completely understood pattern of deformation (Tchalenko & Ambraseys 1970; Jackson & McKenzie 1984; Jackson *et al.* 1995; Berberian & Yeats 1999; Allen *et al.* 2004; Vernant *et al.* 2004; Walker & Jackson 2004; Allen *et al.* 2011; Fig. 1). South of latitude 34°N, active deformation is taken up on N–S right-lateral strike slip faults, which represent the boundaries between the Yazd, Tabas and Lut blocks of Central Iran, whereas north of latitude 34°N, E–W left-lateral strike slip faults prevail, the most prominent of which are the Doruneh and Dasht-e-Bayaz faults (Walker et al. 2003; Walker & Jackson 2004; Meyer & Le Dortz. 2007; Cifelli et al., 2013; Walker et al. 2013) (Fig. 1). These strike-slip faults, which in many cases link with other major structures at their ends, can adjust the NNE–SSW the Arabia-Eurasia convergence if they can rotate clockwise and counterclockwise, respectively (Jackson et al., 1995; Walker and Jackson, 2004; Allen et al., 2011; Mattei et al., 2012; Mattei et al.,, 2015; Walperdorf et al., 2014).

The Ferdows thrust-fold system is located at the western end of the E-W left-lateral strike slip Dasht-e-Bayaz fault in the northern part of Lut block (Fig. 2). The Dasht-e-Bayaz left-lateral strike-slip fault system ruptured over a length of *ca.* 80 km during the earthquake of August 30, 1968 (Mw 7.1) (Tchalenko & Ambraseys 1973; Ambraseys & Melville 1982; Walker et al. 2004; 2011), which was followed in the Ferdows area by two thrust earthquakes on the 1st (*Mw* 6.3) and 4th

(*Mw* 5.5) of September. The Ferdows earthquakes occurred at the western termination of the left-lateral strike slip fault, shortly after the Dasht-e-Bayaz earthquake, suggesting that the E-W oriented Dasht-e-Bayaz fault and the NNE-SSW oriented thrust faults in Ferdows area were probably tectonically linked (Walker et al., 2004; Berberian, 2014). The two earthquakes did not produce surface faulting that was recognised at the time, and the thrust faults responsible for the earthquakes in the Ferdows area have not yet been recognized with certainty (Walker et al., 2003; 2011; Berberian, 2014).

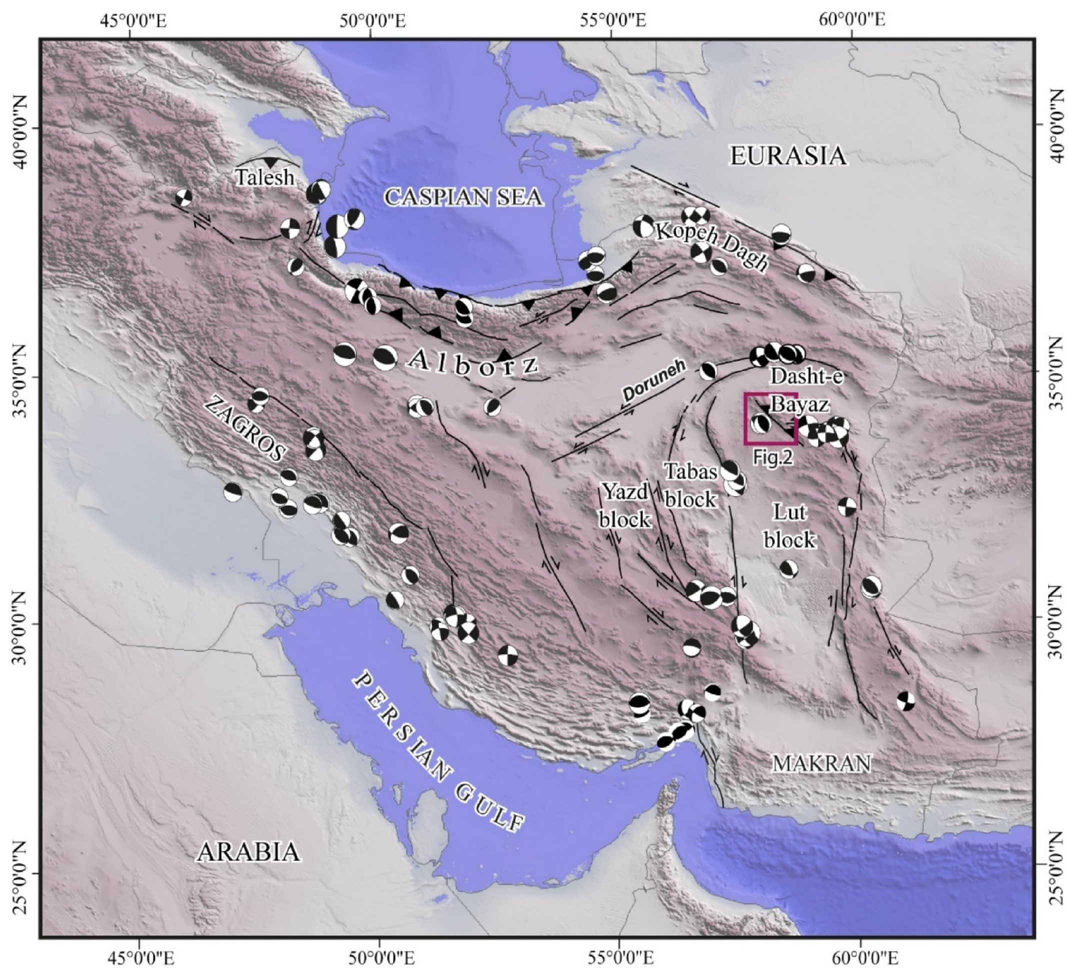

Fig. 1. Shaded relief map of Iran (a) Regional structure and seismicity, highlighting the active fault systems of Iran. Focal mechanisms are from Jackson (2001) for earthquakes between 1959 and 2000 August 22 (modified from Allen et al., 2011).

The Ferdows thrust-fold system, located at the footwall of the Kuh-e-Siah and Kuh-e-Tun mountain range (Fig. 2), is cored by a Neogene succession which includes conglomerates, red marls, siltstones and sandstones belonging to the Middle-Upper Miocene Upper Red Formation (URF), followed by lacustrine dark clays and conglomerates (Fig. 3). Satellite images and new field

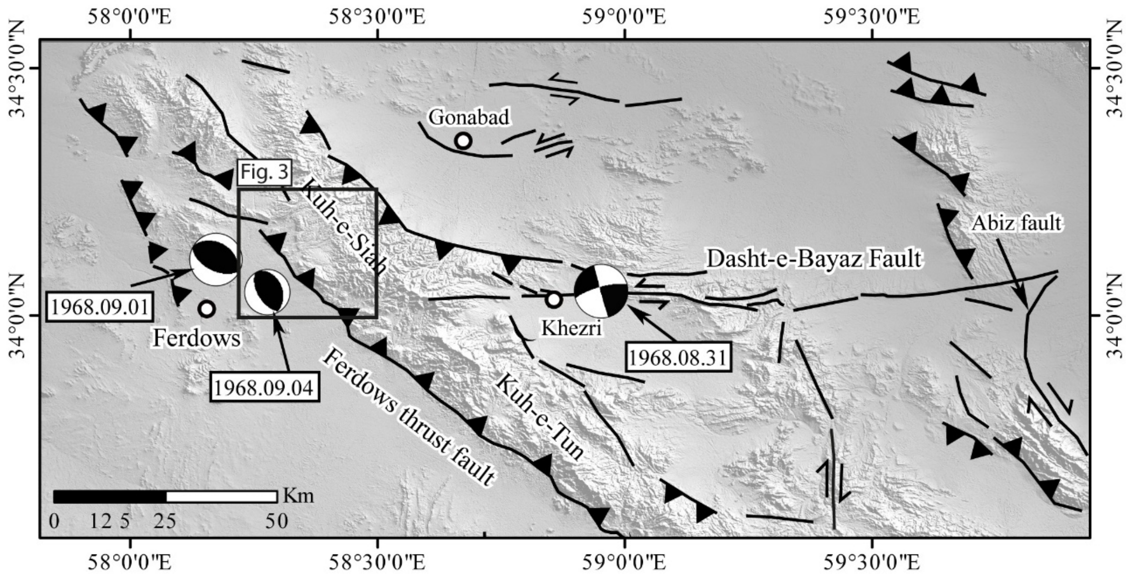

Fig. 2. Shaded-relief topographic map (SRTM data) of the northern part of Lut block, and main active faults of the area. Focal mechanisms of Ferdows and Dasht-e-Bayaz earthquakes (1968) are also reported (modified from Walker et al., 2011).

observation allow recognizing a complex geometry of the Ferdows thrust-fold system, which is well visible at the northwest end of the structure, where the URF units are deformed in a system of NW-SE to N-S folds (Fig. 4). The Neogene succession is covered with a sharp angular unconformity by Quaternary alluvial deposits feeded from the western margin of the Kuh-e-Kalat range, which also shows clear evidence of folding and recent tectonic uplift (Walker et al., 2003). The Quaternary alluvial deposits form a gentle anticline with the eastern flank gently dipping to the east (adverse to the topographic slope) and the western limb that becomes very steep (up to 70°) close to the frontal scarp which separates the uplifted structure (to the east) from the alluvial plain (to the west) (Walker et al., 2003). This geometry suggests that the Ferdows fold system is located at the hangingwall of a east-dipping thrust fault which has been active during recent time causing the overall uplift of the Neogene and Quaternary units (Walker et al., 2003; Berberian, 2014).

3. Methods and sampling

AMS is defined by a symmetric second rank tensor and represented geometrically by an ellipsoid with principal axes $K_1 \geq K_2 \geq K_3$. Several parameters have been defined both for the quantification of the magnitude of anisotropy and for defining the shape of the ellipsoid (see Table 1; Hrouda 1982). The T-shape parameter varies from –1 (perfectly prolate ellipsoid, $K_1 >> K_2 = K_3$) to 1 (perfectly oblate ellipsoid, $K_1 = K_2 >> K_3$), while a value of 0 corresponds to a triaxial ellipsoid. The magnetic lineation L (K_1/K_2) is defined by the orientation of K_1, while the magnetic foliation F (K_2/K_3) is defined as the plane perpendicular to K_3. The anisotropy degree is expressed by the parameter P'. The mean magnetic susceptibility ($K_{mean} = (K_1 + K_2 + K_3)/3$) gives a relative estimation of the amount of magnetic minerals in the sample.

Ninety-two oriented samples were collected from nine sites (7-12 samples from each site) from Neogene red marls and siltstones of Upper Red Fm. from the hanging wall of the Ferdows thrust (Fig. 3). The sampling sites are generally characterized by the absence of tectonic structures visible at the mesoscale, and show a gentle to steep dipping of the bedding planes toward ENE. Only in two sites tectonic mesostructures have been observed, consisting in a decimetric scale shear zone, formed by S-C structures oriented NNW-SSE, almost parallel to the bedding planes (site FE08), or system of fractures-cleavages orthogonal to the bedding planes and oriented NNW-SSE (FE03).

At each site, cores were drilled with a portable petrol powered drilling machine and oriented *in situ* with a magnetic compass. All cores were cut in standard cylinders (25 mm diameter × 22 mm height) and at least one specimen per core was measured. The magnetic mineralogy was investigated on representative specimens using standard rock magnetic techniques. The stepwise acquisition of an isothermal remanent magnetization (IRM) was applied using a pulse magnetizer up to 0.9 T fields. A three component IRM was imparted at 2.7 T, 0.6 T and 0.12 T fields along samples' orthogonal axes and thermally demagnetized following the Lowrie's (1990) procedure. The low-field AMS at room temperature was measured with an AGICO KLY-3S Susceptibility Bridge in the Palaeomagnetic laboratory of the Department of Science, University statistics.

4. Results

Most of the samples acquired the 90% of the intensity of saturation at 100 mT, suggesting that low coercivity ferromagnetic minerals are the main magnetic carrier, with a small component of

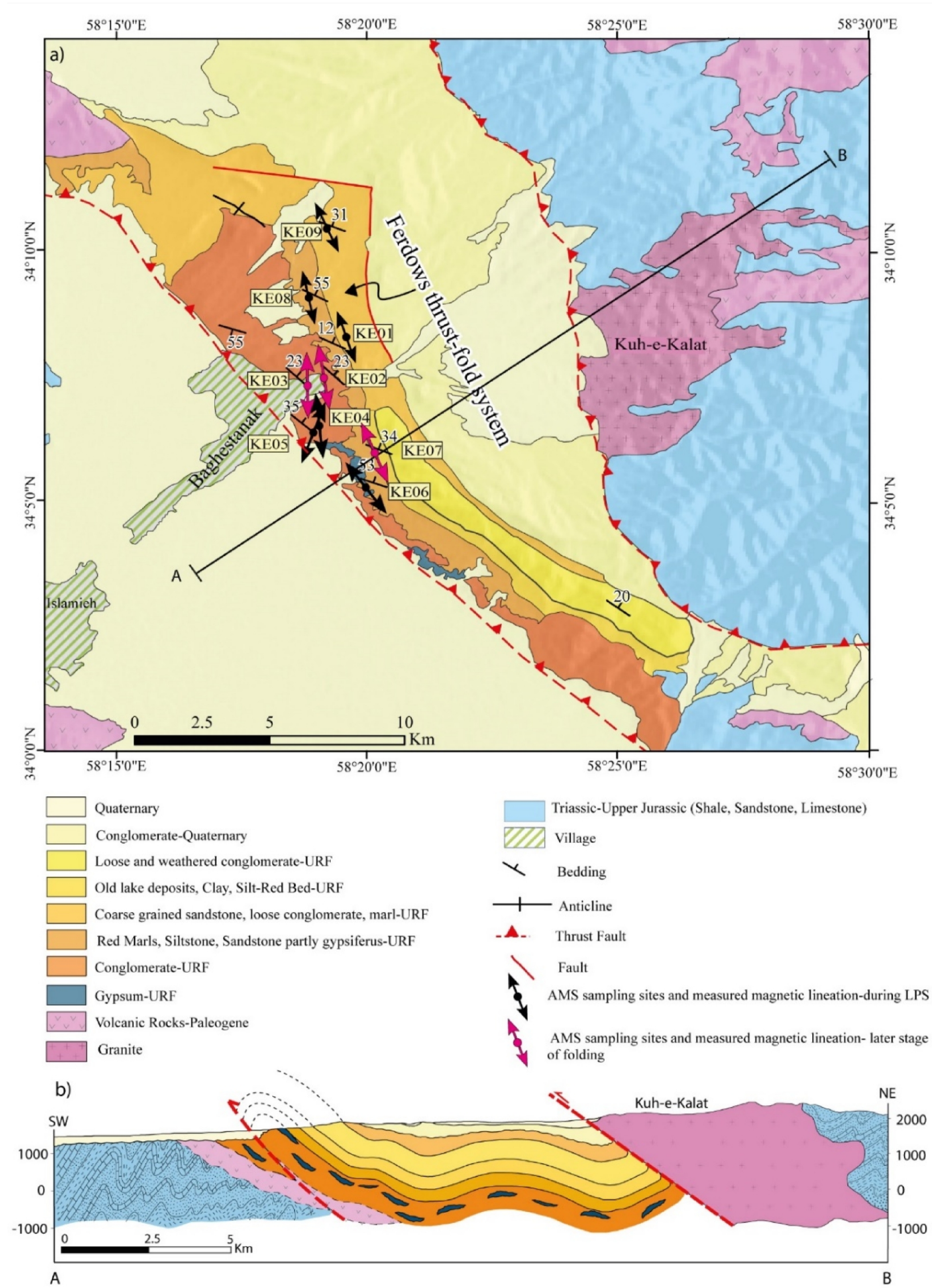

Fig. 3. (a) Geological map of the Ferdows area. The magnetic orientation of magnetic lineation in the sampling sites is also reported; (b) geological cross-section of the Ferdows fold and thrust system.

high coercivity minerals (Fig. 5a). The low coercivity minerals show maximum unblocking temperatures below 630°C, indicating magnetite as main magnetic mineral. The high-coercivity magnetic phases show maximum unblocking temperatures of about 680° C, which we attributed to hematite (Fig. 5b). These findings are fully in agreement with previous magnetic mineralogy (Ballato et al., 2008; Mattei et al., 2012; Cifelli et al., 2015) and mineralogy analyses (Amini and Anketel, 2015) recently carried out in the URF from Central and Northern Iran.

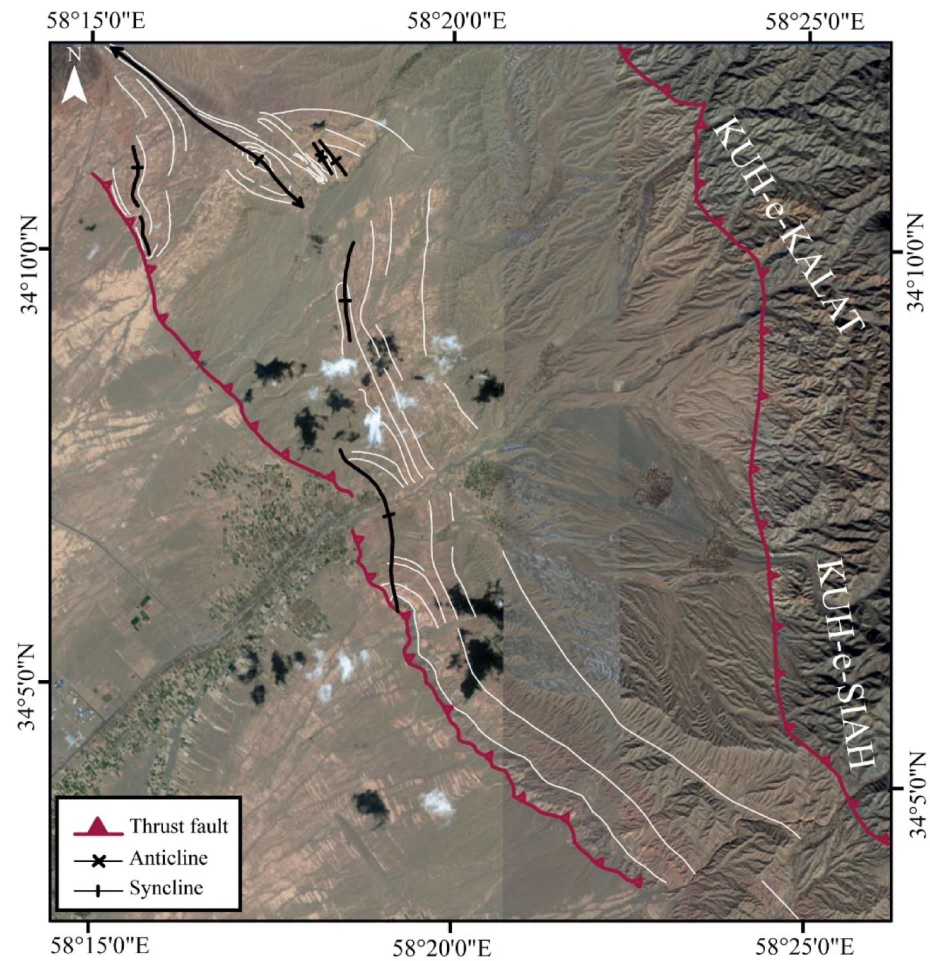

Fig. 4. Bing map view of the Ferdows fold and thrust system showing the main tectonic features of the study area.

The mean magnetic susceptibility (K_{mean}) of the analyzed samples ranges between 400-1700 x 10^{-6} SI (Fig. 6a and Table 1) with most of the samples having susceptibility values in the range of 600-1300 x 10^{-6} SI, which suggest that the ferromagnetic fraction contributes significantly to the magnetic susceptibility in addition to paramagnetic minerals. The magnetic lineation (L) values range between 1.005 to 1.016, while the magnetic foliation (F) values range from 1.006 to 1.018 (Table 1). The site mean degree of anisotropy (P’) values range between 1.014 to 1.031, whereas the shape parameter (T) values show a range from -0.346 to 0.498. The magnetic susceptibility ellipsoid shapes vary from moderately oblate (0 < T < 1, F > L) to moderately prolate (0 < T < -1, L > F) with most of the sites showing triaxial ellipsoids (F ≈ L, T ≈ 0) (Figg. 6b, c and Table 1). This variability of AMS ellipsoids shape parameters appears to be controlled mainly by the angular relationships between bedding and cleavage planes. In fact, in sites where oblate fabrics (T>0) are observed (e.g. FE08), the bedding and cleavage planes, which show both a NNW-SSE direction, are very steep with a small angle between the two planes (Fig. 7e). Conversely, prolate shapes (T<0) have been observed at sites where the cleavage plane system is at high angle with the bedding plane (FE03, Fig. 7h).

1 Table 1 – *List of magnetic anisotropy factors computed at each site of the sampled Ferdows area.*

Site	Lat	Lon	S0	N	km	L	F	Pj_1	Tj_1	D,I (K_1)	D,I (K_3)	e_{121}
FE01	34°08′14″	58°19′31″	66,12	7	857	1.016	1.011	1.028!	-0.259	340/7	242/46	8
FE02	34°07′26″	58°19′05″	49,23	11	1180	1.005	1.009	1.014	0.289	351/25	258/7	10
FE03	34°07′17″	58°18′46″	49,23	11	877	1.012	1.008	1.021	-0.154	1/14	268/10	9
FE04	34°06′29″	58°19′01″	84,60	11	707	1.012	1.006	1.018	-0.346	174/3	82/35	14
FE05	34°06′19″	58°18′53″	52,35	9	838	1.012	1.017	1.030	0.144	22/21	281/28	8
FE06	34°05′14″	58°19′56″	72,53	8	658	1.016	1.014	1.031	-0.096	322/11	225/33	9
FE07	34°05′55″	58°20′06″	70,34	11	1130	1.015	1.009	1.024	-0.275	336/7	68/12	8
FE08	34°09′02″	58°18′48″	68,55	12	1070	1.006	1.018	1.025	0.498	167/7	71/42	12
FE09	34°10′22″	58°19′10″	70,31	9	1100	1.007	1.011	1.019	0.085	155/10	290/76	18

Notes: For each locality the line shows the arithmetic means of the individual site mean values (standard deviation in parenthesis). So = bedding plane (mean value for each site); N = number of specimens; D,I (K_1) = declination and inclination of the maximum susceptibility axis (geographic coordinates); D,I (K_3) = declination and inclination of the minimum susceptibility axis (geographic coordinates); km = ($k_1 + k_2 + k_3$)/3 (mean susceptibility, in 10^{-6} SI units); L = K_1/K_2 (lineation); F = K_2/K_3 (foliation); Pj = exp{2[(η_1– η)2+(η_2– η)2+ (η_3 – η)2]}1/2 (corrected anisotropy degree); T = 2 (η_2– η3)/(η_1– η_3) – 1(shape factor; Jelinek 1981); So = bedding attitude (azimuth of the dip and dip values); η_1 = ln K_1 ; η_2 = ln K_2; η_3= ln K_3; η (η_1 + η_2 + η_3)/3; $e_{1\text{-}2}$ = semi-angle of the 95 per cent confidence ellipses around the principal susceptibility axes.

The magnetic lineation (K_1) is well defined in all sites, with $e_{1\text{-}2}$ angles (the semi-angle of the 95% confidence ellipse in the K_1-K_2 plane) never exceeding 18° (Table 1). K_1 is NNW-SSE oriented in all the sites but FE05, where it is NNE-SSW oriented, sub-horizontal, or slightly plunging northward (Fig. 7c). In most of the sites (FE01, FE04, FE06, FE07) the magnetic lineation lies along the bedding strike. Where cleavage is recognizable the magnetic lineation lies within the cleavage planes (e.g., site FE08), or close to the intersection between the cleavage planes and bedding (FE03). In all the other sites (FE02, FE05 and FE09) the magnetic lineation lies at small angle with the direction of the bedding plane (Fig. 7).

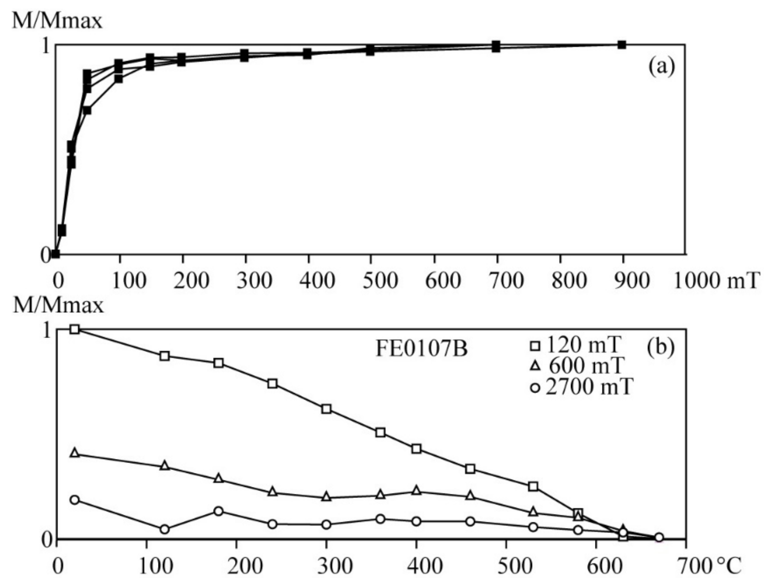

Fig. 5. Magnetic mineralogy of the analyzed samples in the Ferdows sites. (a) IRM acquisition curves showing the prevalence of low-coercivity minerals in the analyzed samples; (b) thermal demagnetization curves of a three-component (hard, medium, soft) IRM (Lowrie, 1990).

The magnetic foliation is generally well defined, showing different relationships with the bedding planes (Fig. 7, 8). In some sites (FE05, FE06 and FE09) the magnetic foliation is well grouped and forms a low angle with the bedding planes (Fig. 7a, b, c). At sites FE01 and FE04 the magnetic foliation is distributed around the bedding plane, forming a girdle orthogonal to the direction of magnetic lineation (Fig. 7d, e). At site FE08 the magnetic foliation lies almost orthogonal to the bedding plane and at high angle with the S-C structures (Fig. 7f). Finally, in some other sites (FE02, FE03, FE07) the magnetic foliation is sub-vertical and shows no apparent relation to bedding orientation, being very steep to sub-vertical even in sites where bedding planes show gentle to sub-horizontal dip (Fig. 7g, h, i).

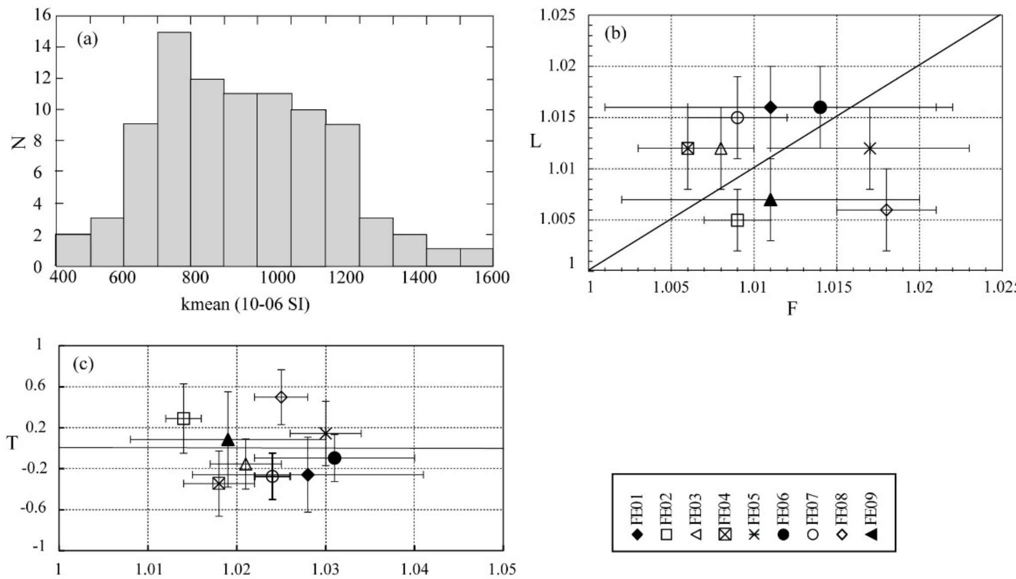

Fig. 6. Magnetic parameters for the entire set of 92 specimens of the Ferdows Red Beds. (a) Frequency distribution of the mean susceptibility (km) values; (b) magnetic foliation (F) vs. magnetic lineation (L) diagram and (c) degree of anisotropy (P) vs. T diagram, calculated using mean site values.

5. Discussion

One of the first applications of the AMS technique to sedimentary rocks was the identification of paleoflow directions in detrital sediments (e.g., Ising, 1942; Hamilton and Rees, 1970; Hrouda, 1982; Baas et al., 2007). Many studies found that the shape and orientation of the magnetic fabrics is controlled by flow regime (Ellwood 1980; Taira 1989; Tarling and Hrouda, 1993; Piper et al., 1996). In particular, it was observed that in natural or laboratory produced sediments, the magnetic fabric orientation was controlled by the orientation of the long axes of magnetic grains, which in turn are aligned in the direction of flow (Runsak, 1957; Rees, 1965). On this basis a large number of AMS data from sedimentary rocks of different age and sedimentary environments have been interpreted as related to sedimentary processes, where the magnetic foliation is almost parallel to the bedding plane, sometime showing an embrication, and the orientation of the magnetic lineation is parallel or orthogonal to the flow direction (Hamilton and Rees, 1970; Ellwood, 1980; Kissel et al., 1998). However, since the pioneering paper of Graham (1966) who first established a link between AMS and LPS fabrics, it was suggested that the magnetic fabric could also reflect the tectonic history of poorly deformed sediments (e.g., Kissel et al., 1986).

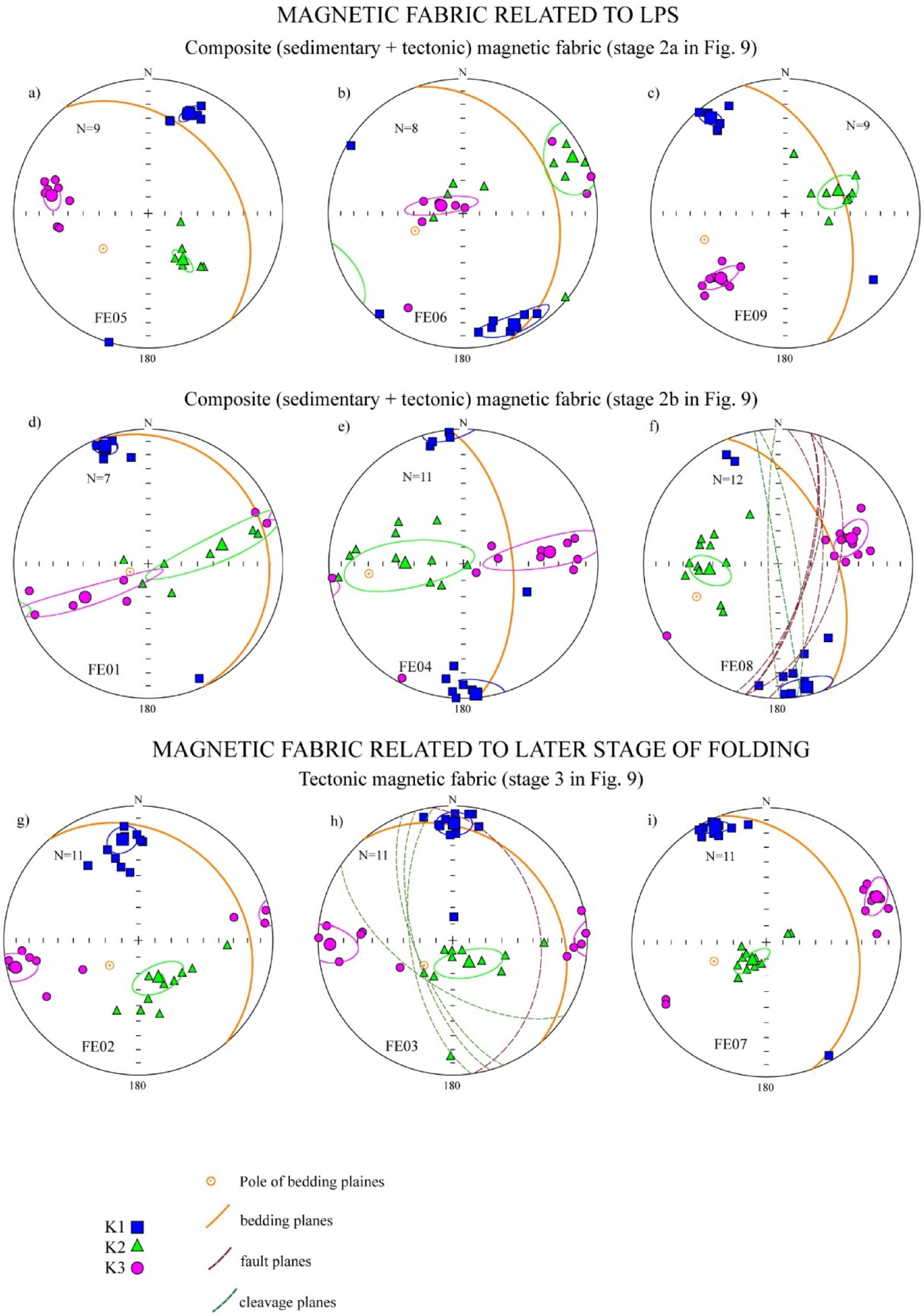

Fig. 7. AMS plots for sites analyzed in this study. Data are plotted on lower hemisphere, equal-area projections, in geographic coordinates. Maximum (squares), intermediate (triangles) and minimum (circles) susceptibility axes together with bedding, cleavage and fault planes are represented.

Subsequent studies have utilized AMS in sedimentary rocks for kinematic analysis of fold-thrust belts. According to the model of the origin of magnetic fabric related to LPS, if sediments undergo an horizontal shortening a tectonic AMS sub-fabric will progressively develop modifying the original sedimentary magnetic fabric, according to the nature and extent of deformation (Fig. 9a). When the LPS deformation is low to moderate, the principal maximum axis K_1 (magnetic lineation) tracks the intersection between LPS and bedding fabrics and will align perpendicular to the shortening direction and subparallel to regional structural trend (Kissel *et al.* 1986; Mattei *et al.* 1997; Sagnotti *et al.* 1998; Pares & Van der Pluijm 2002; Cifelli *et al.* 2009; Oliva-Urcia *et al.* 2009). K_3 remains perpendicular to the bedding plane, still marking the primary magnetic fabric acquired during compaction (Fig. 9a, stage 2a). If shortening increases, the K_3 becomes distributed along a girdle that is parallel to the tectonic LPS direction, and the magnetic ellipsoid becomes prolate (e.g., Kligfield et al., 1981; 1983; Pares & Van der Pluijm 2002) (Fig. 9a, stage 2b). Additional LPS leads the magnetic ellipsoid back to the flattening field with the magnetic foliation parallel to the flattening plane and mesoscopic cleavage (Lowrie & Hirt 1987; Housen & Van der Pluijm 1991; Hirt *et al.* 1995; Luneburg *et al.* 1999; Debacker *et al.* 2009), whereas the magnetic lineation is aligned parallel to the stretching direction, with the development of a purely tectonic magnetic fabric (Fig. 9, stage 3).

In the Ferdows thrust-fold system, all the measured sites show a good agreement among the axes of the magnetic fabric and those of the tectonic structures at local and regional scale (Fig. 7). The magnetic lineation is well defined in all the sites, with the mean direction of K_1 oriented NNW, gently plunging toward NNW (the mean direction of the K_1 calculated from all the sites is N347, 5 ($e_{1\text{-}3}$= 15.9°) (Fig. 8). The distribution of magnetic foliation is more variable and only partially related to LPS deformation: some sites show a K_3 sub-orthogonal to the bedding planes, some sites show a girdle distribution of K_3 around the maximum susceptibility axis K_1, one site shows a magnetic foliation almost orthogonal to bedding, whereas other sites do not show any relationships between bedding planes and magnetic foliation (Fig. 7). When all the sites are taken together, the magnetic foliation is distributed in a girdle with a WSW-ENE orientation, with the maximum concentration around the vertical (the mean direction of the K_3 calculated from all the sites is N256, 11, and $e_{1\text{-}2}$ = 58.4°) (Fig. 8). At the regional scale, both magnetic foliation and magnetic lineation are oriented parallel to the fold axis, as resulting by the bedding attitude distribution, and are almost parallel to the main direction of the joint system measured at site FE03 and of bedding parallel shear zone measured at site FE08 (Figg. 7,8). Furthermore, both magnetic foliation and magnetic lineation are oriented orthogonal to the slip direction observed during the 1968 Ferdows earthquakes, suggesting a close relationship between the development of the magnetic fabric and the regional stress field (Fig. 2). Taken all together, these observations give strong evidence that the formation of the magnetic fabric has been mainly driven by tectonic processes.

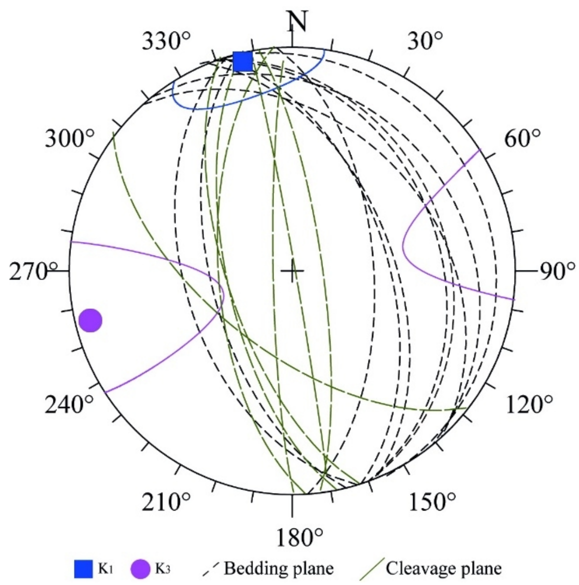

Fig. 8. Mean direction of magnetic foliation and magnetic lineation computed for all sites from the Ferdows area compared with structural data directions.

The most peculiar feature of the observed magnetic fabric in the Ferdows thrust-fold system is represented by the orientation of the magnetic foliation, which allows describing its progressive development related to both LPS and internal strain during folding. Low degree pre-folding LPS is responsible of the development of the magnetic fabric observed at sites FE05, FE06, and FE09, characterized by a well-defined magnetic lineation parallel to the fold axis, and a magnetic foliation sub parallel to the bedding plane (Figg. 7, 9a). The magnetic lineation is considered as an intersection lineation between the bedding plane and a cryptic tectonic foliation (cleavage), orthogonal to the bedding, which is not visible at the outcrop scale. For moderate LPS, the strengths of tectonic and primary fabrics become similar, the magnetic foliation start to disperse along a girdle orthogonal to the magnetic lineation, K_1 strongly clusters parallel to the intersection of LPS and bedding fabrics, and the AMS ellipsoid becomes prolate (sites FE01 and FE04, Figg. 7, 9a). For high LPS, the tectonic fabric becomes dominant, magnetic foliation clusters perpendicular to bedding plane, K_1 clusters parallel to structural trend, and the AMS becomes oblate (FE08) (Figg. 7, 9a). These three types of magnetic fabric are consistent with the evolution of magnetic fabric related to different degrees of LPS and described in many fold-thrust belts, which suggest an early development of magnetic foliation that was acquired when the bedding was still horizonthal (Graham, 1966; Borradaile & Tarling, 1981; Parés & Dinarès-Turell, 1993; Sagnotti and Speranza, 1993; Parés and van der Pluijm, 2003; Cifelli et al., 2015).

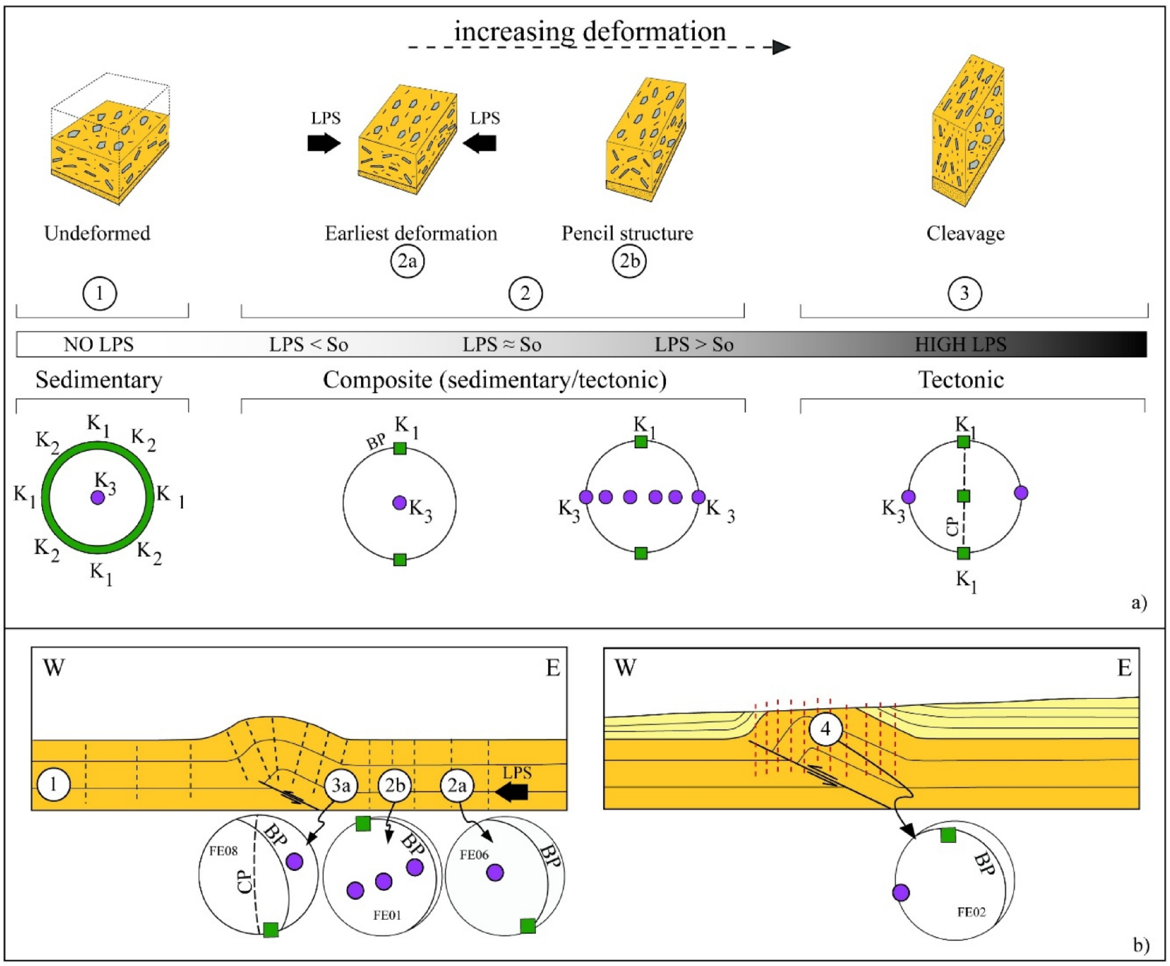

Fig. 9. Evolution of the directional and shape characteristics of AMS and strain ellipsoids during progressive deformation related to LPS (a); (b) schematic geological section of a thrust-related fold showing the observed geometry of magnetic fabric formed during LPS (1) and later stage of folding (2). Representative results from the Ferdows area are also reported.

The more interesting magnetic fabric observed in the Ferdows thrust-fold is represented by a sub-vertical magnetic foliation (sites FE02, FE03, FE07) that is oblique to the bedding planes and cannot attributed to a LPS shortening, implying a different mechanism of deformation during the fold growth, that include flexural-slip and horizontal flattening (Averbuch et al., 1992; 1995; Saint-Bezar et al., 2002). In the active thrust-fold structures of Central Iran several evidences of active flexural-slip movements have been observed during recent earthquakes (Berberian, 1979; Berberian et al., 2000; Walker et al., 2003). In these structures surface ruptures and bedding-planes slip associated to co-seismic deformation have been observed in sub-vertical bedding planes located on growing thrust-related anticlines. In the 1968 Ferdows earthquakes no surface ruptures have been observed in the field, but flexural-slip deformation is present at site FE08, where a decimetric shear zone parallel to the high angle bedding planes (55°) is visible, showing S-C structures with a top-to-the west sense of shear. Several Authors suggested that the formation of oblique magnetic foliation by flexural-slip mechanism is limited to the steep forelimbs of thrust-fold anticlines, where deformation is stronger (Averbuch et al., 1992; Saint-Bezar et al., 2002). In the Ferdows thrust-fold structure the sub-vertical magnetic foliation also occurred in sites located in gentle east-dipping fold limbs (FE02, FE07) that do not show evidence of strong deformation and are located at different position respect to the buried thrust front. A possible hypothesis is that this magnetic fabric is related to late folding horizontal shortening, associated with the stress field responsible of the activity of the Ferdows thrust, which completely erased the primary sedimentary magnetic fabric, with the developing of a sub-vertical foliation (cryptic cleavage) not visible at the outcrop scale (Fig. 9b). This model appears in agreement with the overall tectonic history of the Ferdows thrust-fold system which is characterized by two distinct phases of fold growing, marked by a sharp angular unconformity between the middle-upper Miocene URF and the overlying alluvial and fluvial Quaternary deposits. We speculate that the magnetic fabric related to LPS deformation (Fig. 9a) has been preserved during the early stages of folding, which caused the steep bedding of the URF, whereas the formation of the fourth magnetic fabric (Fig. 9b), characterized by sub-vertical magnetic foliation oblique to bedding, is related to the later stage of folding testified by the gentle anticline of the Quaternary alluvial and river deposits, which lie unconformably on top of the steep URF units.

6. Conclusions

A previously unknown regional fold system, oriented NNW-SSE, has been recognized in the Neogene URF, cropping out in the hanging-wall of the Ferdows thrust fault. The Quaternary deposits, which lay unconformably on top of the URF, are gently folded and describe a NNW-SSE oriented anticline in the hanging-wall of the Ferdows thrust. AMS analyses show that the URF have a well-defined magnetic fabric of tectonic origin, with both magnetic lineation and magnetic foliation oriented parallel to the regional fold axes. In most of the cases magnetic fabric, acquired when the bedding were still horizontal, is related to different degrees of LPS shortening. In some other cases, the magnetic foliation is vertical and oblique to the bedding, suggesting that in the Ferdows thrust-fold structure a cleavage system, not visible at the outcrop scale, has been developed as a consequence of later shortening related to the activity of the thrust system responsible of the recent earthquakes in the area.

Chapter VI

Discussion and conclusion

Discussion and conclusion

Numerous tectonics' investigations used paleomagnetic evidences to infer crustal motions and rotations. The application of the paleomagnetic approach has ranged from the reconstruction of major plate motions (e.g. Irving, 1977) to smaller-scale studies dealing with more local tectonic events (Van der voo and Cannell, 1980).

Iran has a complex deformation history which has been controlled by the presence of continental blocks (Alborz, Lut, and central Iran), whose margins were reactivated during the Cenozoic to accommodate shortening due to Arabia-Eurasia convergence (Mattei et al., 2012). Despite some paleomagnetic researches which has mainly focused on the reconstruction of the late Paleozoic-early Mesozoic northward drift of the Cimmerian blocks (Besse et al., 1998; Muttoni et al., 2009a, 2009b), few paleomagnetic available data from Jurassic to Cenozoic units (Wensink, 1982; Bina et al., 1986; Soffel et al., 1996; Ballato et al., 2008, Mattei et al, 2012, 2014), leaving the post-Cimmerian history of Iran poorly constrained. In this thesis, I carried out a detailed study combining (1) paleomagnetic analysis of the central Iran in the late Jurassic-early Cretaceous to reconstruct the history of paleomagnetic rotations and latitudinal drift of Iran during the Mesozoic; (2) utilization of the paleomagnetic results to give constraints on the origin of the curved shape of the Alborz and Kopeh-Dagh orogens and Shahdad Thrust-belt; (3) applying the paleomagnetic data to define the amount of paleomagnetic rotations in Central Iran since the Miocene, and the relationship between these rotations and the major strike-slip faults kinematics (4) AMS studies on the Late Jurassic-Early Cretaceous and Miocene deposits to define the deformation style across this tectonic boundary and understanding a relationships between the recent tectonics evolution of these areas.

1. Paleogeographic evolution of the CEIM during the Mesozoic

Paleomagnetic results of this study and the literature give some new constraints on the tectonic and paleogeographic evolution of Iran during Middle Jurassic-Late Cretaceous, taking into account latitudinal drifting events, vertical axis rotations, facies distribution, and main geodynamic processes in the area.

During the Middle Jurassic (170 Ma), the Central-East-Iranian Microcontinent (CEIM) consisting of the Yazd, Tabas and Lut continental blocks, was situated in the mid-latitude (~40°N) temperate belt, whereas during the Late Jurassic (145 Ma), it shifted to the low latitude tropical arid belt (~15°N). At these times, the CEIM was oriented WSW-ENE, and had the same lateral arrangement with respect to each other as they have today. The Yazd Block was emergent for most of the Jurassic period and the marine influence increased from the Tabas to the Lut blocks. The Lut Block was bordered to the south by Neo-Tethys Ocean and to the southeast by Neo-Sistan oceanic seaway. Subsequently, the CEIM experienced significant counter-clockwise (CCW) rotation during the Late Jurassic–Early Cretaceous. Our data are not conclusive for indicating if the measured CCW rotation of the CEIM resulted from the northward propagation of rifting-spreading in the Sistan basin during Late Jurassic to Early Cretaceous times, or to the subsequent (late Early Cretaceous?) eastward subduction and closure of the Sistan oceanic basin underneath the continental margin of the Afghan Block (Rossetti et al., 2010).

2. Tertiary tectonic evolution: block-rotation and oroclines

Paleomagnetism is a powerful tool to measure the amount and sense of vertical-axis block rotations and evaluate oroclinal processes within the collision zone. I used the paleomagnetic results to interpret the effect of shortening related to the Arabia-Eurasia convergence in high rate deformation (Alborz) and low rate Deformation (Central Iran)

2.1. Oroclines in Alborz Range and Shahdad thrust- fold belt

The paleomagnetic data mainly obtained from the Upper Red Formation (URF), and in some sites from Lower Red and Qom Formation of Western, Central and Eastern part of Alborz Range and from URF sediments along the Shahdad thrust-fold belt. Paleomagnetic results imply that, the western arm of the Alborz, oriented NW-SE, rotated 17.8° CW (±10°) and 6.2° (±9.2°) CW, whereas the Central part, oriented SW–NE, rotated 21.1° (± 10.6°) CCW and the eastern arm, oriented NW-SE, rotated 17.4° (± 7.7°) CW. Taken together, an oroclinal bending mechanism is proposed for the origin of the curved Alborz Mountains, which acquired most of its curvature in the last 8 Myr. Most likely, the bending processes caused by relative motion between the stable and rigid South Caspian Basin, and the Central/Eastern Iranian blocks, which are located to the north and south of the Alborz range, respectively. In Shahdad thrust-fold Belt, the paleomagnetic results demonstrate the CCW rotation of 22.8° (±18.6°), the NNW-SSE oriented, in the northern part, 13.8° (±7.9°) and 16° (±17.9°) CCW rotation, the N-S oriented, in the central part, and CCW rotation of 5.4° rotation, the NNE-SSW oriented, South-Center and CW in Southern part. Therefore, by the preliminary results, the Shahdad thrust-fold belt may have resulted from orocline bending.

2. 2. Block Rotations in Central Iran

Shortening related to the Arabia-Eurasia convergence has been mainly accommodated in high mountain ranges, Zagros, Alborz, and Kopeh Dag fold-thrust belts of Iran, whereas fault-bonded crustal blocks of CEIM are relatively undeformed. Paleomagnetic data demonstrate that slip on the strike slip-fault of central Iran adjusts vertical axis rotation of the fault bounded crustal blocks. These strike-slip faults have different direction and kinematics. The NE-SW to E-W left-lateral strike slip faults (e.g. Doruneh and Dasht-e- Bayaz), determine the tectonic boundary between Central Iran and the Alborz, whereas N-S right-lateral strike-slip faults prevail along the tectonic boundary between the Yazd, Tabas and Lut blocks. In Central Iran, CW paleomagnetic rotations have been measured in areas where E-W oriented left-lateral strike-slip faults (e.g. Doruneh and Dasht-e-Bayaz) are predominant (e.g. Ferdows area in the Lut block) and north of the Great Kavir fault (Torud and Jandaq), whereas CCW paleomagnetic rotations have been measured in the Tabas, Yazd and Anarak areas, which are characterized by N-S to NNW-SSE oriented right-lateral strike-slip faults. Our new finding show that from the Late Cretaceous to the Oligocene, no significant paleomagnetic rotations have been observed in these area and an important phase of

CCW rotations occurred after the Middle–Late Miocene. Our paleomagnetic results confirm the block-rotation model suggested by Walker and Jackson (2004) and Allen et al. (2004, 2011) to account for late Cenozoic shortening in central Iran, which was based on structural, geomorphologic, and seismic data.

3. Anisotropy of Magnetic Susceptibility

Since Graham (1954) has introduced the Anisotropy of magnetic susceptibility (AMS) as a petrofabric indicator, it has been used to reconstruct the deformation history of sediments widely, even if they appear almost undeformed at the outcrop scale (e.g. Kissel et al., 1986). In particular, it has been demonstrated that magnetic fabric analyses can provide insights into the deformation pattern in different tectonic settings, such as fold and thrust belts (e.g.Borradaile and Tarling, 1981; Mattei et al., 1995, 1997), foreland basins (e.g. Pares et al., 1999), accretionary prisms (e.g. Lee et al., 1990), and sedimentary basins developed under extensional tectonic regime (e.g. Mattei et al., 1997; Cifelli et al., 2007; Porreca and Mattei, 2012). These investigations, indicate a direct connection between the magnetic fabric and the structural setting, and confirm the capacity of AMS to record history of deformation in different tectonic positions.

3.1. Magnetic fabric of the Garedu red beds across the tectonic boundary of Yazd and Tabas Blocks and URF of Ferdows thrust-fold system (Lut Block)

Iran represents one of the most instructive regions to study continental deformation, as here the present-day Arabia–Eurasia convergence is accommodated in a very wide area over a range of structures. To better understanding the deformation style across the tectonic boundary and within the blocks of Central Iran, we integrated AMS and structural analysis of Upper Jurassic Garedu Red Beds Fm. (boundary of the Tabas and Lut Blocks), and Neogene URF of Ferdows thrust-fold system. In the Garedu syncline, AMS and structural results show a magnetic fabric typical of an intermediate stage of deformation, with a magnetic foliation parallel to the cleavage and magnetic lineation often lying at the intersection between cleavage and bedding. Magnetic fabric and cleavage are rotated about 15° CCW respect to the fold hinge, suggesting that the Garedu Red Beds syncline is a transected fold, which formed as a consequence of a right-lateral transpressional regime at the boundary between the Tabas and Lut blocks of Central Iran, between the Lower Cretaceous and Palaeocene. In the Ferdows Thrust-fold system, AMS analyses show that in most of the cases, magnetic fabric acquired when the bedding were still horizontal, is related to different degrees of LPS shortening. In some cases, magnetic fabric has been developed as a consequence of later shortening related to the activity of the thrust system responsible of the recent earthquakes in the area. Results from this study establish a relationships between the recent tectonics of the area and the evolution of the magnetic fabric and demonstrate that a well defined magnetic fabric of pure tectonic origin can also develop in poorly deformed rocks lacking field evidence of pervasive internal deformation.

Bibliography

Aghanabati, A., 1994a. Geological map of Boshruyeh, Series No. J7, scale 1:00,000. Geological survey of Iran.

Aghanabati, A., 1994b. Geological map of Shirgesht, No. Series 7358, scale 1:100,000. Geological survey of Iran.

Alavi, M., 1991. Sedimentary and structural characteristics of the Paleo-Tethys remnants in northeastern Iran. Geological Society of America Bulletin, *103*, 983-992.

Alavi, M. 1994. Tectonics of the Zagros orogenic belt of Iran: new data and interpretations. Tectonophysics, *229*, 211-238.

Alavi, M., 1996. Tectonostratigraphic synthesis and structural style of the Alborz mountain system in northern Iran. Journal of Geodynamics, *21*, 1-33.

Alimohammadian, H., Hamidi, Z., Aslani, A., Shahidi, A., Cifelli, F., Mattei, M., 2013. A tectonic origin of magnetic fabric in the Shemshak group from Alborz Mts. (Northern Iran). Journal of Asian Earth Science, 73, 419–428, doi.org/doi.org/ 10.1016/j.jseaes.2013.05.014.

Allen, M.B., Ghassemi, M.R., Shahrabi, M., Qorashi, M., 2003. Accommodation of late Cenozoic oblique shortening in the Alborz range, northern Iran. Journal of structural geology, 25, 659–672.

Allen, M., Jackson, J. & Walker, R., 2004. Late Cenozoic reorganization of the Arabia-Eurasia collision and the comparison of short-term and long-term deformation rates. Tectonics*,* 23, TC2008, doi: 10.1029/2003TC001530.

Allen, M. B., Armstrong, H. A., 2008. Arabia–Eurasia collision and the forcing of mid-Cenozoic global cooling. Palaeogeography, Palaeoclimatology, Palaeoecology, *265*(1), 52-58. doi: 10.1016/j.palaeo.2008.04.021

Allen, M.B., Kheirkhah, M., Emami, M.H., Jones, S.J., 2011. Right-lateral shear across Iran and kinematic change in the Arabia-Eurasia collision zone. Geophysical Journal International*,* 184, 555–574.

Ambraseys, N.N., Melville, C.P., 1982. A History of Persian Earthquakes. Cambridge University Press, London, p. 219.

Amidi, S. M., Emami, M. H., Michel, R., 1984. Alkaline character of Eocene volcanism in the middle part of Central Iran and its geodynamic situation.Geologische Rundschau, *73*, 917-932.

Amini, A., 1997. Provenance and Depositional Environment of the Upper Red Formation*, Central* Zone Iran*,* Ph.D. thesis, The University of Manchester.

Amini, A., Anketell, J.M., 2015. Textural and geochemical studies of detrital Fe–Ti oxides and test of their validity in provenance determination, a case study from Central Iran. Journal of African Earth Sciences, 103, 140–152. doi.org/10.1016/ j.jafrearsci.2014.12.008.

Aubourg, C.B., Smith, H., Bakhtari, N., Guya, A., Eshragi, S., Lallemant, S., Molinaro,M., Braud, X,. Delaunay,S., 2004. Post-Miocene shortening pictured by magnetic fabric across the Zagros-Makran syntaxis. Geological Society of America Special Papers, 383, 17-40

Aubourg, C., Smith, B., Eshraghi, S., Lacombe, O., Authemayou, C., Amrouch, K., Bellier, O., Mouthereau, F., 2010. New magnetic fabric data and their comparison with palaeostress markers in the Western Fars Arc (Zagros, Iran): tectonic implications. Geological Society of London, Special Publication, 330**,** 97–120.

Averbuch, O., Frizon de Lamotte, D., Kissel, C., 1992. Magnetic fabric as a structural indicator of the deformation path within a fold–thrust structure: a test case from the Corbieres (NE Pyrenees, France). Journal of Structural Geology, 14, 461–474. doi.org10.1016/0191-8141 (92)90106-7.

Averbuch, O., Mattei, M., Kissel, C., Frizon de Lamotte, D., Speranza, F., 1995. Cinématique des déformation au sein d'un système chevauchant aveugle: l'exemple de la ''Montagna dei Fiori'' (front des Apennins Centraux, Italie). Bulletin de la Société géologique de France, 166, 451–461. doi.org/10.2113/gssgfbull.166.5.451. 2332.

Azizan, A., Shahraki, A., Seifouri, S., 1999. Geological map of Kerman, Series No. 7450, Scale 1:100000. Geological Survey of Iran.

Baas, J.H., Hailwood, E.A., McCaffrey, W.D., Kay, M., Jones, R., 2007. Directional petrological characterisation of deep-marine sandstones using grain fabric and permeability anisotropy: methodologies, theory, application and suggestions for integration. Earth-Science Reviews. 82, 101–142. doi.org/10.1016/j.earscirev.2007.02.003.

Babazadeh, S.A., De Wever, P., 2004a. Early Cretaceous radiolarian assemblages from radiolarites in the Sistan Suture (eastern Iran). Geodiversitas 26, 185–206.

Bagheri, S., Stampfli, G.M., 2008. The Anarak, Jandaq and Posht-e-Badam metamorphic complex in central Iran: new geological data, relationships and tectonic implications. Tectonophysics, 451, 123–155.

Ballato, P., Nowaczyk, N. R., Landgraf, A., Strecker, M. R., Friedrich, A., Tabatabaei, S. H., 2008. Tectonic control on sedimentary facies pattern and sediment accumulation rates in the Miocene foreland basin of the southern Alborz Mountains, northern Iran. Tectonics, *27*. doi: 10.1029/2008TC002278.

Ballato, P., Stockli, D.F., Ghassemi, M.R., Landgraf, A., Strecker, M.R., Hassanzadeh, J., Friedrich, A. and Tabatabaei, S.H., 2013. Accommodation of transpressional strain in the Arabia-Eurasia collision zone: new constraints from (U-Th)/He thermochronology in the Alborz Mountains, north Iran.Tectonics, *32*, 1-18.

Barrier, E., & Vrielynck, B., 2008. Palaeotectonic maps of the Middle East.*Commision for the* Geological Map of the World*, Paris*.

Barrier, E., Vrielynck, B., 2008. Palaeotectonic maps of the Middle East. Tectono sedimentary-palinspastic maps from Late Norian to Pliocene. 14 maps. Paris: CGMW/CCGM.

Baud, A., Stampfli, G, Steen, D., 1991. The Triassic Aghdarband Group: volcanism and geological evolution. Abhandlungen der Geologischen Bundesanstalt, *38*, 125-137.

Becker, H., Förster, H., Soffel, H., 1973. Central Iran, a former part of Gondwanaland. Paleomagnetic evidence from Infracambrian rocks and iron ores of the Bafq area, Central Iran: Zeitschrift fuer Geophysik, 39, 953-963.

Berberian, M., 1979. Earthquake faulting and bedding thrust associated with the Tabas-e-Golshan (Iran) earthquake of September 16, 1978. Bulletin of the Seismological Society of America*,* 69, 1861–1188.

Berberian, M., King, G.C.P., 1981. Towards a paleogeography and tectonic evolution of Iran, Canadian journal of earth sciences*.* 18, 210–265.

Berberian, F., Berberian, M., 1981. Tectono-plutonic episodes in Iran. Zagros Hindu Kush Himalaya Geodynamic Evolution, 5-32.

Berberian, F., Muir, I. D., Pankhurst, R. J., & Berberian, M. 1982. Late Cretaceous and early Miocene Andean-type plutonic activity in northern Makran and Central Iran. Journal of the Geological Society, 139, 605-614.

Berberian, M., Yeats, R.S., 1999. Patterns of historical earthquake rupture in the Iranian plateau, Bulletin of the Seismological Society of America. 89, 120–139.

Berberian, M., Jackson, J.A., Qorashi, M., Talebian, M., Khatib, M.M., Priestley, K., 2000. The 1994 Sefidabeh earthquakes in eastern Iran: blind thrusting and bedding-plane slip on a growing anticline, and active tectonics of the Sistan suture zone. Geophysical Journal International. 142, 283–299. doi.org/10.1046/j.1365-246x.2000.00158.x.

Berberian, M., 2014. Earthquakes and Coseismic Surface Faulting on the Iranian Plateau – A Historical, Social and Physical Approach. Developments in Earth Surface Processes 17. pp. 2–714. ISBN: 978-0-444-63292-0.

Besse, J., Torcq, F., Gallet, Y., Ricou, L.E., Krystin, L., Saydi, A., 1998, Late Triassic paleomagnetic data from Iran: Constraints on the migration of the Iranian block through the Tethyan Ocean and initial destruction of Pangea: Geophysical Journal International, 135, 77–92. doi:10.1046/j.1365-246X.1998.00603.x.

Besse, J., Courtillot, V., 2002. Apparent and true polar wander and the geometry of the geomagnetic field over the last 200 Myr. Journal of Geophysical Research. 107. doi.org/2310.1029/2000JB000050.

Besse, J., Torcq, F., Gallet, Y., Ricou, L.E., Krystyn, L., Saidi, A., 1998. Late Permian to Late Triassic palaeomagnetic data from Iran: Contrains on the migration of the Iranian block through the Tethyan Ocean and initial destruction of Pangea. Geophysical Journal International. 135, 77–92. doi.org/10.1046/j.1365246X.1998.00603.x.

Bina, M.M., Bucur, I., Prévot, M., Meyerfeld, Y., Daly, L., Cantagrel, J.M., Mergoil, J., 1986. Palaeomagnetism, petrology and geochronology of Tertiary magmatic and sedimentary units from Iran. Tectonophysics 121, 303–329.

Borradaile, G.J., 1978. Transected folds: a study illustrated with examples from Canada and Scotland. Geological Society of America Bulletin, 89, 481–493.

Borradaile, G.J., Tarling, D.H., 1981. The influence of deformation mechanisms on magnetic fabrics in weakly deformed rocks. Tectonophysics, 77, 151–168. doi.org/10.1016/0040-1951(81)90165-7.

Borradaile, G.J. & Henry, B., 1997. Tectonic applications of magnetic susceptibility and its anisotropy, Earth-Science Reviews. 42, 49–93.

Bottrill, A. D., van Hunen, J., Allen, M. B., 2012. Insight into collision zone dynamics from topography: numerical modelling results and observations. Solid Earth, *3*, 387-399.

Brönnimann, P., Zaninetti, L., Moshtaghian, A., Huber, H., 1973. Foraminifera from the Sorkh Shale Formation of the Tabas area, east-central Iran. Riv. Ital. Paleont, *79*, 1-32.

Brunet, M. F., Cloetingh, S., 2003. Integrated peri-Tethyan basins studies (peri-Tethys programme). Sedimentary Geology, *156*, 1-10.

Brunet, M.-F., et al. (Eds.), South Caspian to Central Iran Basins. Geological Society of London Special Publication 312, 31–55. doi.org/10.1144/SP312.3.

Carey, S.W., 1955. The orocline concept in geotectonics-Part I. In Papers and proceedings of the Royal Society of Tasmania, 89, 255-288.

Cifelli, F., Rossetti, F., Mattei, M., Hirt, A.M., Funiciello, R., Tortorici, L., 2004. An AMS, structural and paleomagnetic study of quaternary deformation in eastern Sicily. Geophysical Journal International, 26, 29–46.

Cifelli, F., Mattei, M., Chadima, M., Hirt, A. &Hansen, A., 2005. The origin of tectonic lineation in extensional basins: combined neutron texture and magnetic analyses on undeformed clays. Earth and Planetary Science Letters, 235, 62–78.

Cifelli, F., Rossetti, F., Mattei, M., 2007. The architecture of brittle postorogenic extension: results from an integrated structural and paleomagnetic study in north Calabria (southern Italy). Geological Society of America Bulletin, 119, 221– 239. doi.org/10.1130/B25900.1.

Cifelli, F., Mattei, M. and Della Seta, M., 2008. Calabrian Arc oroclinal bending: The role of subduction. Tectonics, 27, TC5001. doi:10.1029/2008TC002272.

Cifelli, F., Mattei, M., Chadima, M., Lenser, S., Hirt, A.M., 2009. The magnetic fabric in undeformed clays: AMS and neutron texture analyses from the Rif Chain (Morocco), Tectonophysics. 466, 79–88. doi.org/10.1016/j.tecto.2008.08.008.

Cifelli, F., Mattei, M., Rashid, H., Ghalamghash, J., 2013. Right-lateral transpressional tectonics along the boundary between Lut and Tabas blocks (Central Iran). Geophysical Journal International, 193, 1153–1165. doi.org/10.1093/gji/ggt070.

Cifelli, F., Ballato, P., Alimohammadian, H., Sabouri, J., Mattei, M., 2015. Tectonic magnetic lineation and oroclinal bending of the Alborz range: implications on the Iran–Southern Caspian geodynamics. Tectonics, 34, 116–132. doi.org/10.1002/2014TC003626.

Conrad, G., Montigny, R., Thuizat, R., Westphal, M., 1981. Tertiary and Quaternary geodynamics of Southern Lut (Iran) as deduced from palaeomagnetic, isotopic and structural data. Tectonophysics, 75, T11–T17.

Daneshian, J., Dana, L. R., 2007. Early Miocene benthic foraminifera and biostratigraphy of the Qom Formation, Deh Namak, central Iran. Journal of Asian Earth Sciences, *29*, 844-858.

Davoudzadeh, M., Soffel, H., Schmidt, K., 1981. On the rotation of the Central-East Iran microplate. Neues Jahrbuch für Geologie und Paläontologie, Monatshefte, *1981*, 180-192.

Davoudzadeh, M., & Schmidt, K., 1984. A review of the Mesozoic paleogeography and paleotectonic evolution of Iran. N. Jb. Geol. Palaont. Abh, *168*.

Davoudzadeh, M., Lammerer, B., Weber-Diefenbach, K., 1997. Paleogeography, Stratigraphy, and Tectonics of the Tertiary of Iran. Neues Jahrbuch fur Geologie und Palaontologie-Abhandlungen, *205*, 33-68.

Debacker, T.N., Hirt, A.M., Sintubin, M., Robion, P., 2009. Differences between magnetic and mineral fabrics in low-grade, cleaved siliciclastic pelites: a case study from the Anglo-Brabant Deformation Belt (Belgium). Tectonophysics, 466, 32–46. doi.org/10.1016/j.tecto.2008.08.008.

Debacker, T.N., Robion, P., Sintubin, M., 2004. The anisotropy of magnetic susceptibility (AMS) in low-grade, cleaved pelitic rocks: influence of cleavage/ bedding angle and type and relative orientation of magnetic carriers. In: Martin-Hernandez, F., Lüneburg, C.M., Aubourg, C., Jackson, M. (Eds.), Magnetic Fabrics: Methods and Applications. Geological Society, London, Special Publications, 238, 77–107.

Demarest, H.H., 1983. Error analysis for the determination of tectonic rotation from paleomagnetic data. Journal of Geophysical Research, 88, 4321–4328. doi.org/10.1029/ JB088iB05p04321.

Dercourt, J.E.A., Zonenshain, L.P., Ricou, L.E., Kazmin, V.G., Le Pichon, X., Knipper, A.L., Grandjacquet, C., Sbortshikov, I.M., Geyssant, J., Lepvrier, C. and Pechersky, D.H., 1986. Geological evolution of the Tethys belt from the Atlantic to the Pamirs since the Lias. Tectonophysics, *123*, 241-315.

Dewey, J. F., Pitman, W. C., Ryan, W. B., Bonnin, J., 1973. Plate tectonics and the evolution of the Alpine system. Geological society of America bulletin, *84*, 3137-3180.

Dewey, J. F., Sengör, A. C., 1979. Aegean and surrounding regions: complex multiplate and continuum tectonics in a convergent zone. Geological Society of America Bulletin, *90*, 84-92.

Dewey, J. F., Helman, M. L., Knott, S. D., Turco, E., & Hutton, D. H. W., 1989. Kinematics of the western Mediterranean. Geological Society, London, Special Publications, *45*, 265-283.

Ellwood, B.B., 1980. Induced and remanent magnetic properties of marine sediments as indicators of depositional processes. Marine Geology. 38, 233–244. doi.org/10.1016/0025-3227(80)90061-4.

Fisher, R.A., 1953. Dispersion on a sphere. In: *Proceedings of the Royal Society of London* A: Mathematical, Physical and Engineering Sciences. The Royal Society, 1130, 295-305.

Fotoohi Rad, G.R., Droop, G.T.R., Burgess, R., 2009. Early Cretaceous exhumation of High-pressure metamorphic rocks of the Sistan Suture Zone, eastern Iran. Geological Journal, 44, 104–116.

Fursich, F.T., Wilmsen, M., Seyed-Emami, K., Schairer, G., Majidifard, M.R., 2003. Platform-basin transect of a middle to late Jurassic large-scale carbonate platform system (Shotori Mountains, Tabas Area, East-Central Iran). Facies, 48, 171–198.

Fürsich, F.T., Wilmsen, M., Seyed-Emami, K. and Majidifard, M.R., 2009. Lithostratigraphy of the Upper Triassic–Middle Jurassic Shemshak Group of Northern Iran. Geological Society, London, Special Publications, *312*,129-160.

Gallet, Y., Krystyn, L., Besse, J., Saidi, A., Ricou, L. E., 2000. New constraints on the Upper Permian and Lower Triassic geomagnetic polarity timescale from the Abadeh section (central Iran). Journal of Geophysical Research*, 105*, 2805-2815.

Ghazi, A.M., Hassanipak, A.A., Mahoney, J.J., Duncan, R.A., 2004. Geochemica characteristics, 40Ar–39Ar ages and original tectonic setting of the Band-e- Zeyarat—Dar Anar ophiolite, Makran accretionary prism, S.E, Iran. Tectonophysics 393, 175–196.

Goldstein, A.G. & Brown, L.L., 1988. Magnetic susceptibility anisotropy of mylonites from the Brevard zone, North Carolina, U.S.A. Physics of the earth and planetary interiors*,* 51, 290–300.

Golonka, J., 2000. *Cambrian-Neogene plate tectonic maps*. Wydawn. Uniwersytetu JagielloĹ „skiego.

Golonka, J., Gahagan, L., Krobicki, M., Marko, F., Oszczypko, N., 2006. Plate-tectonic evolution and paleogeography of the circum-Carpathian region.

Golonka, J., 2007. Late Triassic and Early Jurassic palaeogeography of the world. Palaeogeography, Palaeoclimatology, Palaeoecology, *244*, 297-307.

Graham, J. W., 1966. Significance of Magnetic Anisotropy in Appalachian Sedimentary Rocks. AGU, Washington, D. C.10, 627–648,

Gray, D.R., 1981. Cleavage-fold relationships and their implications for transected folds: an example from southwest Virginia, USA. Journal of Structural Geology*,* 3, 265–277.

Guest, B., Axen, G. J., Lam, P. S., Hassanzadeh, J., (2006a). Late Cenozoic shortening in the west-central Alborz Mountains, northern Iran, by combined conjugate strike-slip and thin-skinned deformation. Geosphere, 2, doi:10.1130/GES00019.00011.

Guest, B., Stöckli, D.F., Grove, M., Axen, G.J., Lam, P.S., Hassanzadeh, J., 2006b. Thermal histories from the central Alborz Mountains, northern Iran: Implications for the spatial and temporal distribution of deformation in Northern Iran. Geological Society of America Bulletin*,* 118, 1507–1521.

Guest, B., Horton, B. K., Axen, G. J., Hassanzadeh, J., McIntosh, W. C., 2007. Middle to late Cenozoic basin evolution in the western Alborz Mountains: Implications for the onset of collisional deformation in northern Iran. Tectonics, 26, TC6011, doi: 10.1029/2006TC002091.

Hamilton, N., Rees, A.I., 1970. The use of magnetic fabric in paleocurrent estimation. In: Runcorn, S.K. (Ed.). Paleogeophysics, 445–464.

Hassanzadeh, J., Fakhari, M., 1997. The Oligo-Miocene Marine Environments of Central Iran-Intra-and Back-Arc Extensions. In *59th EAGE Conference & Exhibition*.

Hassanzadeh, J., Axen, G. J., Guest, B., Stokli, D. F., Ghazi, A. M., 2004. The Alborz and NW Urumieh-Dokhtar magmatic belts, Iran: rifted parts of a single ancestral arc. In 2004 Denver Annual Meeting.

Hatzfeld, D., and Molnar, P., 2010. Comparisons of the kinematics and deep structures of the Zagros and Himalaya and of the Iranian and Tibetan Plateaus and geodynamic implications: Reviews of Geophysics, 48, 1–48. doi:10.1029/2009RG000304.

Hempton, M. R., 1987. Constraints on Arabian plate motion and extensional history of the Red Sea. Tectonics, *6*, 687-705.

Hessami, K., KOYI, H. A., Talbot, C. J., Tabasi, H., Shabanian, E., 2001. Progressive unconformities within an evolving foreland fold–thrust belt, Zagros Mountains. Journal of the Geological Society, *158*, 969-981.

Hirt, A.M., Evans, K.F. & Engelder, T., 1995. Correlation between magnetic anisotropy and fabric for Devonian shales on the Appalachian Plateau. Tectonophysics*,* 247, 121–132.

Hirt, A.M., Julivert, M., Soldevila, J., 2000. Magnetic fabric and deformation in the Navia-Alto Sil slate belt, Northwestern Spain. Tectonophysics 320, 1–16. doi.org/10.1016/S0040-1951(00)00047-0.

Holdsworth, R.E., Strachan, R.A., Dewey, J.E. (Eds.), 1998. Continental Transpressional and Transtensional Tectonics. Geological Society, London, Special Publications, 135.

Hollingsworth, J., Fattahi, M., Walker, R., Talebian, M., Bahroudi, A., Bolourchi, M.J., Jackson, J., Copley, A., 2010. Oroclinal bending, distributed thrust and strike-slip faulting, and the accommodation of Arabia–Eurasia convergence in NE Iran since the Oligocene. Geophysical Journal International. 181, 1214–1246.

Homke, S., Vergés, J., Garcés, M., Emami, H., Karpuz, R., 2004. Magnetostratigraphy of Miocene–Pliocene Zagros foreland deposits in the front of the Push-e Kush arc (Lurestan Province, Iran). Earth and Planetary Science Letters, *225*, 397-410.

Hounslow, M.W., 1985. Magnetic fabric arising from paramagnetic phyllosilicates minerals in mudrocks, Journal of the Geological Society, London*,* 142, 995–1006.

Housen, B.A. & van der Pluijm, B.A., 1991. Slaty cleavage development and magnetic anisotropy fabrics. Journal of Geophysical Research*,* 96, 9937–9946.

Housen, B.A., Kanamatsu, T., 2003. Magnetic fabrics from the Costa Rica margin: sediment deformation during the initial dewatering and underplating process. Earth and Planetary Science Letters*,* 206, 215–228. doi.org/10.1016/S0012821X (02)01076-2.

Hrouda, F., 1982. Magnetic anisotropy of rocks and its application in geology and geophysics. Geophysical surveys*,* 5, 37–82.

Ising, G., 1942. On the magnetic properties of varved clay. Arkiv för matematik, astronomi o.fysik 29A, 1–37.

Jackson, J. & McKenzie, D., 1984. Active tectonics of the Alpine-Himalayan belt between western Turkey and Pakistan. Geophysical Journal International*,* 77, 185–264.

Jackson, M.J., Tauxe, L., 1991. Anisotropy of magnetic susceptibility and remanence: developments in the characterization of tectonic, sedimentary, and igneous fabric. Reviews of Geophysics*,* 29, 371–376

Jackson, J., Haines, J., Holt, W., 1995. The accommodation of Arabia– Eurasia plate convergence in Iran. Journal of Geophysical Research*,* 100, 15 205–15 219.

Jackson, J., 2001. Living with earthquakes: know your faults. Journal of Earthquake Engineering*,* 5, 5–123.

Jackson, J., Priestley, K., Allen, M., Berberian, M., 2002. Active tectonics of the South Caspian Basin. Geophysical Journal International, 148, 214–245.

Jelinek, V., 1977. The statistical theory of measuring anisotropy of magnetic susceptibility of rocks and its application. Geofyzika Brno*,* 77 p.

Jelinek, V., 1981. Characterization of magnetic fabric of rocks. Tectonophysics*,* 79, 63–67.

Johnson, T.E., 1991. Nomenclature and geometric classification of cleavagetransected Folds. Journal of Structural Geology, 13, 261–274. Jolivet, L., & Faccenna, C. 2000. Mediterranean extension and the Africa-Eurasia collision. Tectonics, *19,* 1095-1106.

Jung, D., Kursten, M., Tarkian, M., 1976. Post-Mesozoic volcanism in Iran and its relation to the subduction of the Afro-Arabian under the Eurasian plate. Afar between continental and oceanic rifting, *2*, 175-181.

Kanamatsu, T., Herrero-Bervera, E., Taira, A., 2001. Magnetic fabrics of soft-sediment folded strata within a Neogene accretionary complex, the Miura group, central Japan. Earth and Planetary Science Letters*,* 187, 333–343. doi.org/10.1016/S0012821X(01)00292-8.

Kananian, A., Juteau, T., Bellon, H., Darvishzadeh, A., Sabzehi, M., Whitechurch, H., Ricou, L.-E., 2001. The ophiolite massif of Kahnuj (western Makran, southern Iran): new geological and geochronological data. Comptes Rendus de L'Académie des Sciences—Series IIA Earth and Planetary Sciences 332, 543–552.

Kargaran, F., Neubauer, F., Genser, J., Houshmandzadeh, A., 2006. The Eocene Chapedony metamorphic core complex in Central Iran: preliminary structural results. In Geophysical Research Abstracts*,* 8, 2006.

Kargaranbafghi, F., Neubauer, F., Genser, J., 2011. Cenozoic kinematic evolution of southwestern Central Iran: Strain partitioning and accommodation of Arabia–Eurasia convergence. Tectonophysics, *502*, 221-243.

Kaz'min, V., Ricou, L.E. and Sbortshikov, I.M., 1986. Structure and evolution of the passive margin of the eastern Tethys. Tectonophysics, *123*, 153-179.

Kaz'min, V. G., Tikhonova, N. F., 2006. Late Cretaceous-Eocene marginal seas in the Black Sea-Caspian region: paleotectonic reconstructions.Geotectonics, *40*, 169-182.

Kaz'min, V. G., Verzhbitskii, E. V., 2011. Age and origin of the South Caspian Basin. Oceanology, *51*, 131-140.

Kent, D.V., Irving, E., 2010. Influence of inclination error in sedimentary rocks on the Triassic and Jurassic apparent polar wander path for North America and implications for Cordilleran tectonics. Journal of Geophysical Research*,* 115, B10103. doi.org/10110.11029/12009JB007205.

Kirschvink, J.L., 1980. The least-squares line and plane and the analysis of paleomagnetic data. Geophysical Journal International*,* 62, 699–718. doi: 10.1111/j.1365-246X.1980.tb02601.x

Kissel, C., Barrier, E., Laj, C. & Lee, T.Q., 1986. Magnetic fabric in undeformed marine clays from compressional zones. Tectonics*,* 5, 769–781.

Kissel, C., Laj, C., Mazaud, A., Dokken, T., 1998. Magnetic anisotropy and environmental changes in two sedimentary cores from the Norwegian Sea and the North Atlantic. Earth and Planetary Science Letters*,* 164, 617–626. doi.org/10.1016/S0040-1951(98)00223-6.

Kligfield, R., Owens, W. H., Lowrie, W., 1981. Magnetic susceptibility anisotropy, strain, and progressive deformation in Permian sediments from the Maritime Alps (France). Earth and Planetary Science Letters*,* 55, 181–189.

Kligfield, R., Lowrie, W., Hirt, A., Siddans, A.W.B., 1983. Effect of progressive deformation on remanent magnetization of Permian redbeds from the Alpes Maritimes (France). Tectonophysics 98, 59–85. doi.org/10.1016/00401951(83)90211-1.

Lafrance, B. & Williams, P.F., 1992. Oblique-cleavage folds: a critical discussion with examples from the Canadian Appalachians, Tectonophysics, 207, 315–330.

Larrasoana, J.C., Pueyo Morer, E.L., Pares, J.M. 2004. An integrated AMS, structural, palaeo- and rock-magnetic study of the Eocene marine marls from the JacaPamplona Basin (Pyrenees, N Spain); new insights into the timing of magnetic fabric acquisition in weakly deformed mudrocks. In: Magnetic fabrics: Methods and applications, Martin Hernadez, F., Hirt, A. (Eds). Geological Society, London, Special Publication 238, 127–143. Doi.org/10.1144/GSL.SP.2004.238.01.10.

Larrasoana, J.C., Gomez-Paccard, M., Giralt, S., Roberts, A.P., 2011. Rapid locking of tectonic magnetic fabrics in weakly deformed mudrocks. Tectonophysics 507, 16–25. doi.org/10.1016/j.tecto.2011.05.003.

Lee, T.Q., Kissel, C., Laj, C., Horng, C., Lue, Y., 1990. Magnetic fabric analysis of the Plio-Pleistocene sedimentary formations of the coastal range of Taiwan. Earth and Planetary Science Letters, 98, 23–32.

Lowrie, W., Hirt, A.M., 1987. Anisotropy of magnetic susceptibility in the Scaglia Rossa pelagic limestone, Earth and Planetary Science Letters, 55, 181–189.

Lowrie, W., 1990. Identification of ferromagnetic minerals in a rock by coercivity and unblocking temperature properties. Earth and Planetary Science Letters, 17, 159–162.

Luneburg, C.M., Lampert, S.A., Lebit, H.D., Hirt, A.M., Casey, M., Lowrie, W., 1999. Magnetic anisotropy, rock fabrics and finite strain in deformed sediments of SW Sardinia (Italy). Tectonophysics, 307, 51–74.

Luo, L. *et al.*, 2009. Magnetic fabric investigation in the northwestern Sichuan Basin and its regional inference. Physics of the Earth and Planetary Interiors, 173, 103–114.

Mattei, M., Sagnotti, L., Faccenna, C., Funiciello, R., 1997. Magnetic fabric of weakly deformed clay-rich sediments in the Italian peninsula: relationship with compressional and extensional tectonics. Tectonophysics 271, 107–122. doi.org/10.1016/S0040-1951(96)00244-2.

Mattei, M., Cifelli, F., Muttoni, G., Zanchi, A., Berra, F., Mossavvari, F., Safar Ali, E., 2012. Neogene block-rotation in Central Iran: evidence from paleomagnetic data. Geological Society of America Bulletin, 124, 943–956. doi.org/10.1130/B30479.1.

Mattei, M., Muttoni, G., Cifelli, F., 2014. A record of the Jurassic massive plate shift from the Garedu Formation of central Iran. Geology. doi.org/10.1130/G35467.1.

Mattei, M., Cifelli, F., Muttoni, G., Rashid, H., 2015. Post-cimmerian (Jurassic– Cenozoic) paleogeography and vertical axis tectonic rotations of Central Iran and the Alborz Mountains. Journal of Asian Earth Sciences*, 102*, 92-101. doi.org/10.1016/j.jseaes.2014.09.038.

McCall, G.J.H., 1997. The geotectonic history of the Makran and adjacent areas of southern Iran. Journal of Asian Earth Sciences*,* 15, 517–531.

McFadden, P.L., 1990. A new fold test for paleomagnetic studies. Geophysical Journal International. 103, 163–169.

McFadden, P.L., Reid, A.B., 1982. Analysis of palaeomagnetic inclination data. Geophys. J. R. Astr. Soc. 69, 307–319.

McQuarrie, N., Stock, J.M., Verdel, C. and Wernicke, B.P., 2003. Cenozoic evolution of Neotethys and implications for the causes of plate motions. *Geophysical Research Letters*, *30*. doi:2010.1029/2003GL017992.

McQuarrie, N., van Hinsbergen, D. J., 2013. Retrodeforming the Arabia-Eurasia collision zone: Age of collision versus magnitude of continental subduction. Geology, *41*, 315-318.

Meyer, B., Le Dortz, K., 2007. Strike-slip kinematics in Central and Eastern Iran: estimating fault slip-rates averaged over the Holocene. Tectonics 26, TC5009. doi.org/10.1029/2006TC002073.

Mirnejad, H., Lalonde, A.E., Obeid, M. and Hassanzadeh, J., 2013. Geochemistry and petrogenesis of Mashhad granitoids: An insight into the geodynamic history of the Paleo-Tethys in northeast of Iran. Lithos, *170*,105-116.

Moghadam, H. S., Stern, R. J. (2015). Ophiolites of Iran: Keys to understanding the tectonic evolution of SW Asia :(II) Mesozoic ophiolites. Journal of Asian Earth Sciences, *100*, 31-59.

Moritz, R., Ghazban, F. and Singer, B.S., 2006. Eocene gold ore formation at Muteh, Sanandaj-Sirjan tectonic zone, Western Iran: A result of late-stage extension and exhumation of metamorphic basement rocks within the Zagros Orogen. Economic Geology, *101*, 1497-1524.

Morley, C.K., Kongwung, B., Julapour, A.A., Abdolghafourian, M., Hajian, M., Waples, D., Warren, J., Otterdoom, H., Srisuriyon, K. and Kazemi, H., 2009. Structural development of a major late Cenozoic basin and transpressional belt in central Iran: The Central Basin in the Qom-Saveh area. Geosphere, *5*, 325-362.

Muttoni, G., Mattei, M., Balini, M., Zanchi, A., Gaetani, M., Berra, F., 2009a. The drift history of Iran from the Ordovician to the Triassic. In: Brunet, M.-F., et al. (Eds.), South Caspian to Central Iran Basins. The Geological Society of London Special Publications 312, pp. 7–29.

Muttoni, G., Gaetani, M., Kent, D.V., Sciunnach, D., Angiolini, L., Berra, F., Garzanti, E., Mattei, M., Zanchi, A., 2009b. Opening of the Neo-Tethys Ocean and the Pangea B to Pangea A transformation during the Permian. GeoArabia 14, 17–48.

Muttoni, G., Dallanave, E., Channell, J.E.T., 2013. The drift history of Adria and Africa from 280 Ma to Present, Jurassic true polar wander, and zonal climate control on Tethyan sedimentary facies. Palaeogeogr. Palaeoclimatol. Palaeoecol. 386, 415–435. doi.org/10.1016/j.palaeo.2013.06.011.

Neill, I., Meliksetian, K., Allen, M. B., Navasardyan, G., Kuiper, K., 2015. Petrogenesis of mafic collision zone magmatism: The Armenian sector of the Turkish–Iranian Plateau. Chemical Geology, *403*, 24-41. doi.org/10.1016/j.chemgeo.2015.03.013.

Nogole Sadat, M. A. A., Almasian, M., Poshtkouhi, M., 1993. Tectonic map of Iran, scale 1:1,000,000. Geological survey of Iran.

Oliva-Urcia, B., Larrasoana, J.C., Pueyo, E.L., Gil, A., Mata, P., Pares, J.M., Schleicher, A.M., Pueyo, O., 2009. Disentangling magnetic subfabrics and their link to deformation processes in cleaved sedimentary rocks from the Internal Sierras (west central Pyrenees, Spain). Journal of Structural Geology, 31, 163–176.

Omrani, J., Agard, P., Whitechurch, H., Benoit, M., Prouteau, G. and Jolivet, L., 2008. Arc-magmatism and subduction history beneath the Zagros Mountains, Iran: A new report of adakites and geodynamic consequences. Lithos, *106*(3), pp.380-398.

Parés, J.M., Dinares-Turell, J., 1993. Magnetic fabric in two sedimentary rock-types from the southern Pyrenees. Journal of geomagnetism and geoelectricity, 45, 193–205.

Parés, J.M., Van Der Pluijm, B.A., Dinares-Turell, J., 1999. Evolution of magnetic fabrics during incipient deformation of mudrocks (Pyrenees, northern Spain). Tectonophysics, 307, 1–14. doi.org/10.1016/S0040-1951(99)00115-8.

Parés, J.M. & van der Pluijm, B.A., 2002. Evaluating magnetic lineations (AMS) in deformed rocks. Tectonophysics, 350, 283–298.

Parés, J.M., Van Der Pluijm, B.A., 2003. Magnetic fabrics in low-strain mudrocks: AMS of pencil structures in the Knobs Formation, mudrocks (Valley and Ridge Province, US Appalachians). Journal of Structural Geology, 25, 1349–1358.

Parés, J.M., 2004. How deformed are weakly deformed mudrocks? Insights from magnetic magnetic anisotropy. In: Martin-Hernandez, F., Lüneburg, C., Aubourg, C., Jackson, M. (Eds.), Magnetic Fabrics: Methods and Applications. Geological Society, London, Special Publication 238, 191–203. doi.org/10.1144/GSL.SP.2004.238.01.13.

Paterson, S.R., Yu, H., Oertel, G., 1995. Primary and tectonic fabric intensities in mudrocks, Tectonophysics*,* 247, 105–119.

Pearce, J.A., Bender, J.F., De Long, S.E., Kidd, W.S.F., Low, P.J., Güner, Y., Saroglu, F., Yilmaz, Y., Moorbath, S. and Mitchell, J.G., 1990. Genesis of collision volcanism in Eastern Anatolia, Turkey. Journal of Volcanology and Geothermal Research, *44*, 189-229.

Piper, D.J.A., Elliot, M.T., Kneller, B.C., 1996. Anisotropy of magnetic susceptibility in a Palaeozoic flysch basin: the Windermere Super group, northern England. Sedimentary Geology*,* 106, 235–258. doi.org/10.1016/S0037-0738 (96)00011-5.

Porreca, M. & Mattei, M., 2012. AMS fabric and tectonic evolution of Quaternary intramontane extensional basins in the Picentini Mountains (Southern Apennines, Italy). International Journal of Earth Sciences*,* 101, 787–802.

Pueyo-Morer, E.L., Millán, H., Parés, J.M., Pocovi, A., 1997. Determination of the folding mechanism by AMS data. Study of the relation between shortening and magnetic anisotropy (Ṕ): A case study in the Pico del Aguila Anticline (Southern Pyrenees). Physics and Chemistry of the Earth, 22, 195–201.

Ramezani, J., Tucker, R. D., 2003. The Saghand region, Central Iran: U-Pb geochronology, petrogenesis and implications for Gondwana tectonics. American Journal of Science, *303*, 622-665.

Rees, A.I., 1965. The use of anisotropy of magnetic susceptibility in the estimation of sedimentary fabric. Sedimentology 4, 257–271. doi.org/10.1111/j.1365-3091.1965.tb01550.x.

Reuter, M., Piller, W. E., Harzhauser, M., Mandic, O., Berning, B., Rögl, F., Korh, A; Aubry, Wielandt-Schuster, U., Hamedani, A., 2009. The Oligo-/Miocene Qom Formation (Iran): evidence for an early Burdigalian restriction of the Tethyan Seaway and closure of its Iranian gateways. International Journal of Earth Sciences, *98*, 627-650.

Rezaeian, M., Carter, A., Hovius, N., Allen, M. B., 2012. Cenozoic exhumation history of the Alborz Mountains, Iran: New constraints from low-temperature chronometry. Tectonics, *31*.

Rieben, H., 1955. The geology of the Teheran plain. American Journal of Science, *253*, 617-639.

Richards, J.P., 2014. Tectonic, magmatic, and metallogenic evolution of the Tethyan orogen: From subduction to collision. Ore Geology Reviews*, 70, 323-345*.

Richter, C., van der Pluijm, B. A., Housen, B.A., 1993. The quantification of crystallographic preferred orientation using magnetic anisotropy. Journal of Structural Geology, 15**,** 113–116.

Ricou, L. E., 1996. The plate tectonic history of the past Tethys Ocean. In *The* Tethys Ocean*,* Springer US, 3-70.

Robert, A.M., Letouzey, J., Kavoosi, M.A., Sherkati, S., Müller, C., Vergés, J. and Aghababaei, A., 2014. Structural evolution of the Kopeh Dagh fold-and-thrust belt (NE Iran) and interactions with the South Caspian Sea Basin and Amu Darya Basin. Marine and Petroleum Geology, 57, 68-87. doi.org/10.1016/j.marpetgeo.2014.05.002.

Robertson, A. H., Ustaömer, T., Parlak, O., Ünlügenç, U. C., Taşlı, K., Inan, N., 2006. The Berit transect of the Tauride thrust belt, S Turkey: Late Cretaceous–Early Cenozoic accretionary/collisional processes related to closure of the Southern Neotethys. Journal of Asian Earth Sciences, *27*, 108-145. doi: 10.1016/j.jseaes.2005.02.004.

Rochette, P., 1987. Magnetic susceptibility of the rock matrix related to magnetic fabric studies. Journal of Structural Geology, 9, 1015–1020.

Rochette, P., Jackson, M. & Aubourg, C., 1992. Rock magnetism and interpretation of anisotropy of magnetic susceptibility. *Reviews of Geophysics,* 30, 209–226.

Rossetti, F., Nasrabady, M., Vignaroli, G., Theye, T., Gerdes, A., Razavi, M., Vaziri, H.M., 2010. Early Cretaceous migmatitic mafic granulites from the Sabzevar range (NE Iran): implications for the closure of the Mesozoic peri-Tethyan oceans in central Iran. TerraNova*,* 22, 26–34.

Rusnak, G.A., 1957. The orientation of sand grains under conditions of ‘‘unidirectional’’ fluid flow: 1. Theory and experiment. The Journal of Geology*,* 65, 384–409.

Ruttner, A., Nabavi, M. & Hadjian, J., 1968a. Geology of the Shirgesht area (Tabas area East Iran). Geological Survey of Iran, Report No. 4.

Ruttner, A., Nabavi, M. & Alavi, M., 1968b. Geological map of the Ozbak-Kuh Mountains. Geological Survey of Iran.

Ruttner, A. W., 1993. Southern borderland of Triassic Laurasia in north-east Iran. Geologische Rundschau, *82*, 110-120.

Sagnotti, L., Speranza, F., 1993. Magnetic fabric analysis of the pliopleistoceneclayey units of the sant’arcangelo basin, southern Italy. Physics of the Earth and Planetary Interiors, 77, 165–176. doi.org/10.1016/0031-9201(93)90096-R.

Sagnotti, L., Speranza, F., Winkler, A., Mattei, M., Funiciello, R., 1998. Magnetic fabric of clay sediments from the external northern Apennines (Italy). Physics of the Earth and Planetary Interiors, 105, 73–93. doi.org/10.1016/S0031-9201(97)00071-X.

Saint-Bezar, B., Hebert, R.L., Aubourg, C., Robion, P., Swenen, R., Frizon de Lamotte, D., 2002. Magnetic fabric and petrographic investigations of hematite-bearing sandstones within ramp-related folds: examples from the South Atlas Front (Morocco). Journal of Structural Geology, 24, 1507–1520. doi.org/10.1016/S01918141(01)00140-7.

Salvini, F., 2004. *Daisy 3, The Structural Data Integrated System Analyzer,* Dipartimento Scienze, Universita degli Studi Roma TRE, Rome.

Sengör, A.M., 1979. Mid-Mesozoic closure of Permo-Triassic Tethys and its implications. Nature, 279**,** 590–593.

Sengör, A. M. C., Kidd, W. S. F., 1979. Post-collisional tectonics of the Turkish-Iranian plateau and a comparison with Tibet. Tectonophysics, *55*, 361-376.

Sengör, A.M.C., 1984. The Cimmeride Orogenic System and the Tectonics of Eurasia. Geological Society of America, Special Paper, 195, pp. 82.

Sengör, A.M.C., Altiner, D., Cin, A., Us- tomer, T., Hsu, K.J., 1988. The origin and assembly of the Tethyside orogenic collage at the expenses of Gondwana land. In: Gondwana and Thethys, Audley-Charles, M.G., Hallam, A. (Eds.). Geological Society Special Publication, 37, 119–181.

Seyed-Emami, K., 2003. Triassic in Iran. *Facies*, *48*, 91-106.

Sheikholeslami, M. R., Kouhpeyma, M., 2012. Structural analysis and tectonic evolution of the eastern Binalud Mountains, NE Iran. Journal of Geodynamics, *61*, 23-46.

Soffel, H., Forster, H., Becker, H., 1975. Preliminary polar wander path of Central Iran. Journal of geophysics, *41*, 541-543.

Soffel, H. C., Förster, H. G., 1980. Apparent polar wander path of Central Iran and its geotectonic interpretation. Journal of geomagnetism and geoelectricity, *32*, SIII117-SIII135.

Soffel, H.C., Davoudzadeh, M., Rolf, C., 1989. Palaeomagnetic investigations on Phanerozoic formations from Iran: reinterpretation of measurements between 1972 and 1982. Muenchner Geophysikalische Mitteilungen. Münchner Univers. Schriften. 4, 23–56.

Soffel, G., Davoudzadeh, M., Rolf, C. Schmidt, S., 1995. New paleomagnetic data from Iran, Geo-sciences, Geological Survey of Iran, 4.

Soffel, H. C., Schmidt, S., Davoudzadeh, M., Rolf, C., 1996. New palaeomagnetic data from Central Iran and a Triassic palaeoreconstruction. Geologische Rundschau, *85*, 293-302

Soper, N., 1986. Geometry of transecting, anastomosing solution cleavage in transpression zones. Journal of Structural Geology, 8, 937–940.

Soper, N.J., Hutton, D.H. W., 1984. Late Caledonian sinistral displacements in Britain: implications for a three-plate collision model. Tectonics*,* 3, 781–794.

Stampfli, G., Marcoux, J., Baud, A., 1991. Tethyan margins in space and Time. Palaeogeography, Palaeoclimatology, Palaeoecology, 87**,** 373–409.

Stampfli, G.M. & Borel, G.D., 2002. A plate tectonic model for the Paleozoic and Mesozoic constrained by dynamic plate boundaries and restored synthetic oceanic isochrones. Earth and Planetary Science Letters, 196**,** 17–33.

Stoneley, R., 1981. The geology of the Kuh-e Dalneshin area of southern Iran, and its bearing on the evolution of southern Tethys. Journal of the Geological Society, *138*, 509-526.

Stöcklin, J., Eftekhar-Nezhad, J., Hushmand-zadeh, A., 1965. Geology of the Shotori Range (Tabas area, East Iran). Geological survey of Iran, Report No. 3.

Stöcklin, J. (1968). Structural history and tectonics of Iran: a review. AAPG Bulletin, 52, 1229-1258.

Stöcklin, J., Nabavi, M.H., 1969. Boshruyeh map, scale 1:250,000. Geological Survey of Iran.

Stöcklin, J., Nabavi, M.H., 1971. Explanatory text of the Boshruyeh Quadrangle Map J7. Scale 1:250.000. Geological Survey of Iran.

Stöcklin, J,. 1974."Possible ancient continental margins in Iran." The geology of continental margins. Springer Berlin Heidelberg, 873-887.

Stöcklin, J., Setudehnia, A., 1977. Stratigraphic lexicon of Iran, Geological Survey of Iran, Tehran, Report 18, 376 pp.

Stringer, P. & Treagus, J.E., 1980. Non-axial planar S1 cleavage in the Hawick rocks of the Galloway area, Southern Uplands, Scotland. Journal of Structural Geology, 2, 317–331.

Sun, W.W., Jackson, M., Craddock, J.P., 1993. Relationship between remagnetization, magnetic fabric, and deformation in the midcontinental Paleozoic carbonates. Tectonophysics, 221, 361–366.

Taira, A., 1989. Magnetic fabric and depositional processes. In: Taira, A., Masuda, F. (Eds.), Sedimentary Facies in the Active Plate Margin. Terra Scientific Publishing, Tokyo, 44–77.

Takin, M., 1972. Iranian geology and continental drift in the Middle East. Nature, 235, 147–150.

Tarling, D.H., Hrouda, F., 1993. The Magnetic Anisotropy of Rocks. Chapman & Hall, London, pp. 217.

Tatar, M., J. Jackson, D. Hatzfeld, and E. Bergman (2007), The 2004 May 28 Baladeh earthquake (Mw 6.2) in the Alborz, Iran: Overthrusting the South Caspian Basin margin, partitioning of oblique convergence and the seismic hazard of Tehran. Geophysical Journal International, 170, 249–261. doi:10.1111/j.1365-246X.2007.03386.x.

Tavani, S., Cifelli, F., 2010. Deformation pattern analysis and tectonic implications of a décollement level within the Central Apennines (Italy). Geological Journal, 45, 582–596. doi.org/10.1002/gj.1198.

Tchalenko, J.S., Ambraseys, N.N., 1970. Structural analysis of the Dasht e-Bayaz (Iran) earthquake fractures. Geological Society of America Bulletin, 81, 41–60.

Tchalenko, J.S., Ambraseys, N.N., 1973. Earthquake destruction of adobe villages in Iran. Annals of Geophysics, 26, 357–389.

Tirrul, R., Bell, I.R., Griffis, R.J. and Camp, V.E., 1983. The Sistan suture zone of eastern Iran. Geological Society of America Bulletin, *94*, 134-150. 1002/2013JB010620.

Torsvik, T.H., Van der Voo, R., Preeden, U., Mac Niocaill, C., Steinberger, B., Doubrovine, P.V., van Hinsbergen, D.J., Domeier, M., Gaina, C., Tohver, E. and Meert, J.G., 2012. Phanerozoic polar wander, palaeogeography and dynamics. Earth-Science Reviews, 114, 325-368.

Van der Voo, R., 1993. Paleomagnetism of the Atlantic, Tethys and Iapetus Ocean, Cambridge University Press, Cambridge, pp 411.

Verdel, C. (2008). Cenozoic geology of Iran: an integrated study of extensional tectonics and related volcanism. Unpublished Ph. D. Thesis*, California Institute of Technology, Pasadena*.

Verdel, C., Wernicke, B. P., Hassanzadeh, J., Guest, B., 2011. A Paleogene extensional arc flare-up in Iran. Tectonics, *30*.

Vernant, P., Nilforoushan, F., Hatzfelad, D., Abbassi, M.R., Vigny, C., Masson, F., Nankali, H., Martinod, J., Ashtiani, A., Bayer, R., Tavakoli, F., Chery, J., 2004. Present-day crustal deformation and plate kinematics in the Middle East constrained by GPS measurements in Iran and northern Oman. Geophysical Journal International, 157, 381–398. doi.org/10.1111/j.1365-246X.2004.02222x.

Walker, R., Jackson, J., Baker, C., 2003. Surface expression of thrust faulting in eastern Iran: source parameters and surface deformation of the 1978 Tabas and 1968 Ferdows earthquake sequences. Geophysical Journal International, 152, 749–765. doi.org/10.1046/j.1365-2 46X.2003.01886.x.

Walker, R., Jackson, J., 2004. Active tectonics and late Cenozoic strain distribution in central and eastern Iran. Tectonics 23, TC5010. doi.org/10.1029/2003TC001529.

Walker, R., Jackson, J., Baker, C., 2004. Active faulting and seismicity of the Dasht-eBayaz region, eastern Iran. Geophysical Journal International, 157, 265–282, doi.org/10.1111/j.1365-2966.2004.02179.x.

Walker, R.T., Bergman, E., Szeliga, A., Fielding, E.J., 2011. Insights into the 1968-1997 Dasht-e-Bayaz and Zirkuh earthquake sequences, eastern Iran, from calibrated relocations, InSAR and high-resolution satellite imagery. Geophysical Journal International, 187, 1577–1603. doi.org/10.1111/j.1365-246X.2011.05213.x.

Walker, R.T., Khatib, M.M., Bahroudi, A., Rodés, A., Schnabel, C., Fattahi, M., Talebian, M., Bergman, E., 2015. Co-seismic, geomorphic, and geologic fold growth associated with the 1978. Tabas-e-Golshan earthquake fault in eastern Iran. Geomorphology 237, 98–118. doi.org/10.1016/j.geomorph.2013.02.016.

Walpersdorf, A., Manighetti, I., Mousavi, Z., Tavakoli, F., Vergnolle, M., Jadidi, A., Hatzfeld, D., Aghamohammadi, A., Bigot, A., Djamour, Y., Nankali, H., Sedighi, M., 2014. Present-day kinematics and fault slip rates in eastern Iran, derived from 11 years of GPS data. Journal of Geophysical Research: Solid Earth 119, 1359–1383.

Weil, A.B. and Sussman, A.J., 2004. Classifying curved orogens based on timing relationships between structural development and vertical-axis rotations. Geological Society of America Special Papers, 383, 1-15.

Weil, A.B., Yonkee, A., 2009. Anisotropy of magnetic susceptibility as a proxy for layer parallel shortening and tangential extension: implications for mountain belt curvature in the Wyoming Salient. Lithosphere, 1, 235–256. doi.org/10.1130/L42.1.

Wensink, H., Zijderveld, J. D. A., Varekamp, J. C., 1978. Paleomagnetism and ore mineralogy of some basalts of the Geirud Formation of Late Devonian-Early Carboniferous age from the southern Alborz, Iran. Earth and Planetary Science Letters, *41*, 441-450.

Wensink, H., 1979. Implications of some paleomagnetic data from Iran for its structural history. Geologie en Mijnbouw 58, 175-185.

Wensink, H., Varenkamp, J.C., 1980. Palaeomagnetism of basalts from Alborz: Iranpart of Asia in the Cretaceous. Tectonophysics, 68, 113–129.

Wensink, H., 1982. Tectonic inferences of paleomagnetic data from some Mesozoic formations in Central Iran. Journal for Geophysic. 51, 12–23.

Wensink, H., 1983. Paleomagnetism of red beds of Early Devonian age from central Iran. *Earth and Planetary Science Letters*, *63*, 325-334.

Wilmsen, M., Fürsich, F.T., Seyed-Emami, K., 2003. Revised lithostratigraphy of the Middle and Upper Jurassic Magu Group of the northern Tabas Block, east- central Iran. Newsletters on Stratigraphy, 39, 143–156.

Wilmsen, M., Wiese, F., Seyed-Emami, K., Fürsich, F.T., 2005. First record and significance of Turonian ammonites from the Shotori Mountains, east-central Iran. Cretaceous Research, 26, 181–195. doi.org/10.1016/j.cretres.2004.10.004.

Wilmsen, M, Fursich, F.T., Seyed-Emami, K & Majidifard, M.R., 2009a. An overview of the lithostratigraphy and facies development of the Jurassic System on the Tabas Block, east-central Iran. Geological Society, London, Special Publications*,* 312, 323-343.

Wilmsen, M., Fursich, F.T., Seyed-Emami, K., Majidifard, M.R., Taheri, J., 2009b. The Cimmerian Orogeny in northern Iran: tectono-stratigraphic evidence from the foreland. TerraNova*,* **21,** 211–218.

Wilmsen, M., Fursich, F.T., Seyed-Emami, K., Majidifard, M.R., ZamaniPedram, M., 2010. Facies analysis of a large-scale Jurassic shelf-lagoon: the Kamar-e-Mehdi Formation of east-central Iran. Facies*,* 56, 59–87.

Woodcock, N.H., Awan, M.A., Johnson, T.E., Mackie, A.H., Smith, R.D.A., 1988. Acadian tectonics of Wales during Avalonia/Laurentia convergence. Tectonics*,* 7, 483–495.

Yilmaz, Y., 1993. New evidence and model on the evolution of the southeast Anatolian orogen. Geological Society of America Bulletin, *105*, 251-271.

Zamani-Pedram, Z., 2011. Source, Facies, and Sedimentary Environments of the Middle to Upper Jurassic Strata in the Kerman and Tabas Areas, East-Central Iran. PHD Thesis, Bayerischen Julius-Maximilians-Universität, Würzburg, Germany.

Zanchi, A., Berra, F., Mattei, M., Ghassemi, M. & Sabouri, J., 2006. Inversion tectonics in central Alborz, Iran. Journal of Structural Geology*,* 28, 2023– 2037.

Zanchi, A., Zanchetta, S., Garzanti, E., Balini, M., Berra, F., Mattei, M., Muttoni, G., 2009a. The Cimmerian evolution of the Nakhlak–Anarak area, Central Iran, and its bearing for the reconstruction of the history of the Eurasian margin. In: Brunet, M.F., Wilmsen, M., Granath, J. (Eds.), South Caspian to Central Iran basins, Geological Society of London Special Publication 312, pp. 261–286. doi.org/10.1144/SP312.13.

Zanchi, A., Zanchetta, S., Berra, F., Mattei, M., Garzanti, E., Molyneux, S., Nawab, A., Sabouri, J., 2009b. The Eo-Cimmerian (Late? Triassic) orogeny in north Iran. Geological Society, London, Special Publications, *312*, 31-55.

Zanchi, A., Malaspina, N., Zanchetta, S., Berra, F., Benciolini, L., Bergomi, M., Cavallo, A., Javadi, H.R. and Kouhpeyma, M., 2015. The Cimmerian accretionary wedge of Anarak, Central Iran. Journal of Asian Earth Sciences, *102*, 45-72.